2021

In situ dissolvable hydrogels for biomedical applications

BOSTON UNIVERSITY

GRADUATE SCHOOL OF ARTS AND SCIENCES

Dissertation

IN SITU DISSOLVABLE HYDROGELS FOR BIOMEDICAL APPLICATIONS

by

KATHERINE ADAMS COOK

B.A., University of Richmond, 2015
B.S., University of Richmond, 2015
M.A., Boston University, 2018

Submitted in partial fulfillment of the

requirements for the degree of

Doctor of Philosophy

2021

Approved by

First Reader

Mark W. Grinstaff, Ph.D.
Distinguished Professor of Translational Research
Professor of Biomedical Engineering
Professor of Chemistry
Professor of Materials Science and Engineering
Professor of Medicine

Second Reader

Arturo J. Vegas, Ph.D.
Assistant Professor of Chemistry
Assistant Professor of Biomedical Engineering
Assistant Professor of Materials Science and Engineering

Third Reader

Scott E. Schaus, Ph.D.
Professor of Chemistry
Assistant Professor of Pharmacology and Experimental Therapeutics

ACKNOWLEDGEMENTS

I would like to thank my research advisor, Professor Mark Grinstaff, for his mentorship, guidance, and support throughout my research endeavors at Boston University. Mark, you have exceeded my expectations as a research mentor and I am forever grateful that you welcomed me into your lab.

I would also like to thank my dissertation advisory committee members, Arturo Vegas, Ph.D., Scott Schaus, Ph.D., John Snyder, Ph.D., and Ara Nazarian, Dr.Sc. for their research guidance, classroom instruction, seminars, and support. You have all significantly challenged and advanced my knowledge of chemistry.

A special thanks goes out to my peers in the Grinstaff Laboratory for their kindness, willingness to teach, and friendships that I will forever hold near and dear to my heart. Thinking back on my experience at Boston University and in the Grinstaff Laboratory, I could not have earned this degree without the daily conversations, laughs and friendly faces day in and day out on the 5th floor of SCI.

I'd like to acknowledge Dr. Chloe Grazon for her mentorship my first two years of graduate school at Boston University. I would not be the scientist that I am today without your kind, detailed, and dedicated mentorship both in and out of the laboratory. I will forever look up to you as an amazing mother, scientist, and friend.

A very special thanks goes to Nada Naguib. Nada, you not only have been an incredible young scientist that I have had the honor to mentor, but an amazing friend as well. I will forever value your help during the two and a half years you

worked on my project with me. I am so thankful that we had that time to grow our professional and personal relationship and friendship, and that we continue to support each other throughout our achievements. I have the utmost confidence that you will succeed with the highest honors in the Biomedical Engineering Ph.D. program at Cornell University. I cannot wait to see where life takes you and I am so proud of the scientist and friend you have become. (p.s. yes, I will still get you a job wherever I work so we can forever be labmates).

I would like to thank my cat, David, and his other mom, Christa Mole, for their friendship, and support throughout this endeavor. Christa, you have always been an amazing friend to me since the first day of graduate school orientation. From the lunch breaks and walks during the day, to the weekly Bachelor nights, I will forever be grateful for our friendship. Not only have you been an incredible friend, but your generosity continues to astonish me. You lent me your cat, David, to try out having a cat before adopting one, and little did I know he would be a lifelong, furry best friend who wakes me up with kisses at 3am every morning. I am so proud of your accomplishments both in and out of the laboratory. I cannot wait to watch you defend your thesis soon.

I would also like to thank my friends, both near and far, for the laughs, cries, hugs, and adventures we have been through together. I will always cherish the late nights in lab, working up reactions, the last-minute Cornwall's get-togethers, game nights, facetimes, and ski trips we have shared together. You have helped me grow as a scientist, a friend, and so much more. I cannot wait to laugh and have more

adventures with you all. Specifically, I'd like to send a special thanks to Helen Warner. Helen, you have been a vital part of my life since the first day of college and I couldn't imagine it any other way. You have supported me beyond anything I could have hoped for throughout graduate school. Your nightly texts checking in during one of the hardest parts of my life got me through day by day. You came to Boston to be my support during my defense even though it was virtual. You have far surpassed anything I could have asked for in a friend. I am forever grateful to have you in my life, and I couldn't imagine it without you. I'm so proud of you for the person you have become over the last 10 years of our friendship.

Lastly, I would like to give an incredibly special thank you to my family. Moving to a new city knowing nobody is difficult, but you all made it so much easier with the phone calls, facetimes, and visits. Thank you to my parents, my brother, and my sister-in-law for all of the laughs, the shoulders to lean on, and the encouragement throughout not only the last 5 years of my life, but the last 28. I would never be where I am without you. From the rides to school growing up, to the nation-wide dive meets, I'm forever grateful for all of the time and energy you have dedicated to ensuring I have every chance to pursue my dreams. To my family around the world, thank you so much for welcoming me into your homes with open arms and showing me what the world has to offer. Thank you for all of the love and kindness you all have given me especially during the last 5 years. I certainly would not have made it to this day without you. I love you all so much.

IN SITU DISSOLVABLE HYDROGELS FOR BIOMEDICAL APPLICATIONS

KATHERINE ADAMS COOK

Boston University Graduate School of Arts and Sciences, 2021

Major Professor: Mark W. Grinstaff, Distinguished Professor of Translational Research, Professor of Biomedical Engineering, Professor of Chemistry, Professor of Materials Science and Engineering, Professor of Medicine

ABSTRACT

Hydrogels are hydrophilic, three-dimensional polymeric networks prepared through chemical or physical conjugation. Hydrogels are recognized for their tunable properties, specifically through changes in the backbone of the polymers, such as 1) modifying the number of hydrophobic chain lengths, 2) adding or removing cleavable linkages, 3) varying reactive-end groups, 4) increasing or decreasing the weight percent of the hydrogel, and 5) combining two or more hydrogel networks into one, namely creating an interpenetrating network. We synthesized and characterized on- and off-demand, dissolvable hydrogels for use as burn wound dressings, polypectomy bandages, and vascular occlusion devices, and within interpenetrating networks. The hydrogels are composed of PEG-based crosslinkers, and PEI-based hyperbranched macromers which were prepared in high yields. In context of burn wound dressings, there is an unmet need for an adherent dressing with ease of removal, such as a dissolvable hydrogel dressing. In a model of *in vivo* porcine burn wounds, our hydrogel shows superior burn healing relative to traditional dressings such as sterile gauze pad and non-adherent foam dressings. When our hydrogel was removed, no newly formed

tissue adhered to the dressing, and immunohistochemical stains exhibit improved inflammation and necrosis. When our hydrogel was used as an *in vivo* polypectomy sealant, we observed ease of application and adhesion to the colon, despite peristalsis. In *in vitro* studies, we observe no migration of bacteria through the hydrogel. As a vascular occlusion device, our hydrogels withstand an *ex vivo* burst pressure of up to 440mmHg on average, over 3x that of arterial pressure. Furthermore, we prepared an interpenetrating network from two hydrogel formulations both using SN2 chemistry with tunable mechanical properties. The hydrogel formulations highlighted in this work vary in gelation, mechanical properties, swelling, dissolution, and adhesion based on the structure of the polymer and reactive groups. These hydrogels represent a future direction in wound dressings and sealants as they prevent bacterial migration into an open wound, adhere to tissue, provide a moist wound environment, demonstrate structure-function relations allowing for tunable mechanical properties, and are biocompatible.

TABLE OF CONTENTS

LIST OF TABLES

LIST OF FIGURES

LIST OF SCHEMES

LIST OF ABBREVIATIONS

ºC……..Degrees Celsius

^{13}C……... Carbon

^{1}H ……..Proton

Å ……..…….Angstrom

α……..…… alpha

AgNPs…… Silver nanoparticles

AMPS……..……..2-acrylamido-2-methylpropane sulfonic acid sodium salt

ASTM……American Society for Testing Materials

β ……beta

b……...……...Broad

β-CD……..…… Beta-cyclodextran

$CDCl_3$……Dueterated Chloroform

cm ……..Centimeter

CP ……Co-polymer

d ……..……...Day

D_2O…… Deuterated water

Da…….Daltons

DBU……... 1,8-Diazabicyclo(5.4.0)undec-7-ene

DCC…….. Dicyclocarboxydiimide

DCM……... Dichloromethane

Dex ……..Dextran

DHR ……..……Discovery h rheometer

DIPEA……..…….Diisopropylethylamine

DMF ……..……Dimethylformamide

DPTB ……..……Deep Partial-Thickness Burn

DSC ……..……..Differential Scanning Calorimetry

DTT ……..……..Dithiothreitol

E ……..……Young's modulus

ECM ……..……Extracellular matrix

Eq ……..……..…….Equivalents

Et_3SiH ……..……Triethylsilane

FGF ……..……Fibroblast growth factor

G' ……..……..Storage Modulus

G" ……..……Loss Modulus

GPC ……..……..Gel Permeation Chromatography

H_2O_2……..……..Hydrogen Peroxide

HA ……..……Hyaluronic acid

His-1……..……..Histatin-1

HOBt ……..……1-Hydroxybenzotriazole

hr ……..……Hour

HUVEC ……..……Human umbilical vein endothelial cell

Hz ……..……...Hertz

IL-1β……..……..Interleukin-1-β

IL-6 ……Interleukin-6

kDa ……..Kilodaltons

kg ……Kilogram

kPa……..Kilopascals

LME ……..Lysine methyl ester

LVER……..Linear viscoelastic region

m……..Multiplet

M……Molar

m ……Mass

MAL ……..Maleimide

MALDI…….. Matrix-assisted Laser Desorption/Ionization

MBA ……..N-N’-methylenebisacrilamide

MC……..Methylcellulose

MESNA ……..Mercaptoethanesulfonate

mg……..Milligram

min ……..Minute

mL ……..Milliliter

mm ……..Millimeter

mM……..Millimolar

mmHg ……..Millimeters of mercury

mmol ……..Millimolar

MMPs ……..Metalloproteinases

Mn……..……..Molecular Number

MRSA……... Methicillin-resistant Staphylococcus aureus

MTS ……..3-(4,5-dimethylthiazol-2-yl)-5-(3-carboxymethoxyphenyl)-2-(4-sulfophenyl)-2H-tetrazolium)

MTT …….……..(3-(4,5-dimethylthiazol-2-yl)-2,5-diphenyltetrazolium bromide

Mw ……..……Molecular Weight

N……..…….Newton

n ……..……Sample size

NADPH…….……Dinucleotide Phosphate, Nicotinamide-Adenine

NC ……..…….Nanocrystalline silver

nCur ……..……Curcumin

NHS ……..…….N-hydroxysuccinimide

NMR ……..……Nuclear Magnetic Resonance

ON……..…….Overnight

Pa ……..……..Pascals

PBS ……..……..Phosphate buffered saline

PDGF……..…….Platelet-derived growth factor

PDI……..……..Polydispersity index

pDNA……..……Plasmid deoxyribonucleic acid

PEG……..……Poly(ethylene glycol)

PEI……..……Poly(ethyleneimine)

PEI-SH……..…….Thiolated Poly(ethyleneimine)

PFP ……..…….Pentafluorophenyl

PGX……..…….……..Pressurized gas to expand liquid

PMNs……..…..……..Polymorphonuclear neutrophils

ppm……..……Parts per million

PVA……..…….Poly(vinyl alcohol)

q ……..Quartet

Res ……..…..…….Resveratrol

RT ……..……..Room temperature

s ……..…….Second

s ……..……..Singlet

SC ……..……Sildenafil citrate

SEM……..…….……..Scanning electron microscopy

SPTB…….Superficial Partial-Thickness Burn

SSD……..……Silver sulfadiazine

SVA……..……Succinimidyl valerate

t……..…….Triplet

$t_{1/2}$……..……..……..……Half life

TG……..……Transglutaminase

TGF-β…..……..Transforming growth factor-beta

TNF-α…..…… Transforming growth factor-alpha

TOF……...…..…….Turnover frequency

Tr ……...…..…….……..Trityl

tt ……..…….……Triplet of triplets

UV ……..…….……Ultraviolet

VEGF…..……... Vascular endothelial growth factor

wt%……...…….……Weight percent

ZOI ……...…….……Zone of inhibition

δ ……...…….……Chemical shift

µL……..……..Microliter

µm……...…….……Micrometer

CHAPTER 1. MANAGEMENT OF SECOND-DEGREE BURNS USING HYDROGELS: CURRENT STATUS AND FUTURE PROSPECTS

1.1 Anatomy of the integument

The integument, or skin, the largest organ in the human body is a physical barrier to injuries and environmental pathogens that maintains homeostasis, modulates inflammation and transmits tactile sensations.[1] Burn injuries can disrupt any of the skin's three anatomic layers: the epidermis, dermis and/or hypodermis. However epidermal cells underlying the outer surface of the skin can regenerate from cells deep within the dermal appendages (including hair follicles, sebaceous glands, and sweat glands) [2,3] and from adipose-derived stem cells found on the hypodermis.[1,4,5] The tightly regulated contiguous healing process involves four phases: I) hemostasis, II) inflammation, III) cellular proliferation, and IV) matrix remodeling and ultimately results in a cross-linking of collagen I fibers to confer adequate tensile strength to the newly formed scar.[6] An in-depth background on the integument and the wound healing process has been performed previously by Lloyd et al [1] and is not within the scope of this review.

1.2 Classification

Burns are classified according to burn depth in four degrees. (**Figure 1.1** and **Table 1.1**).[7]

First-degree burns (**Figure 1.2A**), known as sunburns, are superficial red and painful injuries that and only affect the top layer of the epidermis and typically heal completely without the need for intervention. *Second-degree burns* penetrate into the dermis and are therefore referred to as partial-thickness burns. These burns are further categorized into *superficial partial-thickness burns (SPTBs)* (**Figure 1.2B**), which entirely injure the epidermis and part of the dermis, and *deep partial-thickness burns (DPTBs)* (**Figure 1.2C**) which extend deeper into the dermis layer. Wounds resulting from second degree burns can be very sensitive and painful when touched due to exposure of intact, sensory nerve endings. Re-epithelialization depends on the level of degradation of the dermis and the number of damaged skin appendages, thereby this wounds are frequently encountered with scarring and contractures.[2] In contrast, *third-degree burns* destroy all skin layers, including the underlying subcutaneous fat, and are therefore considered full-thickness burns. These burn wounds present no sensitivity to touch due to destruction of the dermal plexus nerves (**Figure 1.2D**).[8] Ultimately, *fourth-degree burns* extend through all skin layers and extend to muscle, tendons and bones (**Figure 1.2E**) consequently affecting nerve endings. These burns are the most challenging to treat and often prompt surgical debridement and grafting.[9]

1.3 Burn wound management

Proper wound management begins with correctly classifying the depth of

the burn alongside early clinical evaluation and management. Differentiation between SPTB, DPTB, and third-degree burns may not be apparent in the first days after the injury. Moreover, these wounds can suffer from burn conversion, a poorly understood process, in which the thermal injury spreads from a superficial to a full-thickness burn.[7,10] For all burns, the goals of management and treatment include pain mitigation, prevention of infection, and promoting rapid healing, with the ultimate goal of restoring the injured region to both full function and visual aesthetic.[8]

Caring for a burn wound begins with debridement followed by covering the wound to create an environment that both promotes re-epithelization and prevents cellular dehydration. Second-degree burns, the most common burns resulting from thermal injuries,[11] are often managed on an outpatient basis. Multiple dressing options are currently available, and their use depends on the burn depth, volume of exudate present, and patient comfort. For the treatment of SPTBs and DPTBs, the gold standard is conventional low-cost gauze impregnated with silver sulfadiazine (SSD).[8] These dressing can provide a temporary protective barrier until tissue integrity can be naturally restored. However, these traditional dressings often adhere to the wound surface and delay the healing process due to frequent perturbations of the wound site. In addition, SSD is thought to delay re-epithelization due to toxicity on the regenerating keratinocytes. Nonetheless, this concern does not appear to prevent their widespread clinical use.[12]

As the understanding of dermal wound healing advances, the range of treatments available for second-degree burns has also expanded (**Table 1.2**). More recent dressings promote wound healing, absorb excess exudate, reduce bacterial burden, and minimize pain during dressing changes.[11] In addition, some innovative dressings accommodate movement of the burned skin[13] and facilitate the patient's return to daily activities.[14]

1.4 Dressing pads

Dressing pads simply refer to simple non-adherent dressings made of gauze, loosely woven translucent cotton fibers. Gauze pads are applied directly to the wound surface to provide a protective barrier to infection while allowing oxygenation of the injured tissue to promote healing. These dressings are either non-medicated or medicated, and are sometimes combined with paraffin to avoid skin damage when removed (i.e., a tulle dressing). However, even with paraffin, dressing changes often result in pain and re-injury of the tissue, increasing the length of the re-epithelialization process, and ultimately requiring anesthetization of the patient. [15,16]

Aforementioned, dressing pads containing silver sulfadiazine are the current standard-of-care for second-degree burn injuries. However, Iodine and chlorhexidine are also used as antimicrobials, if less commonly. The major advantages of antimicrobial-containing gauze dressings are their low cost, widespread availability, and effective prevention of local bacterial infection.[8]

Local cytotoxicity of the silver ions over keratinocytes and fibroblasts along with pain eliciting from constant dressing changes are commonly expected following treatment of second-degree burns with SSD dressings. [12,17–23] Nonetheless, silver ions have been historically recognized as potent antimicrobials with cytotoxic activity against numerous bacteria, viruses, yeast, and fungi,[24] and therefore newer formulations with silver are being manufactured to maintain the broad antibacterial spectrum while posing less local toxicity. [25] Clinical trials comparing nanocrystalline silver to traditional SSD formulations for the treatment of deep partial-thickness burns show that nanocrystalline silver (NC) dressings present lower incidence of infections in comparison to SSD formulations (9.5% vs 27.8% with an odds ratio of 0.14, 95% CI [0.06-0.35]).[25] Moreover, two studies report significantly less pain with the Acticoat™ NC dressings compared to SSD dressings using a visual analog scale (VAS) for pain (1-10; 0 being no pain, 10 being severe pain).[26,27] Varas et al. report a mean VAS pain difference of 3.2 for NC dressing vs 7.9 for SSD ($p<0,001$)[27] whereas Muangman et al. report a VAS difference of 4 ± 0.6 for NC dressing vs 5 ±0.7 for SSD.[26] However, the authors of this meta-analysis conclude that despite the proven lower incidence of infections and higher satisfaction with NC dressing, further randomized studies are needed to confirm the results and change the current guidelines for the management of second-degree burns.[25]

Another historically well-described treatment for second-degree burns is Honey. [28–30] Benefits of using honey include: 1) improving wound contraction

while promoting formation of granulation tissue and epithelialization, 2) reducing debridement, 3) soothing and deodorizing the wounds, 4) preventing dry scab formation, and 5) decreasing scarring.[28] Wijesinghe et al., compare the use of honey covered by sterile gauze to SSD impregnated gauze for the treatment of second-degree burns in a meta-analysis including 8 randomized controlled clinical trials. [30] The fixed and random effect odds ratios for complete wound healing at 15 days both show superiority for honey dressings for the treatment of second-degree burns (fixed effects odds ratio of 6.1 (95%CI [3.7-9.9]) and pooled random effect odds ratio of 6.7 (95%CI [1.8-15.8]).[30]

A weakness of antimicrobial impregnated gauze pads is insufficient adsorption of wound exudate. Gauze dressings require daily changes that, as previously mentioned, traumatize the newly epithelialized surfaces, disrupting the granulation process, resulting in unwanted pain and discomfort to the patient. Chaganti et al. systematically review three randomized controlled clinical trials in the United States and China comparing the rate of re-epithelization and time to wound healing of second-degree burns using traditional SSD with gauze versus highly absorptive foam dressings - dressings consisting of layers of semipermeable polyurethane manufactured specifically to absorb large amounts of exudate. These absorptive foam dressings 1) enhance autolytic debridement 2) provide a moist wound environment and 3) promote healing.[31,32,33] According to Chaganti et al., [11] healing periods for second-degree burns are similar regardless of the type of dressing used, as results show no statistically significant

difference in time to complete healing between using foam dressings and SSD with gauze (**Table 1.3**). In contrast, results from the three trials indicate that, unlike healing time, pain varies with the type of dressing. All trials used the Johns Hopkins VAS, but specific data collection timepoints varied between trials:[34] Silverstein et al report pain scores during dressing application, during wear, and on dressing removal; Yang et al.[35] report pain scores before wound treatment and after treatment at day 7, 14, 21 and 28; and Tang et al report pain scores before, during, and after dressing removal from week 1 to 4.[31] Despite the differences in the clinical study designs, the use of foam dressings causes less pain and is more comfortable for patients, particularly at earlier stages of healing.[11]

1.5 Hydrocolloid dressings

Hydrocolloid dressings consist of a layer of gel-forming material adhered to a semi-permeable film or foam backing. This gel layer comprises an adhesive polymer matrix containing a combination of absorbent materials including gelatin, pectin, and sodium carboxymethylcellulose that absorb exudates and swell into a gel-like substance providing a moist environment. Hydrocolloids are waterproof, flexible dressings that assist in tissue regeneration and granulation, are impermeable to bacteria, and promote autolytic debridement of dry and/or necrotic wounds.[14] Application and removal of hydrocolloid dressings is easy and painless. These dressing are available in a variety of sizes, shapes, thicknesses

and may also include adhesive borders making them ideal for wounds in high friction areas of the body, such as the sacrum, heels, and elbows, where they reduce the likelihood of rucking, wrinkling or edge rolling.[36] In addition, some of these dressing may be transparent, allowing visualization of the wound without removal of the dressing. However, efficacy depends on the amount of exudate, as these dressings are not designed to treat wounds with high volume exudates. Leakage and discharge of unpleasant color and odor, which is often mistaken for infection, can result if the wound presents with high exudate production, requiring more frequent dressing changes and overall compromising the cost-effectiveness of this product.

A systematic review comparing three randomized clinical trials reveals superior efficacy (time to complete healing) of hydrocolloid dressings over chlorhexidine impregnated paraffin gauze dressings.[14,37–39] Moreover, the incidence of infection, adverse events, and pain levels are also superior in the hydrocolloid dressing group**.** Similarly, Wright et al., [36] report higher satisfaction for the hydrocolloid dressings versus the chlorhexidine impregnated paraffin gauze (satisfaction levels recorded for both investigators and participants using a 10-item VAS, with 0= useless and 10= excellent). Satisfaction levels rate higher for hydrocolloid dressings from both participants and investigators (**Table 1.4**).[40] However, unlike to what would be expected, the authors report a more frequent need to change the hydrocolloid dressings in comparison to the gauze. The number one reason is that patients treated with hydrocolloid dressings presented

extensive leakage (15%) compared to those treated with the conventional gauze dressings (3%). The difference in reasons for dressing change between groups is significant (p=0.01) and besides leaking, other reasons included pain, discomfort and detachment of the dressing. [36] In addition, the authors report no significant difference in the difficulty between removing either of the dressings, questioning whether patient satisfaction could be diminished if they had to buy more dressings to treat the same wound.

1.6 Silicon-coated nylon dressings

Silicon coated nylon dressings are flexible, porous, semitransparent polyamide nets coated with a silicone that facilitates the application and retention of the dressing in the wound area.[14] These highly pliable, and stretchable dressings are amenable to placement on tissue with complex surface contours. The dressing's open mesh structure protects the wound while allowing free passage of exudate into a secondary dressing, reducing frequent dressing changes. In addition, these dressings are non-adherent and therefore removal is easy and atraumatic.[41]

Important to note that some modern silicon coated nylon dressings contain biological compounds, such as collagen peptides, and serve as biosynthetic skin substitutes. [42] The collagen component allows adhesion to fibrin on the clean wound surface and contributes to pain reduction, while the silicone outer layer allows some water loss to promote adequate moisture and induce healing.[42]

Demling and DeSanti compare the efficacy of topical antibiotic management with bacitracin versus TransCyte™, a commercially available biosynthetic silicon-coated dressing (on a nylon mesh coated with porcine collagen and newborn human fibroblast cells) [43], for the treatment of mid-partial thickness burns of the face.[44] The results indicate a significant decrease in the daily care time**,** pain between and during wound care (VAS, assessed pain from 0-10, with 0 being the lowest), and healing time (time to re-epithelization) favoring the skin substitute group (**Table 1.6**).[45] However, despite satisfactory results, the authors conclude that the complex design associated with the use of live cells in this product in addition to the high-cost production decreases availability and therefore the potential clinical translatability of this dressing.[46]

1.7 Hydrofiber dressings

Hydrofiber dressings are absorbent and biodegradable dressings prepared from sodium carboxymethyl cellulose specifically designed to treat moderate to heavily exudating wounds.[47,48] Similar to hydrocolloid dressings, hydrofiber dressings transform into a gel-like substance to create a moist microenvironment that promotes healing while limiting wound secretion and bacterial communication.[49] The advantages of these dressings include 1) highly absorbent material, 2) mechanical stability, and 3) ease of removal with saline irrigation, minimizing the pain and tissue damage during and after dressing changes. Muangman et al.,[50] underline the superior efficacy of hydrofiber

dressings coated with ionic silver (Aquacel Ag™) for the treatment of partial-thickness burns in outpatients as these dressings require less time for wound closure, reporting a difference in time of 3.7 days (95%CI [1.9-5.4]) (**Table 1.7**) when compared to SSD dressings. In addition, patients report less pain with hydrofiber dressings during dressing changes showing a reduction of pain scores at days 1, 3, and 7 post-treatment (pain scores are registered on a 10 point VAS, with 0 representing no pain) (**Table 1.8**). Treatment with hydrofiber dressings is more cost-efficient than SSD dressings (including both hospital and travel costs).[50] However, despite satisfactory results, this product remains expensive, and may be unavailable due to low demand.

1.8 Hydrogels as burn wound dressings

Hydrogels are hydrophilic, three-dimensional, polymeric networks, that swell upon exposure to aqueous environment. They are comprised of natural and/or synthetic materials and are well designed for the treatment of second-degree burns as they protect the burn from the outside environment, absorb excessive wound exudates, and exhibit mechanical properties similar to skin. Hydrogels, as well as the materials that comprise them, can be prepared through a variety of chemical and physical processes and are primarily characterized via mechanical properties, weight percent, adhesion, swelling, gelation, gel fraction, morphology, degradation and cytotoxicity. Furthermore, hydrogel burn wound dressings are prepared targeting specific properties beneficial to supporting

wound healing such as antimicrobial effects, drug delivery, and degradation of the dressing.

1.9 Hydrogel preparation

Physical crosslinking results in reversible, weak interactions between polymers to construct a three-dimensional polymeric network.[51–53] Preparation involves heating, cooling, or self-assembly at room temperature, pH stimulated crosslinking, cation/anion interactions, or hydrogen-bond interactions between aqueous polymer solutions.[51,54,55]Physically crosslinked hydrogels are prepared by mixing either one or multiple macromolecules interacting through non-covalent linkages such as **ionic interactions, hydrogen bonding, hydrophobic interactions, metal coordination,** and **molecular entanglements.** Such examples of physical crosslinking, previously mentioned, include calcium-alginate hydrogels, acrylamide or acrylic acid and 2-ureido-4[1*H*]-pyrimidinone motif, modifying acrylamide or acrylic monomers with n-alkyl groups, polyacrylamide-co-acrylic acid and carboxyl-Fe^{+}, and tropocollagen networks, respectively (**Figure 1.3A**).[56–60] Physical crosslinking may be reversed by an external stimuli such as temperature, pH, or mechanical stress.[51,61] In addition, the weak mechanical strength of physically crosslinked hydrogels and their disassembly upon external stimuli limit the applicability of these hydrogels as burn wound dressings.

Chemical crosslinking is the covalent conjugation of two or more macromers to form a three-dimensional network.[51,53] Chemical crosslinking is typically irreversible and primarily occurs through **condensation** or **addition** reactions.

Condensation reactions are defined as the conjugation between a nucleophile and an electrophile, resulting in one, larger macromolecule, with the loss of a smaller molecular weight side product (e.g., water). Specifically in hydrogels, the macromers contain multiple nucleophile and electrophile reactive groups in order to form an intertwined, polymeric network. Common nucleophiles in hydrogel condensation reactions include amines, hydroxyls, and thiols, while electrophiles include activated esters, aldehydes, nitrenes, epoxides, and alkyl halides. Common condensation reactions for hydrogel assembly are **esterification** via carboxylic acid-hydroxyl reactive groups**, amidation** via N-hydroxysuccinimide-amine reactive groups**,** and **enzymatic crosslinking** via gamma-carboxamide-epsilon amino reactive groups (**Figure 1.3B**).[51,61,62] From these condensation reactions, enzymatic crosslinking using transglutaminase (TG) as a common catalyst has become an emerging method for preparing hydrogels due to its biocompatibility, mild reaction conditions, and capability to react *in situ*.[51,63,64,65,66]

Addition reactions chemically conjugate two molecules together to form one, larger molecule. Similar to condensation reactions, a hydrogel network prepared through addition reactions require multiple reactive groups per each

nucleophile and electrophile. Common nucleophiles of hydrogel addition reactions include hydroxyls, amines, thiols, enolate ions, organometallics, and cyanides. Corresponding hydrogel electrophiles include nitriles, carbonyls, and alkenes. For example, hydrogels assembled through addition reaction typically utilize **nucleophilic addition** via Michael-type reactions such as thiol-ene reactive groups, **cycloaddition** via DBCO-azide reactive groups, and **free radical addition** via acrylate reactive groups.[51,54,56,61,62,67,68]

Condensation and addition reaction methods have been widely used to develop polysaccharide, poly(ethylene glycol), poly(vinyl alcohol), and protein-based hydrogel burn wound dressings. However, the tunability of condensation and addition crosslinked hydrogel networks is limited by reactive group kinetics, pH, and temperature.[69,70]

1.10 Hydrogel characterization

Hydrogel characteristics must be assessed to appropriately tune them for their application. Physical and chemical characterization can be obtained through methods such as kinetic gelation studies, mechanical properties, adhesion, swelling, among others.

Mechanical properties

After preparing the hydrogel, rheological measurements are taken to determine the viscoelastic properties of hydrogels via strain sweep, to determine the linear viscoelastic region, and frequency sweep, to determine the storage

moduli and loss moduli overtime after swelling. Another method of characterizing mechanical properties of hydrogels utilizes Young's modulus (*E*). Young's modulus defines the stiffness of a material via compression or tension tests. *E* is measured as the slope of the linear portion of the resulting stress-strain curve. Hydrogels must maintain mechanical properties on the same order as tissue and structural integrity stable for the duration of the dressing's usage.

Weight percentage

The mechanical properties of hydrogels can be tuned by weight percent of the hydrogel. Hydrogels weight percent determines the amount of material in the polymer using the following equation:

$$wt\% = \frac{W_{materials}}{W_{gel}} x100$$

where $W_{materials}$ is the total weight of polymer used divided by the total weight of the hydrogel (W_{gel}). A higher weight percent hydrogel exhibits stiffer mechanical properties than a lower weight percent. This allows for the tunability of hydrogels to mimic the stiffness of the tissue.

Adhesion

Peel, lapshear, and torsion tests assess the adhesive properties of hydrogels on a particular surface, in the case of second-degree burns adhesion is measured on skin, utilizing an Instron mechanical testing load frame. A hydrogel is prepared between two pieces of skin, and the skin is pulled at a 90^{o} or 180^{o} angle for a peel test, or in opposite directions for a lapshear test. The force (N) required to pull the pieces of skin apart is measured. Torsion tests

involve dressing a hydrogel on tissue and applying torsional strain to assess, qualitatively, how well the hydrogel adheres to tissue.

Swelling

Due to the hydrophilic nature of hydrogels, they swell in aqueous environments. Swelling is typically reported as a percentage increase in weight calculated from the following equation:

$$Swell\ \% = \frac{mf}{mi} x100$$

where m_i = the initial mass of the hydrogel before swelling in solution, and m_f = the final mass of the hydrogel at a particular timepoint after swelling in solution. Swelling is an important characteristic for burn wound dressings in order to absorb wound exudate, an aqueous inflammatory response containing electrolytes, proteins, enzymes, and waste products among other biological molecules.

Gelation

Gelation time is defined as the time it takes for a hydrogel solution to solidify. Gelation can be measured quantitatively on the rheometer via a time sweep, qualitatively by the inverted test tube method or assessed quantitatively via Nuclear Magnetic Resonance by following peak shifts of the crosslinking reactive groups within the hydrogel.

Gel fraction

Gel fraction measures the amount of material that reacts to form a gel. Gel fraction can be calculated using the following equation:

$$Gel\ fraction = \frac{mf}{mi}$$

where m_f = the mass of the dry hydrogel after swelling in water for 24-48 hours, and m_i = the mass of the dry hydrogel before swelling in water for 24-48h.

Scanning electron microscopy (SEM)

Scanning electron microscopy (SEM) is a characterization technique used to visualize the internal structure of a hydrogel including pore shape and size.

Hydrogel degradation

In burn wound dressings, hydrogel degradation minimizes mechanical debridement during dressing changes. Degradation is achieved by synthesizing hydrogel components containing internal, cleavable linkages such as esters, thioesters, glycosidic linkages, phosphodiesters, nitrobenzyl linkages, sulfonamide linkages, or nitrosamine linkages, among others.

Cytotoxicity

High cell viability is vital to designing an ideal burn wound dressing. Cytotoxicity should be assessed against NIH3T3 fibroblasts, as this cell line is required for safety testing of a medical device, as outlined by the 10993 FDA regulatory documents. Intact hydrogels, the starting materials, and, where applicable, the degradation components should be assessed for cytotoxicity prior to applying these hydrogels *in vivo*.

1.11 Pre-clinical hydrogels with antimicrobial properties

Antimicrobial impregnated hydrogels aim to minimize burn wound bacterial

infection through three main modes: 1) utilizing antimicrobial chitosan polymers in the hydrogel backbone, 2) loading hydrogels with antibiotics, or 3) locally delivering silver nanoparticles (AgNPs), among other antimicrobial agents, directly to the burn wound dressing.

Chitosan-based hydrogels are widely used due to their antimicrobial activity. Chitosan's innately antimicrobial activity comes from its ability to bind the negatively charged bacterial cell wall causing disruption of the membrane and ultimately increasing permeability that culminates with the bacterial cell wall destruction.[71] Subsequently, chitosan aggregates with DNA, inhibiting replication of the bacterial genetic material resulting in apoptosis of the cell.[71] Specifically, Dang et al. prepare chitosan-curcumin copolymer hydrogels (nCur-CP) and determine the bacterial zone of inhibition (ZOI), the area around the treatment where growth is inhibited. Specifically, nCur-CP hydrogel shows significant antimicrobial effects via an increased ZOI against *E. coli*, *E. typhimurium*, *P. aeruginosa*, and *S. aureus* relative to curcumin treatment alone (**Table 1.8**).[72] Additionally, nCur-CP hydrogel copolymers exhibit similar antimicrobial effects to the commercially available antibiotic, chloramphenicol.[72] Similarly, gentamicin-, an aminoglycoside antibiotic, loaded chitosan hydrogels (CS-GT) act as antimicrobial burn wound dressings against *S. aureus* and *S. aeruginosa*. The CS-GT hydrogel promotes skin repair after a scalding burn and significantly increases the ZOI against *S. aureus* and *P. aeruginosa* ($p<0.05$) compared to chitosan and gentamicin alone after 24h of treatment at 37ºC (**Table 1.8**).[73]

A chitosan-PVA hydrogel loaded with antimicrobial silver nanoparticles (AgNPs) significantly decreases bacterial growth of *S. aureus* and *E. coli* as compared to a chitosan-PVA dressing without AgNPs based on ZOI according to Rinehart et al. (**Table 1.8**).[74] The hydrogel is composed of 15% chitosan and 85% PVA hydrogel loaded with 5mM silver nanoparticles. The low ZOI of the chitosan-PVA hydrogel alone suggests that chitosan and PVA have minimal antimicrobial activity against *S. aureus* and *E. coli*.

Jackson et al. utilizes a similar approach using PVA-based hydrogels with silver nanoparticles (PVA-AgNP). PVA-AgNP hydrogels are applied to burn wound dressings post-hydrogel preparation (**Table 1.8**). The resulting PVA-AgNP hydrogel significantly inhibits bacterial growth compared to PVA hydrogels alone (**Table 8**).[75].

Likewise, Boonkaew et al. report an Ag-NP loaded hydrogel prepared via UV-irradiation from 2-acrylamido-2-methylpropane sulfonic acid sodium salt (AMPS) and *N-N'*-methylenebisacrilamide (MBA) (AMPS-MBA). AgNP loaded AMPS-MBA hydrogels exhibit microbial inoculum below the detection limit after 24h against *S. aureus,* MRSA, and *P. aeruginosa* (>6.01 ±0.00, 6.28 ± 0.00, and 7.26 ± 0.00 (log reduction), respectively) relative to commercially available Acticoat™. However, AgNP loaded AMPS-MBA hydrogels show bacterial growth inhibition at 3 hours, whereas Acticoat inhibits bacterial growth within 30 minutes.[76]

Kim et al. describes an injectable methylcellulose (MC) hydrogel

containing silver nanoparticles (MC/AgNP) as an antimicrobial burn wound dressing. MC/AgNP hydrogels are prepared through sol-gel transition induced by hydrophobic interactions via temperature increase. MC/AgNP hydrogels at both 0.5 wt% and 1.0 wt% AgNP concentration exhibit 99.9% antibacterial activity against *K. pneumoniae*, *E. coli*, and *S. aureus,* while MC hydrogels without silver nanoparticles demonstrate no bacterial growth inhibition under the same experimental conditions.[77] Kim et al. suggests that the antimicrobial properties of the MC/AgNP hydrogels are due to Ag^+ from the silver nanoparticles binding to, and penetrating bacteria cell walls, disrupting their structural integrity, increasing permeability and ultimately resulting in bacteria cell destruction.[77]

1.12 Pre-clinical hydrogel-drug delivery systems

Drug delivery via hydrogel loading remains a challenge due to the large pore size of the hydrogel resulting fast, initial drug release, described as a burst release. Johnson et al. reports an ibuprofen-encapsulated hydrogel as a burn wound dressing, prepared via pressurized gas to expand liquid-processed alginate hydrogel scaffolds (PGX technique). PGX hydrogel preparation loads up to 8 wt% ibuprofen as compared to 0.0 ± 0.7 wt% in hydrogels without PGX technique.[78] This ibuprofen-loaded alginate hydrogel reduces discoloration and scabbing/hardness at day 3 and accelerates overall burn wound healing as early as day 14, while untreated burn wounds and those treated with alginate hydrogels alone do not heal until day 28. The reduction in the wound healing time

is attributed to ibuprofen's anti-inflammatory properties.[78] Additionally, it is proposed that healthy granulation tissue growth is promoted by an ion exchange between calcium and sodium ions in the alginate dressing and the wound, respectively, ultimately stimulating mitosis.[78]

Zheng et al. describes a histatin-1(His-1)-loaded gelatin hydrogel crosslinked *in situ* with acrylic acid-modified cyclodextrin, coupled with loading resveratrol (Res) to promote vascularization, reduce inflammation, and act as an antioxidant to eliminate reactive oxygen species in burn wounds.[64] Anti-inflammatory and pro-angiogenic properties of the Res/His-1/gel were analyzed via inflammatory cytokines. *In vitro,* the Res/His-1/gel increases angiogenesis and primary human umbilical vein endothelial cell (HUVEC) migration after incubation for 5 and 10h. *In vivo,* second-degree burn wounds treated with the Res/His-1/gel exhibit replacement of granulation tissue with healthy epidermis by day 7, as compared to no present epidermis at day 7 in the control groups.[64] Additionally, skin appendages and sebaceous glands develop in the Res/His-1/gel group by day 14, but do not form in control groups.[64] The Res/His-1/gel not only exhibits promising anti-inflammatory properties but it also promotes angiogenesis both *in vitro* and *in vivo*.

Similarly, Wang et al. deliver biocompatible Res- and plasmid DNA (pDNA) encoding vascular endothelial growth factor (VEGF) via hydrogels to reduce inflammation and promote angiogenesis. The hydrogel is composed of hyaluronic acid (HA), dextran (Dex), and β-cyclodextran (β-CD) with alkene

functionalized reactive groups that crosslink via UV-irradiation. Polyethyleneimine-conjugated pDNA and Res is encapsulated into the hydrogel scaffold and accelerates burn wound healing in an *in vivo* rat model via inhibition of inflammation and by promoting microvascular formation. Healing rates of burn wounds treated with the hydrogel alone, a Res-loaded hydrogel and the Res/pDNA-loaded hydrogel all significantly increase by days 14 and 21, with the fastest wound closure time observed in the Res/pDNA-loaded hydrogel treatment group compared to the no treatment group at 15.6 ± 1.3 % wound area and 29.6 ± 2.3% wound area, $p<0.01$, respectively.[79] The Res/pDNA-loaded hydrogel exhibits promising burn wound healing properties including inhibition of the inflammatory cascade as well as angiogenesis.

Samadi et al. utilized a chitosan/PVA hydrogel film loaded with AgNPs, for antimicrobial treatment, and sildenafil citrate (SC) for its pro-angiogenesis properties. Hydrogels are loaded with SC via swelling in a 5% aqueous SC solution, and burns are treated immediately after swelling. *In vivo* burn wounds are treated with SC/AgNP-hydrogel, AgNP-hydrogel, and SC-hydrogel, and healing is assessed by time and appearance. The SC/AgNP-hydrogel group exhibits complete skin epithelial remodeling by day 14, while scarabs remain on wounds in both the AgNP-hydrogel and SC-hydrogel treatment groups at day 14. Additionally, the SC/AgNP-hydrogel group shows fewer inflammatory cells than the other treatment groups. Further, silver staining is performed to evaluate the presence of type III collagen, an indicator for scarless wounds. Increases in

collagen type III are detected at day 4 in burns treated with SC/AgNP-hydrogels as compared to minimal collagen type III detected in the AgNP-hydrogel and SC-hydrogel groups.[80] Additionally, increased angiogenesis is reported in the SC-AgNP-hydrogel group as compared to the AgNP-hydrogel and SC-hydrogel groups. Overall, the SC/AgNP—hydrogel treatment group outperforms the controls with regards to *in vivo* accelerated epithelialization, and tissue regeneration.

Although these drug-loaded hydrogels show promise as novel burn wound dressings, rigorous preclinical validation of efficacy needs to be conducted to determine the optimal formulations that will ensure and promote wound healing in the clinical setting.

1.13 Pre-clinical dissolvable hydrogels

Dissolvable hydrogels are advantageous burn wound dressings because they minimize the mechanical debridement that occurs during a dressing change and therefore protect the newly formed granulation tissue. These hydrogels disassemble upon exposure to an external stimulus. Ghobril et al., describes a first-of-its-kind dissolvable hydrogel via thiol-thioester exchange between the terminal thiol on a cysteine methyl ester (CME) solution and the internal thioester linkage within the hydrogel network. Thiol-thioester exchange reaction with CME occurs at physiological relevant pH (7.4) and exhibits increased reaction kinetics at basic pH. Dissolution time may be controlled through CME concentration,

where an increased concentration of CME from 0.3M to 0.5M at pH 7.4 decreases the dissolution time from 1 hour to 36 minutes, respectively.[51,62,81] Hydrogels with the same structure, but lacking a thioester functional group do not exhibit dissolution, confirming the role of thiol-thioester exchange in the dissolution mechanism.

Similarly, Lu et al. prepare a dissolvable hydrogel as a burn wound dressing containing a polyethyleneimine (PEI) backbone with selenide reactive end groups. Crosslinking in this system occurs via formation of intra- and inter-diselenide bridges upon exposure to air. Diselenide hydrogels dissolution occurs via two mechanisms, 1) an oxidation reaction upon exposure to excess 3 wt% H_2O_2 solution for 15 minutes or 2) a reduction reaction using dithiothreitol (DTT).[82] Diselenide hydrogels applied to *ex vivo* porcine tissue and subsequently exposed to H_2O_2-soaked gauze dissolve after 30 minutes. Dissolution of diselenide hydrogels is a promising burn wound dressing property as it minimizes the need for the painful, mechanical debridement that damages new tissue growth.[82]

Incorporating drug delivery or antimicrobial properties within these dissolvable dressings may allow for accelerated wound healing and improved infection rates in burn patients.

1.14 Conclusions

This review provides an overview on current practices and novel

developments in the field of second-degree burn wound dressings. Specifically, it summarizes ways in which second-degree burn wounds can be treated and managed using polymeric hydrogels as dressings, as well as key characteristics and evaluations utilized for their optimization. Optimal burn wound dressings should: 1) adhere to tissue without mechanical debridement, 2) possess antimicrobial activity, and 3) decrease wound healing time. Though encapsulation of anti-inflammatory, pro-angiogenic, and antibiotic drugs into hydrogels there appears a promising solution to promote rapid wound healing, future studies are still necessary to evaluate and improve sustained and efficient drug release in an attempt to reduce the need for frequent dressing changes. In conclusion, hydrogels offer a novel approach for the treatment of second-degree burn wounds. Hydrogel dressings are biocompatible, can be easily manipulated and removed, and are highly tunable to incorporate biologically active molecules that improve wound healing.

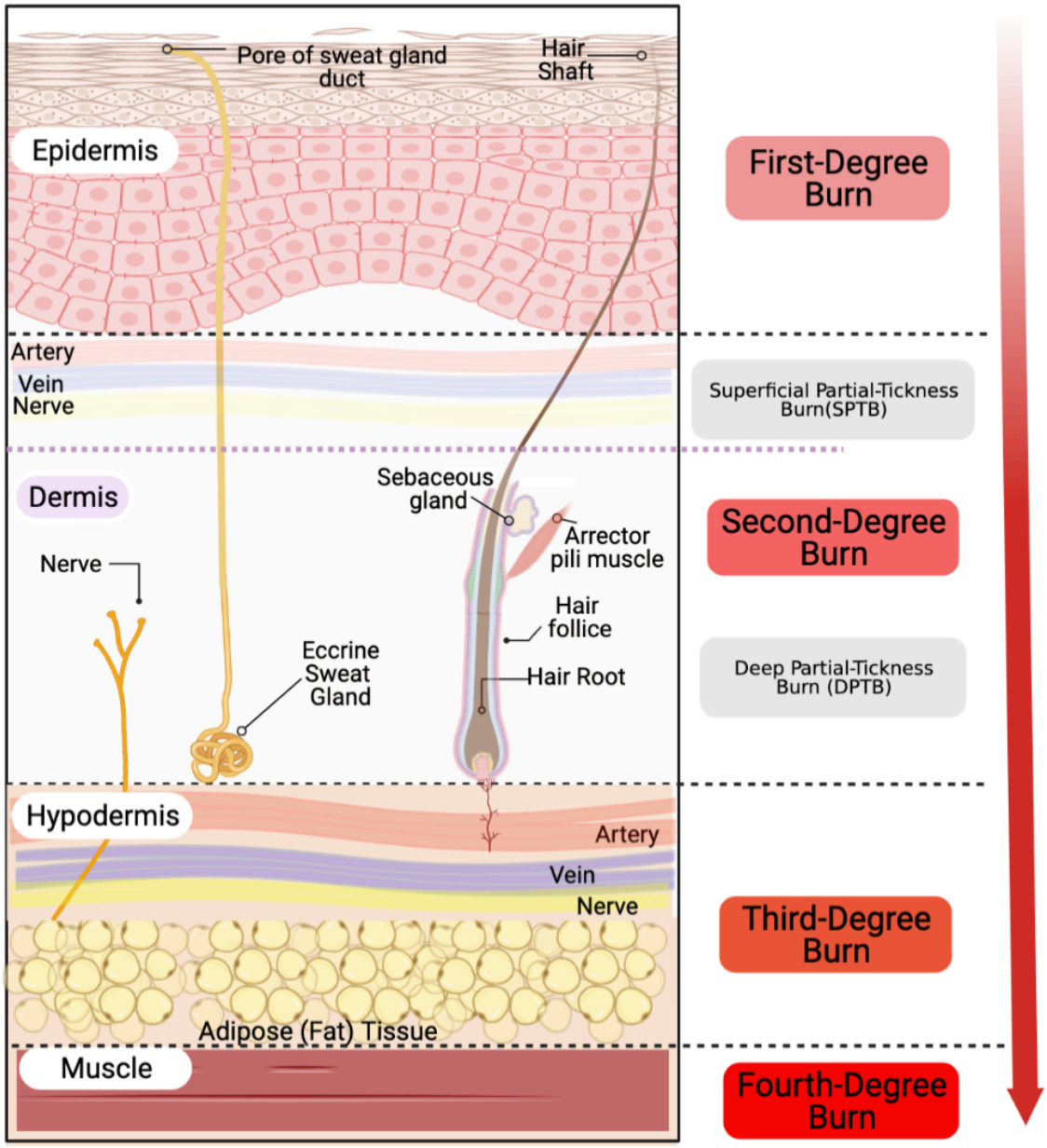

Figure 1.1. Anatomy and classification of burn wound depth.

Figure 1.2. Clinical examples of burn degrees and their associated nomenclature.

A) First Degree burn, commonly referred as “sunburn”. B) Second Degree-Superficial Partial-Thickness Burn (SPTB). C) Second Degree-Deep Partial-Thickness Burn (DPTB). D) Third Degree burn with eschar formation. E) Fourth Degree burn affecting tendons from the hand.

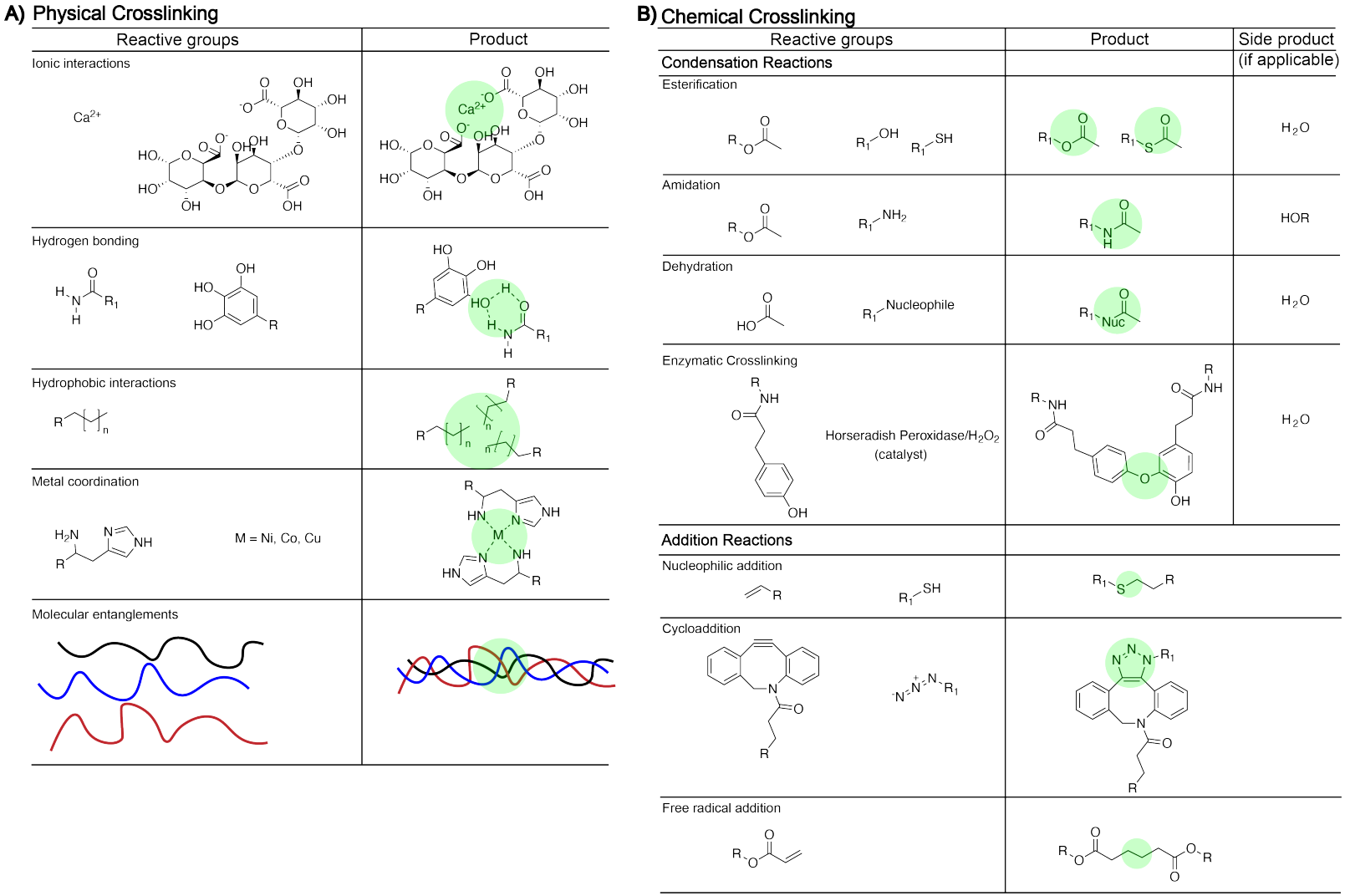

Figure 1.3. Hydrogel crosslinks, highlighted in green, representing A) physical crosslinking examples, B) chemical crosslinking examples

	First Degree	*Second-Degree*		*Third-Degree*	*Fourth-Degree*
Depth of burn	Epidermis (Superficial)	**SPTB** Epidermis and upper 1/3 dermis	**DPTB** Epidermis and dermis, affecting appendages	Full thickness (including subcutaneous fat)	Extends into muscle, tendons and/or bone
Most common causes	Sunburn (Prolonged UV exposure)	Brief contact with hot liquids, chemicals, flames or electric discharge (such as lightning)		Exposure to hot liquids, chemicals, flames or electric discharge	Prolonged time in direct contact with hot liquids, chemicals, flames or electric discharge
Appearance	Dry burns with erythema and desquamation Absence of blisters Blanch with pressure	Wet/weeping burns with erythema Blisters present Blanch with pressure	Moist burns with erythema and a red-waxy white appearance Blisters present easily unroof Delayed blanch when pressure is applied	Waxy white to dark -leathery dry and inelastic burns Do not blanch with pressure	White or black burns Do not blanch with pressure
Sensation	Painful	Extremely painful	Painful only with pressure	Painless unless deep pressure is applied	
Healing time	3-6 days	7-14 days	>21 days, usually require surgical treatment	Require surgical treatment to start healing	
Scarring	No scarring observed	No scarring, but skin dyspigmentation is expected	Hypertrophic and keloid scarring expected with or without skin contracture		Hypertrophic and keloid scarring with severe skin contracture

Table 1.1. Classification of Burn wound's depth. Second Degree-Superficial Partial-Thickness Burn **(SPTB)**. Second Degree-Deep Partial-Thickness Burn **(SPDB).**

	Advantages	*Disadvantages*	*Commercially available options*
Dressing pads	• Low cost • Antibacterial protection • Ideal for clean and dry wounds	• Requires frequent dressing change and tape to secure the pad • Changing dressing disrupts the wound bed and may be painful • Not for wounds with high exudates	Xeroform™, Bactigras™, Jenolet™
Antimicrobial dressings	• Low cost • Minimize bacterial colonization	• Cytotoxicity may cause would healing delay • Constant removal may result traumatic, disrupting the granulation tissue	Acticoat™, Aquacel ™
Hydrocolloid dressings	• Semi-permeable molecules swell with exudates and form a gel to protect against bacteria and moisture penetration • Can be easily detached • Ideal for areas of great friction	• Destruction of dressing results in unpleasant color and odor often confused with infection • Not capable of absorbing big amounts of exudate	Duoderm™, Comfeel™, Tegasorb™
Silicon coated nylon dressings	• Easy and atraumatic removal • Protect new tissue growth	• Not for wounds with high exudates • Sensitivity has been reported to silicone	Mepitel™, Biobrane™, TransCyte™
Hydrofiber dressings	• Moist microenvironment promotes healing	• High Cost • Destruction of dressing results in unpleasant color and odor often confused with infection	Durafiber ™, Opticell ™
Hydrogels	• Outer surface impermeable to bacteria and water • Transparent structure allows wound visualization without dressing removal • Flexible and easy to detach • Assists in autolytic debridement	• Low absorption capacity usually demands secondary dressing • Maceration can occur if exudate is abundant	Intrasite ™, Nu-gel™, Aquaform™

Table 1.2. Advantages and disadvantages of commercially available dressings to treat second-degree burns.

Trial	Follow up	Percentage of patients with Complete healing (RR)	Time to complete healing
Silverstein et al.[14]	21 days post burn or until full reepithelization	1.2 [95%CI, 0.95–1.53]	Mean days: 17 for SSD vs. 13 for foam dressing (p>0.05)
Tang et al. [12]	28 days post burn or until full reepithelization	1.0 [95%CI, 0.85–1.17]	Median days: 15 for SSD vs. 16 for foam dressing (p 0.74)
Yang et al.[13]	28 days post burn	1.0 [95% CI, 0.87–1.2]	Mean days: 25 ± 4 SD for SSD vs. 22 ± 3 SD (p<0.05)

Table 1.3. Results from Chaganti et al systematic review comparing traditional SSD with gauze and foam dressings for the treatment of second degree thermal burns.[7]

Information from Deutsch et al.[6], Oryan et al.[9] and Broussard and Powers [84].

Trial	*Follow up*	*Percentage of patients with Complete healing (RR)*	*Time to complete healing*
Silverstein et al.[33]	21 days post burn or until full reepithelization	1.2 [95%CI, 0.95–1.53]	Mean days: 17 for SSD vs. 13 for foam dressing (p>0.05)
Tang et al.[31]	28 days post burn or until full reepithelization	1.0 [95%CI, 0.85–1.17]	Median days: 15 for SSD vs. 16 for foam dressing (p 0.74)
Yang et al.[32]	28 days post burn	1.0 [95% CI, 0.87–1.2]	Mean days: 25 ± 4 SD for SSD vs. 22 ± 3 SD (p<0.05)

Table 1.4. Results from Chaganti et al systematic review comparing traditional SSD with gauze and foam dressings for the treatment of second degree thermal burns. [11]

Dressing	*Participants*	*Investigators*
Hydrocolloid	9.04	9.31
Chlorhexidine impregnated paraffin gauze	6.86	6.9
P value	p <0.02	p=0.05

Table 1.5. Satisfaction levels from Wright et al study comparing hydrocolloids to clorhexidine impregnated paraffin gauze

*Data reported using a 10 item VAS.[40]

Mean ± S.D.	**Face care (h/day)**	**Pain scale wound care**		**Healing time (days)**
		During	**Between**	
Topical agents	2.2±0.4	5 ± 1	3±2	12±3
TransCyte™ skin substitute	0.4±0.01*	2±1*	1±0.5*	8±1

Table 1.6. Comparison between Opsite™ and Jenolet™ according to Poulsen et al.[38]

Dressing	***AquacelAg ™***	***SSD***	***P value***
Time to wound closure (days)	10±3	13.7±4.3	p<0.02
Pain scores			
Day 1	4.1±2.1	6.1±2.3	P<0.02
Day 3	2.1±1.8	5.2±2.1	
Day 7	0.9±1.4	2.2±1.9	
Total cost US$	52 ± 2	93 ± 36	P<0.01

Table 1.7. Comparison between AquacelAg™ and SSD acoording to Muangman et al.[50]

Hydrogel formulation	*P. aeruginosa*	*S. aureus*	*E. coli*	*S. typhi*
nCur-CP	27 ± 1.2mm	27 ± 0.5mm	24 ± 0.3mm	20 ± 0.5mm
Curcumin	11 ± 0.5mm	20 ± 1.0mm	14 ± 0.3mm	9 ± 0.2mm
Chitosan	7.0 ± 1.0 mm	7.0 ± 1.0 mm	N/A	N/A
Gentamicin	21.3 ± 0.6 mm	17.7 ± 1.2 mm	N/A	N/A
CS-GT hydrogel	20.3 ± 1.0 mm	20.0 ± 1.0 mm	N/A	N/A
Chitosan-PVA hydrogel + AgNPs	N/A	10.2 ± 1.0 mm	9.7 ± 1.3 mm	N/A
Chitosan-PVA hydrogel	N/A	1.0 ± 0.5 mm	0.8 ± 0.6 mm	N/A
PVA-AgNP (4h)	1.00×10^0	1.00×10^3	1.00×10^0	N/A
PVA-AgNP (48h)	1.00×10^2	1.00×10^4	1.00×10^2	N/A
10% PVA gel (4h)	3.73×10^7	3.73×10^7	3.73×10^7	N/A
10% PVA gel (48h)	3.73×10^7	3.73×10^7	3.73×10^7	N/A
PVA powder (4h)	3.73×10^7	3.73×10^7	3.73×10^7	N/A
PVA powder (48h)	3.73×10^7	3.73×10^7	3.73×10^7	N/A

Table 1.8. Comparison between AquacelAg™ and SSD acoording to Muangman et al.[48]

CHAPTER 2. *In situ* gelling and dissolvable hydrogels for use as on-demand wound dressings for burns

2.1 Introduction

According to the world health organization, approximately 11 million people require medical attention due to burns each year.[78] In low-income countries, burns cause nearly 200,000 deaths annually.[78] Within higher income countries, such as the United States, there are approximately 2 million fires, with 1.2 million people sustaining burn injuries.[79] Death rates are as high as 75% for patients with burn wounds on 40% or more of their body surface area due to infection, dehydration, and pain.[79] The greater the surface area of burns, the more serious the burn, such that a burn covering 15% or more of the total body surface area (TBSA) in adults requires hospitalization while only a 10% TBSA necessitates hospitalization in children.[78,80–86] Even when patients survive and recover from their injuries, many burn survivors must manage life-long disabilities and psychological trauma due to burns.[79,81,82,87] A second degree burn results in damage to both the epidermis and dermis layers of tissue, and is a challenging wound to manage due to inflammation, fluid loss, tissue damage, and loss of barrier function by the tissue.[88,89] Today, treatments for second degree burn wounds include antibiotics, fluid replacement, debridement (if necrotic), and dressings.[47,86,90] Wound healing is an evolving process that takes place over days to months depending on the size and severity of the burn, and dressings can be applied and replaced as many as 1-2 times per

day in order to contain and remove the discharge of wound exudate.[84] These dressing changes require significant time (57 ± 34 min) and multiple personnel.[80] In addition to lengthy dressing changes, the act of dressing replacement often requires mechanical debridement and cutting, which traumatizes new tissue, affords longer healing times, and causes pain.[79–82,84,85,87,91–93] In fact, the pain can be severe enough to require anesthesia.[80,81,94]

To address the unmet need for alternative and facile methods to replace a dressing for the management of second degree burns, we recently introduced the concept of a dissolvable hydrogel or dressing.[95] Hydrogels are three-dimensional, hydrophilic networks used for a variety of biomedical applications such as tissue engineering, drug delivery and wound management.[58,60,76,82,96–101] The two-part hydrogel dressing, described herein, forms *in situ* when mixed and applied to the wound as an aqueous solution or spray. Once applied, this dressing adheres and protects the tissue. To remove the dressing, an aqueous cysteine methyl ester (CME) solution is applied which selectively cleaves the internal covalent thioester linkages within the dressing. With a mindset towards translation, we report the synthesis of a small library of hydrogels, their physical and mechanical properties, and performance of an optimized hydrogel dressing in a large animal, second degree burn, pig model. Specifically, a poly(ethyleneimine) (PEI) crosslinks with a NHS activated poly(ethylene glycol) (PEG) containing internal thioester linkages to form an amide-crosslinked linked hydrogel (Figure 2.1). The hydrogel dressing is applied via a syringe to the wound and removed by dissolution utilizing thiol-

thioester exchange chemistry upon exposure to CME solution.

2.2 Synthesis of hydrogel burn dressing

Current burn dressings include gauze dressings, hydrocolloid dressings, silver-impregnated dressings, and hydrogel dressings.[85,102] With regards to wound dressing design and composition, our work focuses on developing hydrogel-based dressings. Hydrogels are ideal burn wound dressing materials as they protect the wound from the outside environment, absorb wound exudates, and possess mechanical properties and elasticity on the same order as that of epithelial tissue.[93,95,102–108] Specifically, we are investigating synthetic hydrogel dressings that form *in situ* via an SN2 reaction between an amine terminated, branched poly(ethyleneimine) (PEI) and a difunctionalized, NHS activated poly(ethylene glycol) (PEG) crosslinker (Figure 2.1). Unique to the dressing design is an internal thioester linkage within the crosslinker which, in the presence of a cysteine methyl ester (CME), undergoes a thiol-thioester exchange to cleave the crosslinker and dissolve the dressing (Scheme 2.1). Herein, we vary the length of methylenes in the crosslinker from 1 to 5 to 10 in order to tune the physical and mechanical properties of the hydrogels, and to identify a hydrogel dressing formulation suitable for evaluation in a large animal porcine second degree burn model.

We synthesized crosslinkers **5-7** starting from PEG (M_w 3000) as shown in Scheme 2.2. Crosslinker **5** was previously synthesized and we adapted this procedure with minor modifications.[61] Briefly, we reacted the starting PEG (M_w

3000) with the appropriate anhydride to form the PEG diacid and subsequently activated it with an NHS ester to give the crosslinker **1**. **1** was reacted with DBU, and the respective thiol-terminal carboxylic acids of 1, 5, and 10 methylenes, to afford intermediates **2**, **3**, and **4**, respectively. Next, we prepared the NHS-activated crosslinkers via DCC coupling chemistry with NHS and purified the products by precipitation in diethyl ether. The yields were high (85-98%) for all the reactions. We characterized and confirmed the structure of the crosslinkers by ^{1}H NMR, ^{13}C NMR, GPC, MALDI and DSC, and the data is provided in section 2.12 and figures 20.22-20.30.

2.3 Hydrogel preparation

Next, we prepared a small library of 10, 15, and 20 wt% hydrogels by mixed the crosslinker, dissolved in 0.1 M phosphate buffer pH 6.5, with branched polyethyleneimine (PEI; M_w 1800) in 0.3 M borate buffer, pH 8.5. However, we observed minimal solubility in buffer with crosslinker **7** due to the hydrophobicity of the methylene chains. In order to overcome the low solubility, we dissolved crosslinker **7** in 0.1 M phosphate buffer pH 6.5 with 50% ethanol prior to mixing it with the PEI solution. The ratio of NHS:NH_2 is 2:1 to ensure amidation of PEI and the crosslinker. We observed no major difference in hydrogel mechanical properties with a 2:1 or 1:1 NHS:NH_2 ratio (Fig 2.14). A transparent, solid hydrogel forms within 5 minutes for all compositions as determined by the inverted tube gelation test. Hydrogel gelation time positively correlates with increasing

hydrophobic chain lengths. The formulation for hydrogel with crosslinkers **5**, **6**, and **7** gel in less than 5 seconds, 90s, and 3-5 minutes, respectively (Figure 2.3A). Gelation time also positively correlates with weight percent, the higher the weight percent the longer the gelation time.

2.4 Morphology

Next, we characterized the morphology of the hydrogels using scanning electron microscopy (SEM). All of the hydrogels possess pore sizes varying from 5μm to 100μm with a honeycomb-like structure. Interestingly, hydrogel **7**, unlike all the other hydrogels, exhibits a more lamellar-like structure (**Figure 2.2**). Because of this observed secondary structure, we assessed the critical aggregation concentration (CAC) of crosslinker **7** using the pyrene assay. We observe a CAC of 0.050mM, a concentration below that of our hydrogel crosslinker concentration (0.053mM) indicating that we are forming a self-assembled structure within the hydrogel itself giving rise to the lamellar structure seen under SEM.

2.5 Reaction kinetics

From a chemical reactivity perspective, the terminal amines of the PEI may react with the terminal NHS ester or the internal thioesters to form an amide bond. Thus, we determined the preferential attack site for the amines via ^{1}H NMR. Specifically, we used N-butylamine, as a model of a primary terminal amine on PEI, and added it to an aqueous solution containing **6** and followed the amidation

reaction via ^{1}H NMR. We observe selective reactivity between PEI and the NHS ester on the crosslinkers, and not the internal thiolester (>99% at the NHS site over 20 minutes). Amidation at the NHS ester is confirmed via an upfield shift from the conjugated NHS ester at 2.82ppm to free NHS at 2.49ppm on crosslinker **6** (Fig 2.6) while the methylene peak at 2.6ppm for the thioester does not shift. The attack of the terminal amine to the NHS-ester occurs quickly, under 10 seconds, however in hydrogels this reaction is likely slower because once one of the amines attacks the NHS-ester, entanglement and solidification occurs with a resulting increase in steric hindrance. Hence the lengthier gelation times. Additionally, a competitive hydrolysis reaction occurs at the NHS ester. Hydrolysis of the NHS ester, however, is negligible at pH 6.5 over twenty minutes, a longer time than necessary to prepare the hydrogel (Fig 2.7). This selectivity of amidation at the NHS ester ensures that we retain the internal thioester linkage, allowing for dissolution through CME.

2.6 Rheological measurements and hydrolysis

With regards to mechanical properties, we perform strain and frequency sweeps at various time points before and after swelling in 50mM PBS. First, we defined the linear viscoelastic region as the linear portion of the storage modulus from the strain sweep (Fig 2.9). We performed a frequency sweep on all hydrogels with 3% strain from 1 to 10 Hz. These hydrogels exhibit viscoelastic, solid-like behavior, storage modulus (G') > loss modulus (G").[109,110]

Over 30 days of swelling, we observe the lowest storage modulus with

hydrogel **5**, sustaining a G' of below 10kPa for the duration of time after swelling. Alternatively, the storage modulus of hydrogels composed of crosslinkers **6** and **7** are each larger, at a peak storage modulus of approximately 12kPa and 20kPa, respectively, all at 15 wt%. (Figure 2.3B-C). We attribute this increase in storage modulus in each hydrogel to the hydrophobicity of methylenes, such that the longer the methylene chain length, the greater the hydrophobic interactions and a stronger hydrogel. This observation holds true for the weight percent dependence. The higher the weight percent, the greater the storage modulus.

To ensure that the presence of ethanol does not increase the storage modulus for hydrogels prepared with crosslinker **7**, we assessed the rheological measurements of hydrogels prepared with crosslinker **6** under the same conditions as those hydrogels used for crosslinker **7**. We observe no significant difference in storage modulus between hydrogels prepared with or without EtOH, indicating that the buffer conditions do not alter mechanical properties of our hydrogels (Fig 2.15).

During the 30 days of swelling, the hydrogels swell between 150-400% depending on weight percent and hydrophobicity of the hydrogel formulation (Figure 2.2D and 2.12). Swelling reaches equilibrium after 48 hours for all formulations. Hydrogels with crosslinker **7** swell the least, likely as a consequence of the hydrophobicity within the long methylene chain length, while hydrogels with crosslinker **5** swell the most.

All of the hydrogels undergo hydrolysis over 30 days of swelling as indicated by a loss of gross structure and a reduction in storage modulus overtime (Figure

2.2B,C). Hydrogel **5** exhibits an immediate loss in storage modulus and gross structure while hydrogels **6** and **7** increase in strength as they swell. However, we ultimately observe a reduction in storage modulus in hydrogels **6** and **7** by 30 days post swelling. We attribute this loss in structure and mechanical properties to hydrolysis of the crosslinker. To further characterize the hydrolysis, we measured the rate of crosslinker hydrolysis in 0.1M sodium bicarbonate buffer, pH 8.0, via ^{1}H NMR. We observe hydrolysis preferentially occurs at the thioester linkage with a rate of $k = 0.055\ min^{-1}$ and $k = 0.003\ min^{-1}$ for crosslinkers **5** and **6**, respectively (Fig 2.8) as opposed to the ester linkage between the glutaric acid and PEG on the crosslinker**. 7** is stable for over 7 days. We attribute the stability of the thioester linkage in crosslinker **7** to the hydrophobic methylene chain length protecting the adjacent thioester from hydrolysis. (Scheme 2.3)

2.7 Hydrogel dissolution

Aside from hydrolysis, the thioester facilitates hydrogel dissolution through thiol-thioester exchange in the presence of cysteine methyl ester (CME).[95] Upon exposure of the dressing to a 0.3M CME solution at pH 8.6, the thiol on the cysteine methyl ester attacks and displaces the internal thioester in the crosslinker. The amine on the now internal cysteine methyl ester subsequently rearranges to form an amide bond by replacing the thioester (Scheme 2.1). This amide bond prevents re-attack of the original, internal thiol (Schemes 2.1 and 2.3). This dissolution process fragments the hydrogel network, degrading the hydrogel over time. Thus,

we assessed the storage modulus of the hydrogel in a CME solution as a function of time at pH 8.6. Complete dissolution, as defined by G' < 300 Pa, occurs in less than 10 minutes to over 90 minutes depending on the hydrogel formulation and weight percent, with a higher weight percent and longer methylene chain length resulting in an increase in time to complete dissolution (Figure 2.4A). Specifically, at 15 wt%, hydrogel **5** dissolves within 10 minutes, while hydrogel **6** dissolves within 30 minutes and gel **7** dissolves within 80 minutes. This trend continues throughout all hydrogels regardless of weight percent. We accredit this slower dissolution of hydrogel **7** to the additional hydrophobic methylenes near the thioester decreasing the local hydrophilicity compared to **5** and **6**. Due to a competitive reaction at the thioester between hydrolysis of water and thiol-thioester exchange, we investigated the rate of dissolution using CME in sodium bicarbonate buffer pH 8.0 via ^{1}H NMR with crosslinker **6** (Scheme 2.3). We monitored the decrease in the methylene proton adjacent to the thioester and determined the thiol-thioester exchange rate to be k=0.084 min^{-1}. This rate is faster than that of hydrolysis and, therefore, indicates that thiol-thioester exchange is the preferred mode of dissolution under 0.3M CME solution conditions.

2.8 Adhesion testing

To investigate the applicability of our hydrogels as burn wound dressings, we assessed their adhesive properties against human skin. We performed a lap shear test to determine adhesion strength on *ex vivo* human breast and abdominal

tissue. All the hydrogels adhere similarly to tissue with values of approximately 0.5 N/cm^2 and display cohesive failure at the hydrogel-skin interface **(Figure 2.4B-C)**. Additionally, the hydrogel adheres similarly to burned skin as well as healthy skin. We attribute the adhesive strength to physical entanglement between the hydrogel and the human skin. The hydrogel, applied *in* situ as a liquid, allows for gelation to occur and take on the morphology of the human skin creating entanglement between the hydrogel and the skin. These hydrogels exhibit lower strength as compared to that of fibrin glue (0.6 ± 0.04 N/cm^2).[111] The hydrogels possess a favorable characteristic that enables their use on damaged soft tissues that are too weak for significant mechanical agitation or debridement.

2.9 Cytotoxicity

Prior to the *in vivo* studies, we assessed cytotoxicity using NIH3T3 fibroblasts. Hydrogels **6** and **7** show >85% viability while **5** shows very low viability due to the rapid release of glutaric acid and increase in local acidity from the dissolution (Fig 2.16).

2.10 *In vivo* porcine burn model

Based on the sum of these results, we selected hydrogel **6** for *in vivo* testing. Specifically, hydrogel **6** exhibits non-toxicity, storage modulus on the same order as that of human skin, maintenance of mechanical strength and structure over 7 days' time, adheres to skin, swelling, and dissolution in 30 minutes. For the *in vivo*

model, we induced second-degree burns on four pigs by heating a brass cylinder to 80°C and placing it on the back of the pig for 20 seconds. We assessed the treatment groups at days 7 and 14, with one or two dressing changes as depicted in Figure 2.5 to observe any differences in healing between groups. Specifically, we compared hydrogel **6** with commercially available gauze sponge dressing, Mepilex™, and xeroform. Triple antibiotic ointment was applied to each burn prior to dressing. Post-necropsy, tissue was dissected, and histopathology analysis was performed (Fig 20.17-20.21, Table 2.1-2.5).

Generally, all treatment groups show mild/moderate necrosis, epidermal ulceration, inflammation, and neovascularization. Hydrogel **6**, however, exhibits less necrosis, epidermal ulceration, and inflammation than other treatment groups, with similar neovascularization, and burn depth (mm) and epidermal dermal thickness (mm) to all treatment groups by day 14 (Figure **2.5C**). Additionally, all hydrogels show some re-epithelialization by day 14, with hydrogel **6** exhibiting complete re-epithelialization on two burns, and partial re-epithelialization on one (N = 3) after two dressing changes; the only dressing with more than one complete re-epithelialized burn. The only treatment groups with complete re-epithelialization on a burn include Hydrogel **6**, on day 14, with 1 dressing change, and sterile gauze dressing on day 14, with two dressing changes. While the differences between the groups are not statistically significant, ($P>0.05$), hydrogel **6** trends towards better performance over conventional gauze, Mepilex™, and xeroform dressings. The spray-on application and removal process of our hydrogels allows ease of

application during dressing and debridement removing the need for mechanical debridement and disruption of newly formed tissue.

2.11 Conclusions

We have synthesized and characterized a small library of dissolvable hydrogels for use as burn wound dressings. We have demonstrated tunable mechanical strength, dissolution, swelling, and adhesion of these hydrogels based on the hydrogel composition. Specifically, hydrogel **6**: 1) is stable for over 7 days, 2) can be applied *in situ* to a burn site, 3) adheres to the tissue, 4) exhibits strength on the same order as human skin, and 4) is dissolvable in under 30 minutes for atraumatic removal. This work highlights the tunability of hydrogels utilizing different methylene chain lengths within the NHS activated PEG crosslinker, the concept of *in situ* hydrogel formation and dissolution, and their successful application as burn wound dressings in a large animal model.

2.12 Materials and methods

Materials

NMR spectra were recorded on a Varian 500 MHz VNMRs instrument; chemical shifts are quoted in parts per million (ppm) calibrated to residual non-deuterated solvent. (^{1}H NMR: $CDCl_3$ at 7.26 ppm; ^{13}C NMR: $CDCl_3$ at 77.16 ppm). Coupling constants (*J*) are quoted in Hertz. Multiplicities are given as: singlet(s), doublet(d), triplet(t), quartet(q), multiplet(m) or broad(br). Gel permeation

chromatography (GPC) was used to determine molecular weight and polymeric distribution in tetrahydrofuran (THF) as the mobile phase with flow rate of 1.0 mL/min. GPC analyses were obtained using an OptiLab DSP Interferometric Refractometer (Wyatt Technology) fitted with two identical Jordi Gel DVB columns (Jordi Labs, 250 mm x 10 mm, 105 Å pore size). Matrix-assisted laser desorption/ionization (MALDI) mass spectra were recorded on a Bruker autoflex Speed MALDI-TOF spectrometer. Positive ion mass spectra were acquired in linear mode. Alpha-cyano-4-hydroxycinnamic acid solution in acetonitrile and water (3:1, 10 mg/mL) was used as a matrix. 8-12 mg of crosslinkers were mixed in 1 mL of 3:1 ACN:H_2O solution and 0.5 μL of the crosslinker matrix solution were each deposited on a MALDI plate layered as matrix:crosslinker:matrix solution. Differential scanning calorimetry (DSC) of crosslinkers were recorded on a DSC Q100 TA instrument.

All anhydrous solvents were purchased from Sigma Aldrich. All reagents were purchased from commercial sources and used without further purification. All reactions were carried out under argon with magnetic stirring. Polyethyleneimine, molecular weight 2000, was purchased from Polysciences, Inc.

Synthesis and characterization of compounds

PEG Diacid. The synthesis of the PEG diacid compound was based on a previously reported protocol.[14] ^{1}H and ^{13}C NMR spectra were similar to the literature.[14]

^{1}H NMR (500MHz), $CDCl_3$: δ 1.93 (q, *J* = 7.21 Hz, 4H), 2.4 (tt, *J* = 7.21, 8H), 3.62 (m, 292H), 4.22 (tt, *J* = 4.73 Hz, 4H) ppm; **^{13}C NMR (500 MHz), $CDCl_3$:** 175.3, 172.8, 70.6, 68.9, 63.4, 33.1, 32.6, 19.9 ppm.

Compound 1. The synthesis of the starting material was based on a previously reported protocol.[14] ^{1}H and ^{13}C NMR spectra were similar to the literature.[14]

^{1}H NMR (500MHz), $CDCl_3$: δ 4.15 (tt, *J* = 3.3, 1.5, 4H), 3.54 (m, 296H), 2.8 (b, 8H), 2.6 (t, *J* = 7.3, 4H), 2.4 (t, *J* = 7.3, 4H), 2.0 (q, *J* = 7.3, 4H) ppm; **^{13}C NMR (500 MHz), $CDCl_3$:** 172.3, 169.0, 168.0, 70.5, 69.0, 63.6, 32.4, 29.9, 25.5, 19.7 ppm

Compound 2. The synthesis of compound **2** was based off of a previously reported protocol.[13,16]

^{1}H NMR (500MHz), $CDCl_3$: δ 4.21 (m, *J* = 4.6, 4.9, 4H), 3.62 (m, 296H), 2.68 (t, *J* = 7.3, 4H), 2.40 (t, *J* = 7.2, 4H), 1.98 (t, *J* = 7.2, 4H) ppm; **^{13}C NMR (500 MHz), $CDCl_3$:** 196.8, 172.6, 169.8, 70.6, 69.0, 63.6, 42.3, 32.8, 31.0, 20.5 ppm;

Compound 3. In a flame dried flask, 1,8-Diazabicyclo(5.4.0)undec-7-ene (265μL) and 6-mercaptohexanoic acid (122μL) were added to a solution of **1** (1g) in anhydrous DMF (5mL). The solution was stirred at room temperature for 16 hours. The organic phase was extracted with a 1M HCl solution, water, and brine. The organic phase was dried over sodium sulfate, filtered, and precipitated in diethyl ether. The precipitate was filtered and dried under vacuum to afford compound **3** as a white solid (96% yield).

^{1}H NMR (500MHz), $CDCl_3$: δ 4.22 (t, *J* = 4.8, 4H), 3.63 (m, 308H), 2.86 (t, *J* = 7.2, 4H), 2.61 (t, *J* = 7.3, 4H), 2.38 (t, *J* = 7.4, 4H), 2.30 (t, *J* = 7.4, 4H), 1.97 (t, *J* =

7.3, 4H), 1.60 (m, 8H), 1.39 (m, 4H), ppm; **^{13}C NMR (500 MHz), $CDCl_3$:** 198.6, 176.1, 172.7, 70.7, 69.0, 42.8, 33.5, 32.9, 29.2, 28.5, 28.1, 24.2, 20.6 ppm;

Compound 4. Synthesis of compound 4 follows the above procedure using 11-mercaptoundecanoic acid (0.190g) as the thiol source (92% yield).

^{1}H NMR (500MHz), $CDCl_3$: δ 4.22 (t, *J* = 4.9, 4H), 2.85 (t, *J* = 7.4, 7.3, 4H), 2.60 (t, *J* = 7.3, 4H), 2.38 (t, *J* = 7.3, 4H), 2.30 (t, *J* = 7.5, 4H), 1.97 (t, *J* = 7.3, 4H), 1.60 (m, 8H), 1.39 (m, 24H) ppm; **^{13}C NMR (500 MHz), $CDCl_3$:** 198.7, 176.5, 172.7, 70.5, 69.0, 63.5, 33.8, 32.9, 29.4, 29.3, 29.2, 29.1, 29.0, 28.95, 28.8, 28.7, 24.7, 20.6 ppm;

Compound 5, 6 and 7. The synthesis of compounds 5, 6 and 7 are based off of a previously reported protocol (yield 96-98%).[13,16] The HNMR and CNMR spectra are similar to those previously reported.

Compound 5:

^{1}H NMR (500MHz), **$CDCl_3$:** δ 4.16 (t, *J* = 4.3, 4H), 3.92 (s, 4H), 3.57 (m, 257H), 2.78 (b, 8H), 2.67 (t, *J* = 7.3, 4H), 2.34 (t, *J* = 7.3, 4H), 1.95 (q, *J* = 7.3, 4H) ppm;

^{13}C NMR (500 MHz), $CDCl_3$: δ ppm;

MALDI-TOF (pos): M_w: 3763 m/z

GPC: M_n: 5077; **M_w:** 5312; **PDI:** 1.05;

Mp (DSC): 46.06°C

Compound 6:

^{1}H NMR (500MHz), $CDCl_3$: δ 4.21 (tt, *J* = 1.5, 3.4, 4H), 3.63 (m, 290H), 2.86 (t, *J* = 7.3, 4H), 2.81 (b, 8H), 2.60 (tt, *J* = 2.5, 4.9, 8H), 2.37 (t, *J* = 7.3, 4H), 1.96 (q, *J*

= 7.3, 7.4, 4H), 1.74 (q, *J* = 7.4, 7.7, 4H), 1.59 (m, 4H), 1.46 (m, 4H) ppm;

^{13}C NMR (500 MHz), $CDCl_3$: δ 198.6, 172.7, 169.1, 168.4, 70.5, 69.1, 63.6, 42.9, 33.0, 29.1, 28.4, 27.8, 25.6, 24.1, 20.6 ppm;

MALDI-TOF (pos): M_w: 3807 m/z

GPC: M_n: 4999; **M_w:** 5196; **PDI:** 1.04;

Mp (DSC): 45.80°C

Compound 7:

^{1}H NMR (500MHz), $CDCl_3$: δ 4.22 (m, 4H), 3.62 (m, 278H), 2.85 (m, 8H), 2.70 (t, *J* = 7.2, 7.3, 2H), 2.60 (tt, *J* = 7.3, 4H), 2.45 (t, *J* = 7.2, 7.4, 4H), 2.37 (t, *J* = 7.2, 7.3, 4H), 2.04 (q, *J* = 7.2, 7.4, 4H), 1.95 (m, 4H), 1.71 (m, 2H), 1.52 (m, 4H), 1.25 (m, 10H) ppm;

^{13}C NMR (500 MHz), $CDCl_3$: δ 198.8, 172.7, 169.2, 168.6, 70.5, 69.0, 63.5, 42.8, 32.9, 30.9, 29.5, 29.3, 29.2, 29.0, 28.8, 28.7, 25.6, 24.5, 20.6 ppm;

MALDI-TOF (pos): M_w: 4210 m/z

GPC: M_n: 6038; **M_w:** 6313; **PDI:** 1.05;

Mp (DSC): 47.42°C

Mechanical properties of hydrogels.

The rheological measurements were obtained from TA Instruments DHR-2 Rheometer. To prepare the hydrogels, PEI in borate buffer with pH adjusted to 8.5 with HCl was reacted with crosslinker **5**, **6**, or **7**, of 3400 MW (NHS-PEG-NHS) in phosphate buffer, pH 6.0. The ratio of amine to NHS was 1:15, and the concentration of the hydrogel was 10, 15, or 20 wt%. Crosslinker **5** formed a

hydrogel instantaneously in under 5 seconds, while crosslinkers **6** and **7** formed hydrogels in 3 to 5 minutes at room temperature. Hydrogels with 8mm width and 2.5mm height were prepared in a cylindrical, Teflon mold and analyzed after sitting in a humid chamber for 1 hour at room temperature, 25^{o}C. The frequency sweeps were measured between 0.1Hz and 10 Hz with an oscillatory strain percent of 3% and a temperature of 22^{o}C. An axial force of 0.15N was applied to the hydrogel using 8mm parallel plate geometry. The oscillatory strain sweeps were recorded at a frequency of 0.1Hz. Human abdominal skin and breast tissue was obtained from Massachusetts General Hospital IRB# 2015P001267. Data are expressed as mean $\pm$ standard deviation (n = 3).

The adhesion of hydrogels between two pieces of human breast tissue at 10, 15 and 20 wt% was determined using an Instron 5944 Micro-tester. Hydrogels were prepared as mentioned above and injected between two pieces of human breast tissue. Hydrogels were left to gel for 1 hour at room temperature. After one hour, a lap shear test following ASTM D3165 protocol adhesion of the hydrogels on human tissue. Tissue pieces were pulled apart at a rate of 5mm/min at room temperature until a break in adhesion was detected and recorded. Data are expressed as mean $\pm$ standard deviation (n = 3).

The kinetics of gelation for hydrogels at all weight percents was determined by the inverted tube test. Gels were formed in glass vials and gelation was determined when the gel no longer runs down the sides of the vial when inverted. Data are expressed as mean $\pm$ standard deviation (n = 3). At the beginning of the

experiment, solutions of crosslinkers and dendrons mixed together were liquid as gelation had just begun. The hydrogels became more viscoelastic and were solid at the end of the experiment.

Swelling ratio was determined by submerging and weighing the hydrogels in 3 mL of 100mM PBS at pH 7.4 over 30 days. At time 0h, 4h, 24h, 48h, 7d, and 30d, the hydrogel was weighed. Swelling ratio is the percentage that the hydrogel swells, determined by $Swelling\ ratio = \frac{final\ mass}{initial\ mass} X\ 100$. Final mass is the mass of the hydrogel at each time point after swelling. Initial mass is the mass of the hydrogel at time 0h.

The solvent system used for the hydrogel formation kinetics study was 0.5mL of $CDCl_3$. Crosslinker **6** was dissolved in this system. An initial ^1H NMR spectrum was taken and subsequently 2.0 eq of *N*-butylamine was added to the NMR tube and an additional ^1H NMR spectrum was taken. Hydrolysis kinetics systems used 0.5mL of D_2O and 10 mg Sodium bicarbonate, pH 8.0 as the solvent system. Crosslinkers **5** and **6** were each dissolved in the solvent system and ^1H NMR was used to follow hydrolysis overtime. The concentration vs time was plotted and a non-linear regression was fitted to the curve. The rate constant, k, was calculated using the first order rate law equation: $[A] = [A]_o e^{-kt}$.

In vivo porcine burn model

An established *in vivo* porcine burn model (CBSET study number TV00008, approved by IACUC project number I00319) was used to assess the healing of cutaneous burns when treated with 1) hydrogel **6** as compared to standard of care

dressings including 2) sterile gauze, 3) Mepilex™, and 4) Xeroform (N=3/treatment). Five female Yorkshire swine (69.0-74.5 kg) were burned at 80°C, for 20s with a 4 cm diameter, 2 kg brass cylinder. Triple antibiotic ointment was applied to each burn sites prior to dressing treatment. Dressing changes and euthanization were performed at the designated time points for each group according to Figure 5. Burn tissues were harvested and stained with H&E at 7 and 14 days post burn.

Necrosis and neovascularization scores were determined using the microscopic changes scoring matrix: 0 = no observable change; 1 = minimal – a nearly imperceptible feature/change, 2 = mild/moderate – an easily identifiable and/or notable feature/change in the tissue; 3 = marked/severe – prominent feature/change in the tissue. Scores were reported as mean ± standard deviation for each dressing in each group.

Individual histopathologic evaluation and hematoxalin & eosin staining are presented in Tables S1-S5 in SI. The Study Pathologist was blinded to the treatment matrix at the time of the pathologist read.

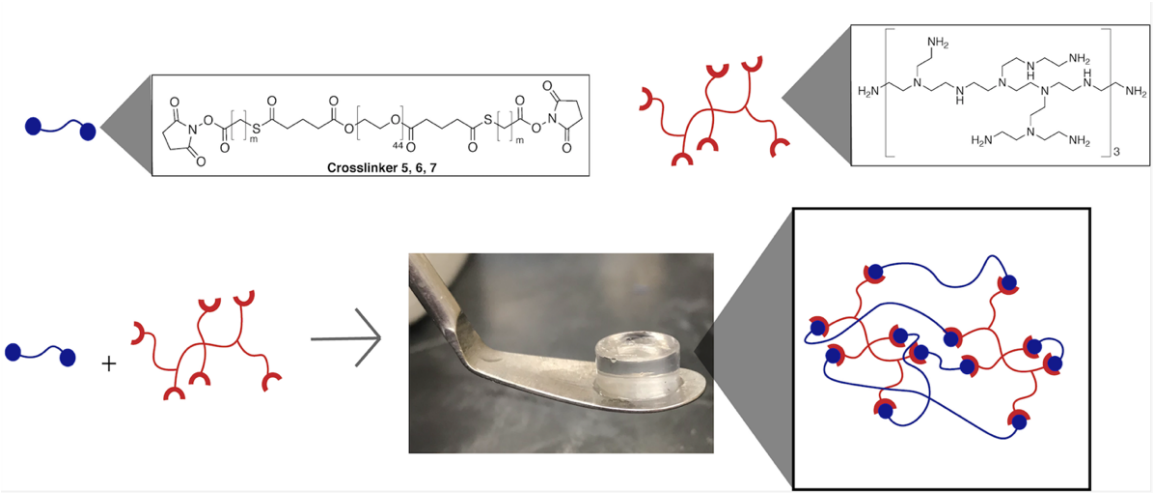

Figure 2.1. Preparation of a three-dimensional hydrogel via the reaction between a poly(ethyleneimine) (PEI) and a NHS activated poly(ethylene glycol) (PEG) crosslinker.

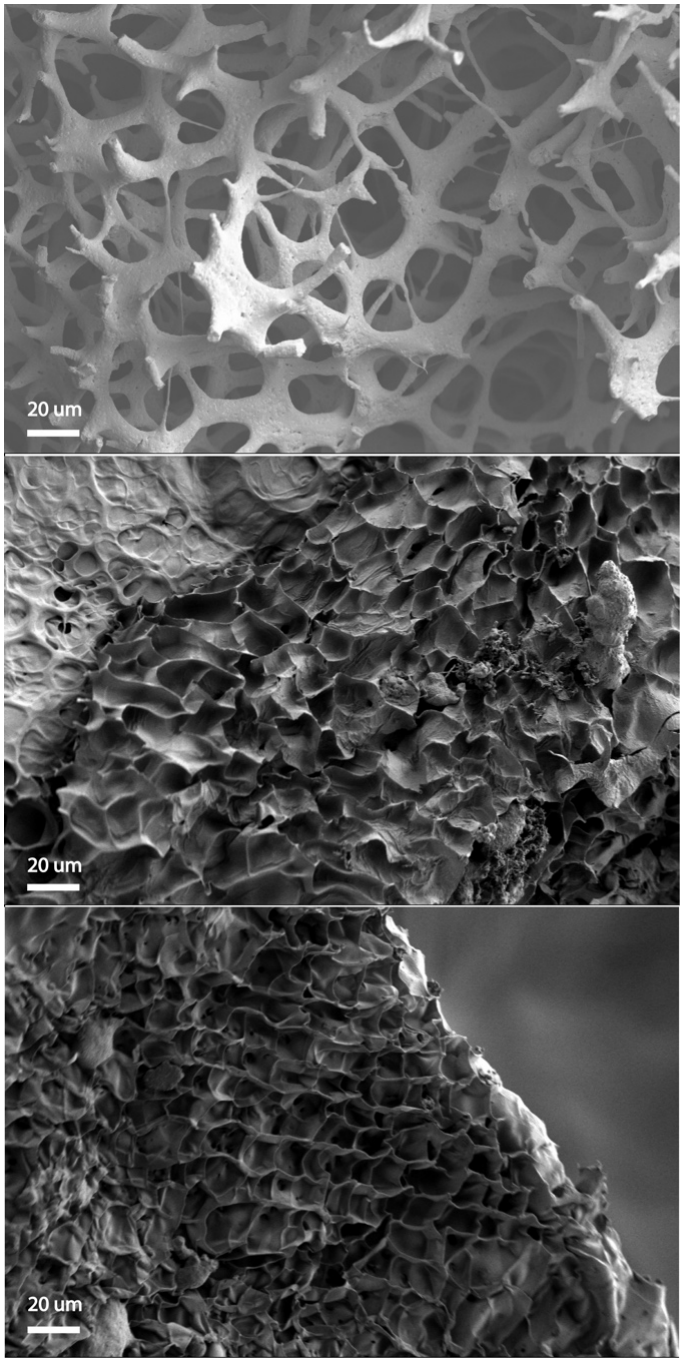

Figure 2.2. SEM images of **5** (top) **6** (middle) and **7** (bottom).

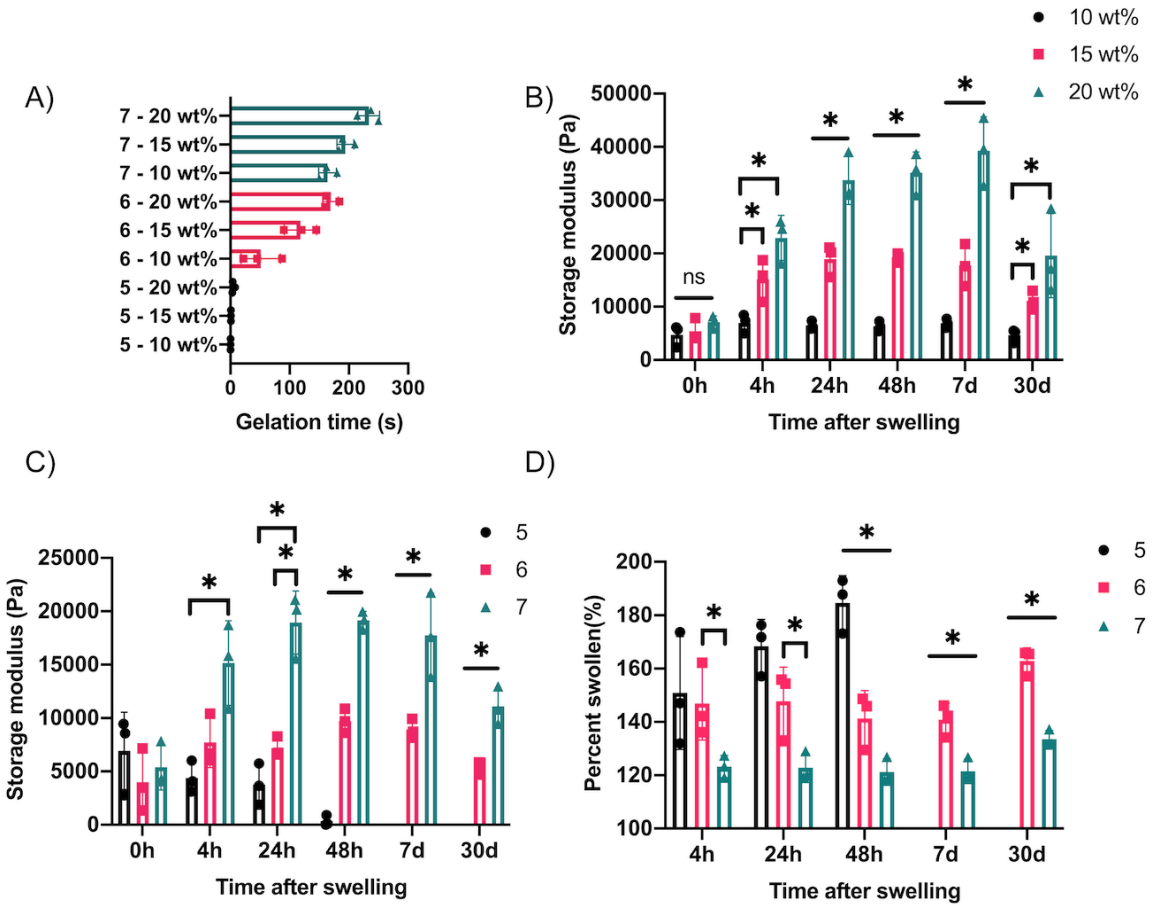

Figure 2.3. A) Gelation times of hydrogels at 10, 15 and 20 wt%. B) m10 hydrogel shows positive correlation between strength of hydrogel and weight percent. C) 15 wt% hydrogels show positive correlation between strength and carbon chain length. D) Swelling of hydrogels decreases with increased methylene chain length.

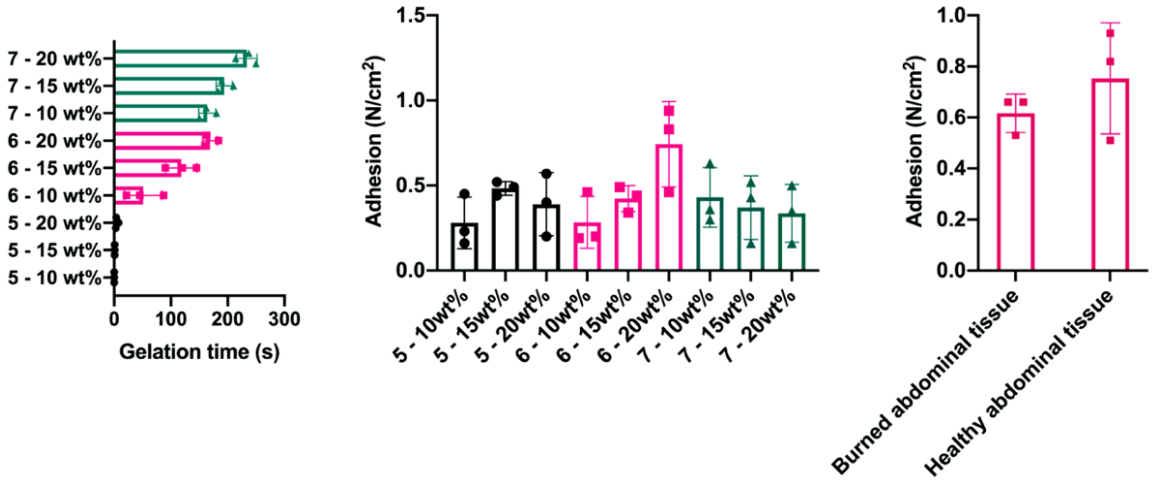

Figure 2.4: A) Dissolution of hydrogels at 15 wt% in 0.3M CME solution. B) Adhesion of hydrogels on human breast tissue using a lap shear test. C) Adhesion of **5**, 15 wt% hydrogels on burned and unburned human abdominal tissue.

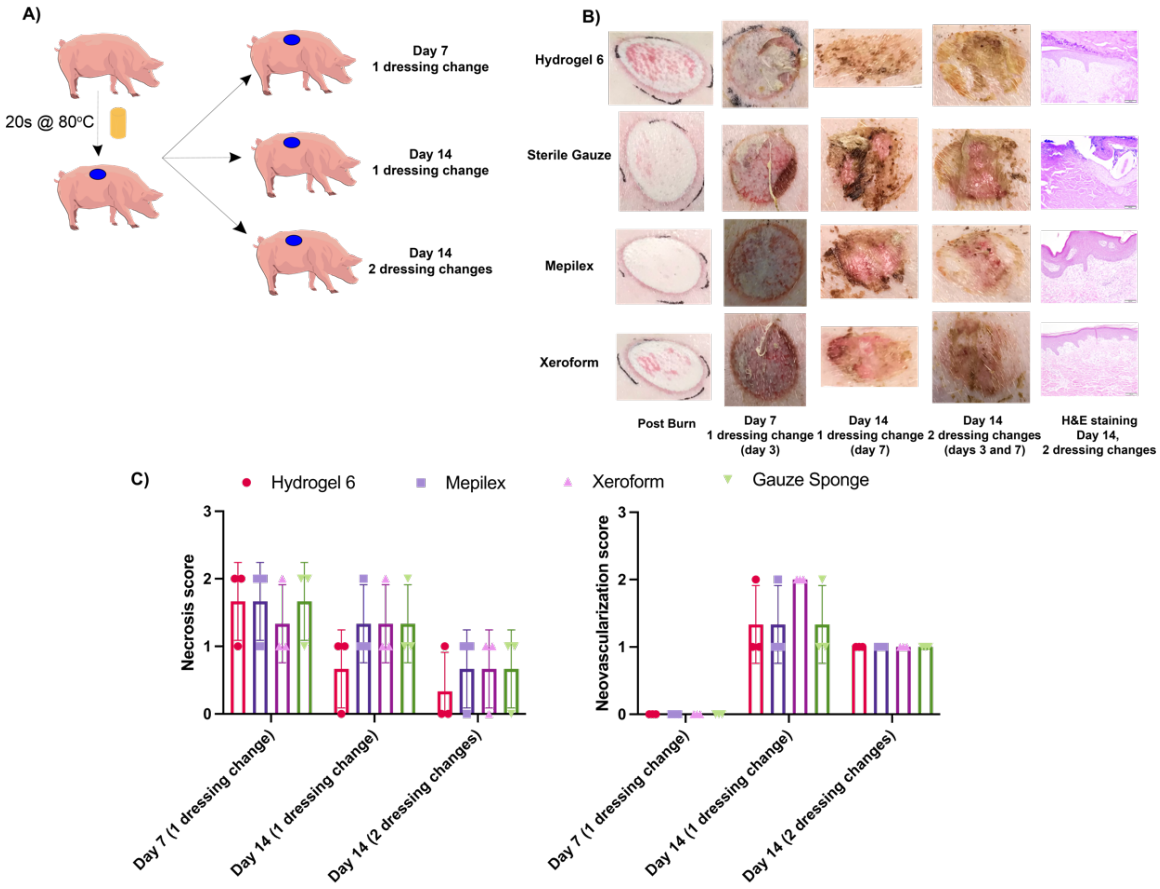

Figure 2.5. *in vivo* study design. Partial-thickness burns (2nd degree) were administered at 80ºC for 20 seconds and treated as detailed in Appendix 2. **A)** Experimental schematic. **B)** Representative photographs of burn sites post burn, during dressing changes at 7 and 14 days with dressing changes prior to sacrifice. Representative H&E of wounds at 14 days, all panels same magnification factor. **C)** Semi-quantitative scoring of wound necrosis, epidermal ulceration, inflammation, and neovascularization.

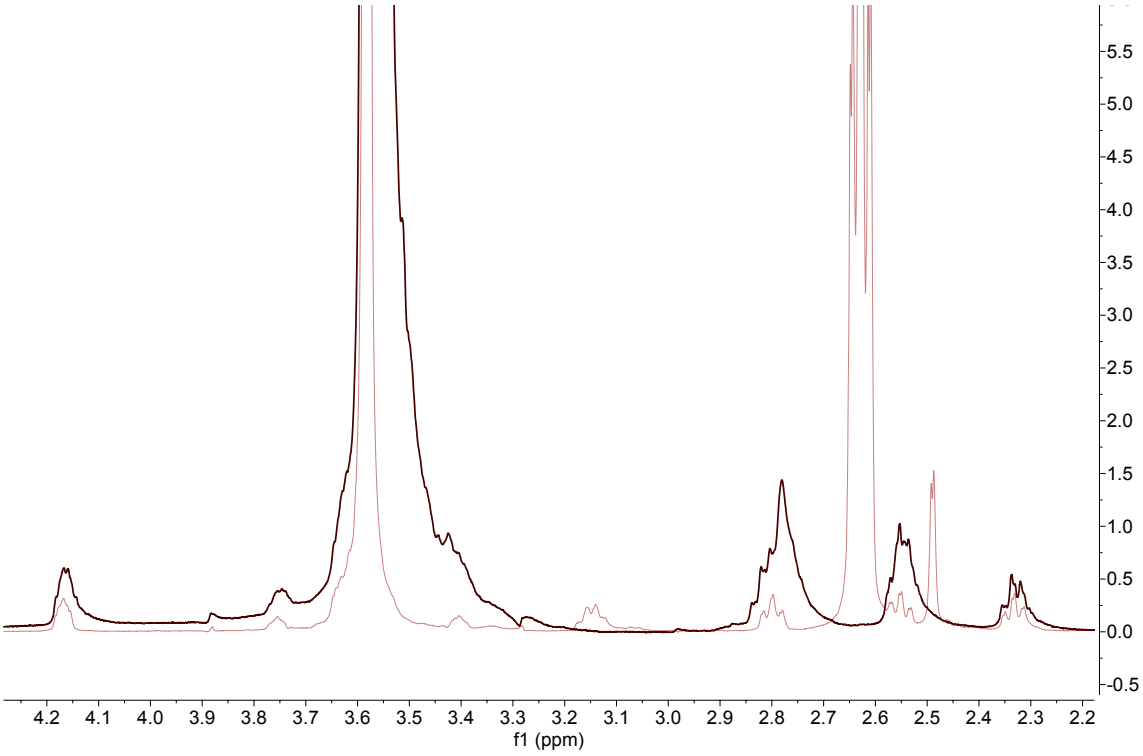

Figure 2.6. Representative ^{1}H NMR spectrum of crosslinker **6** before (red bold) and after (red) reaction with PEI mimetic, *N*-butylamine. NHS peak shifts from 2.78ppm (red bold) to 2.49ppm (red) when reacted with *N*-butylamine.

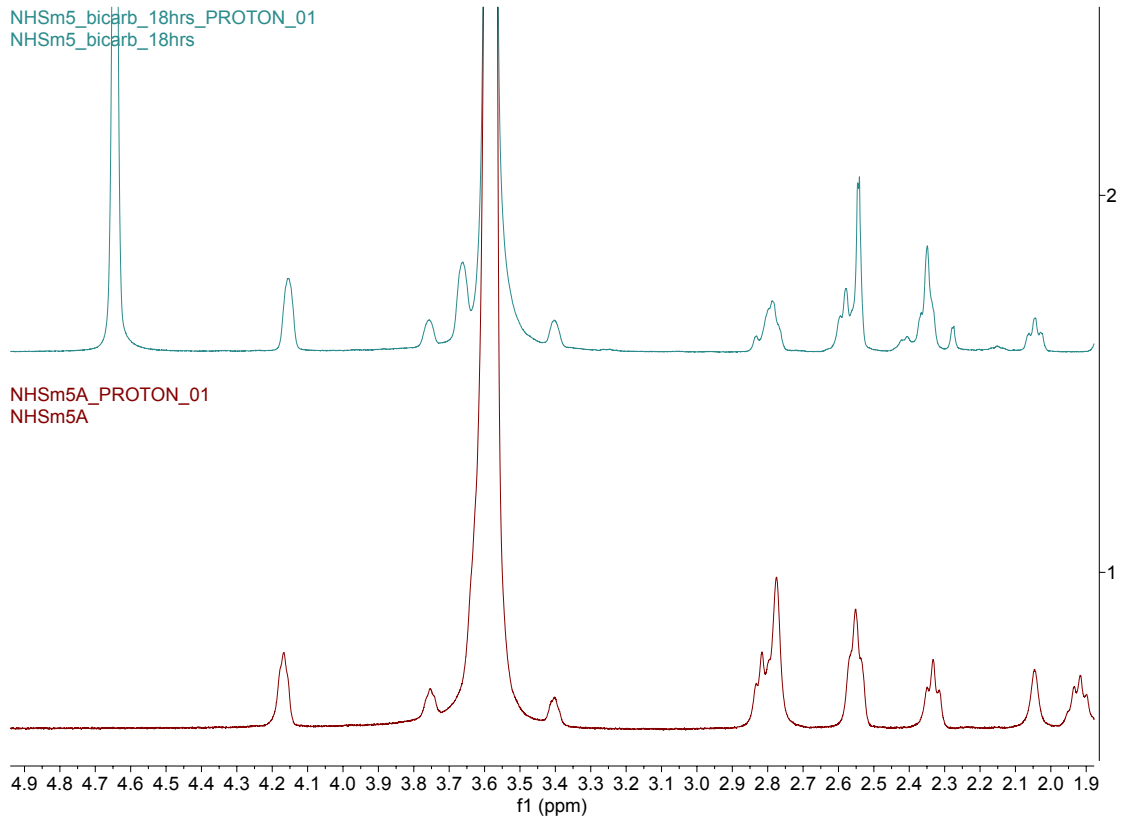

Figure 2.7. Representative ^{1}H NMR spectrum of intact crosslinker **6** (bottom) (NHS at 2.78ppm), and NHS-hydrolyzed (2.54ppm) crosslinker **6** in 0.3M sodium bicarbonate buffer, pH 8.0 (top).

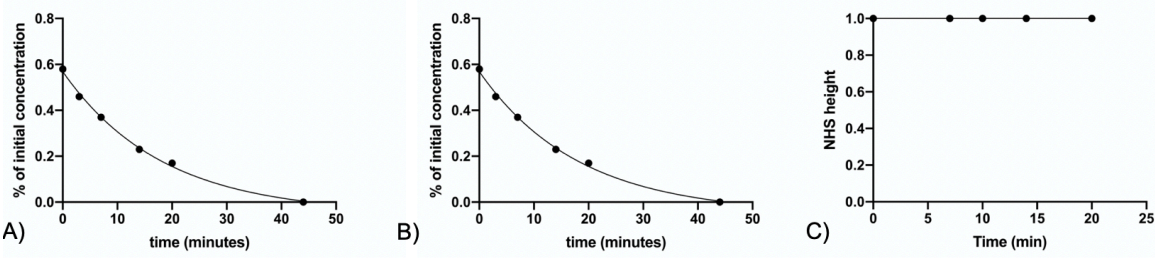

Figure 2.8. Rate order of A. thioester hydrolysis in crosslinker **4** in 0.3M Borate buffer, pH 8.0, B. thioester hydrolysis in crosslinker **5** in 0.3M Borate buffer, pH 8.0, C. **NHS** ester stability in 0.1M phosphate buffer pH 6.5.

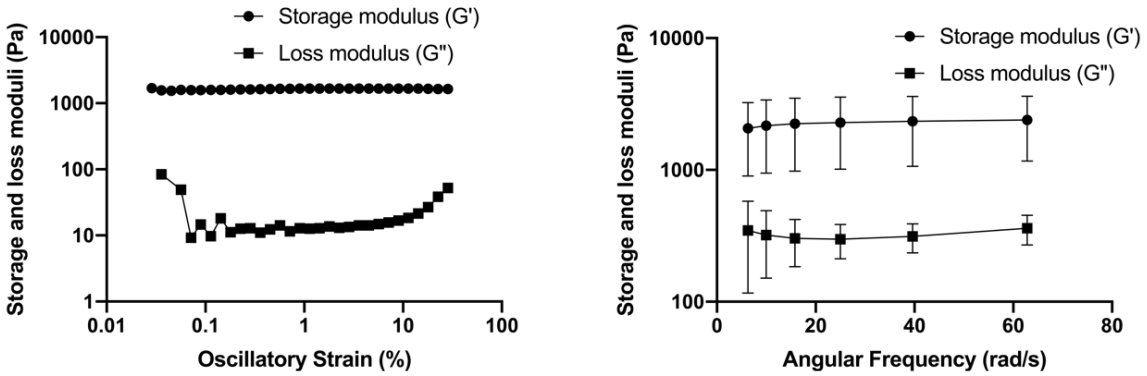

Figure 2.9. Strain sweep (left) and frequency sweep (right) of hydrogel **6**.

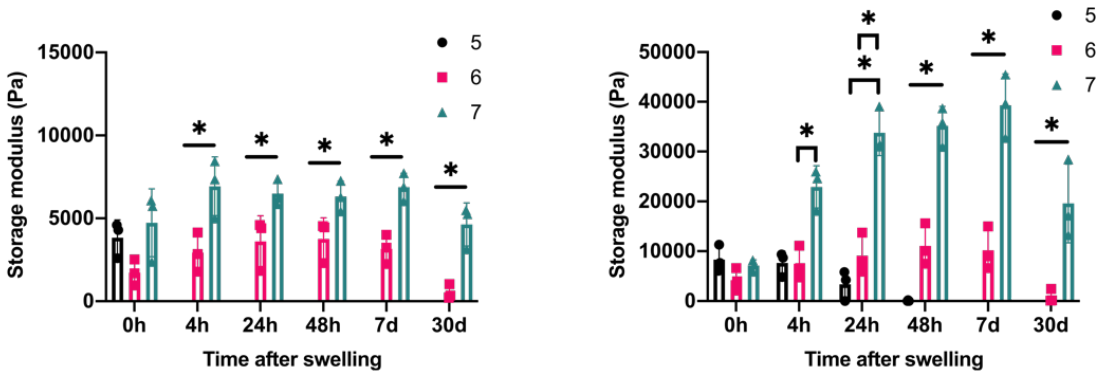

Figure 2.10. Storage modulus of hydrogels composed of crosslinkers **5, 6,** and **7** and 10 wt% (left) and 20 wt% (right)

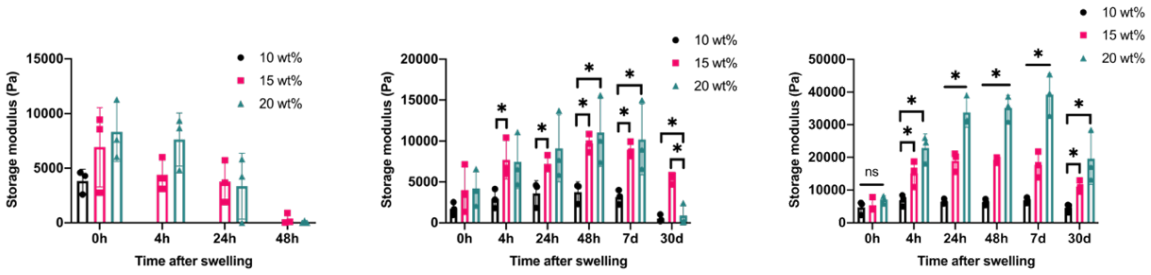

Figure 2.11. Storage modulus for crosslinkers **5** (left), **6** (middle), and **7** (right) at varying weight percents over 30 days of swelling.

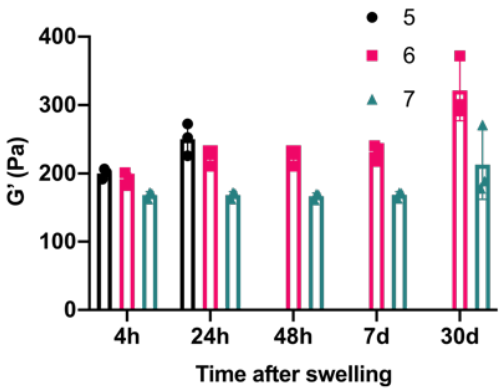

Figure 2.12. Swelling of hydrogels at 20 wt%.

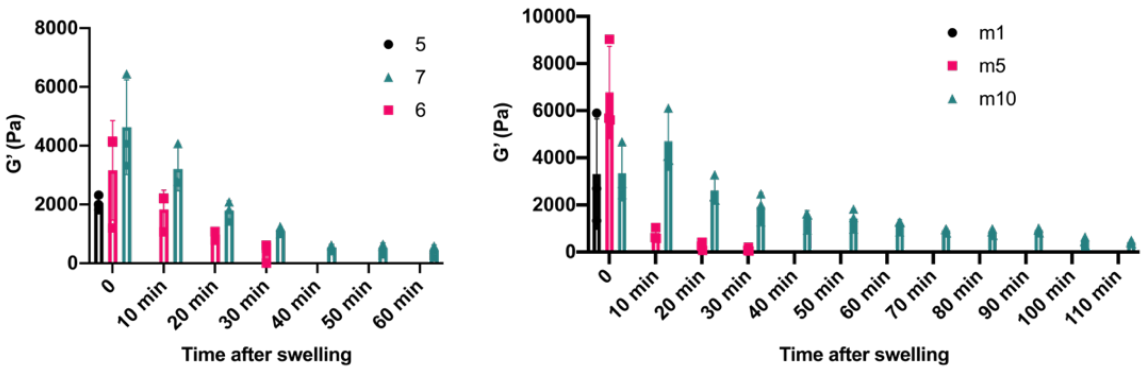

Figure 2.13. Dissolution of crosslinkers **5, 6,** and **7** at 10 and 20 wt%.

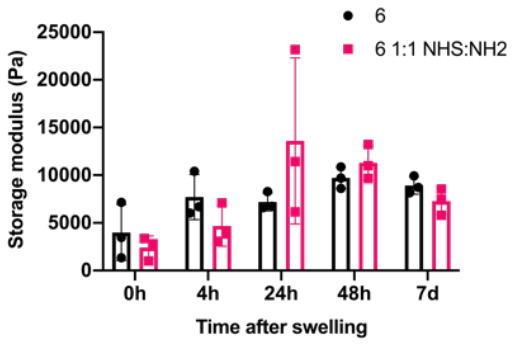

Figure 2.14. Rheological measurements on hydrogels from crosslinker **6** with 2:1 (black) or 1:1 (pink) NHS:NH_2 mole ratio

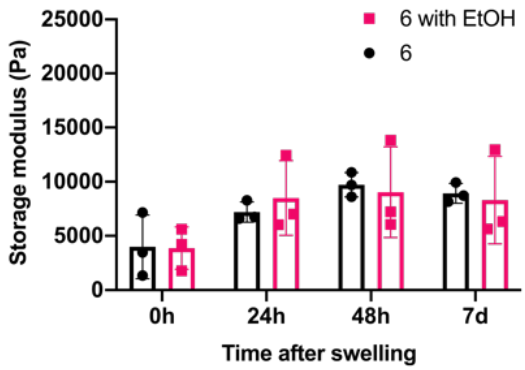

Figure 2.15. Rheological measurements of hydrogels made of crosslinker **6** with and without EtOH.

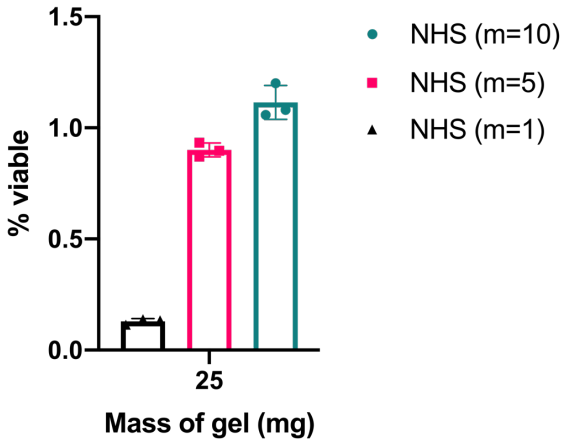

Figure 2.16. Cell viability of hydrogels **5, 6,** and **7**.

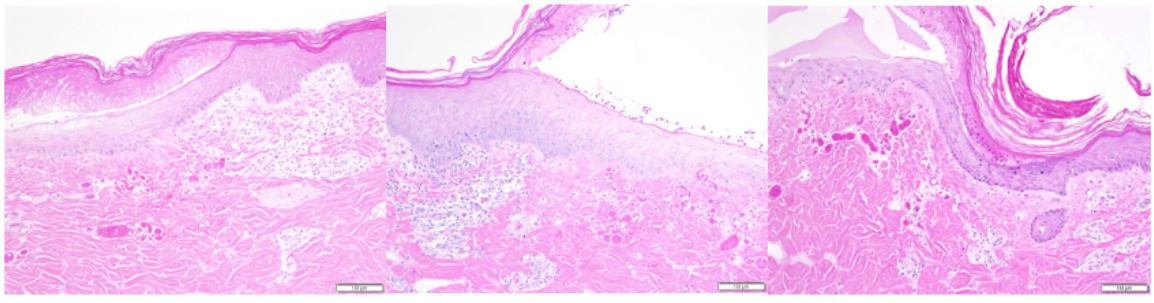

Figure 2.17. H&E of Group 1 for gauze (left), no dressing (middle), and hydrogel dressing (right).

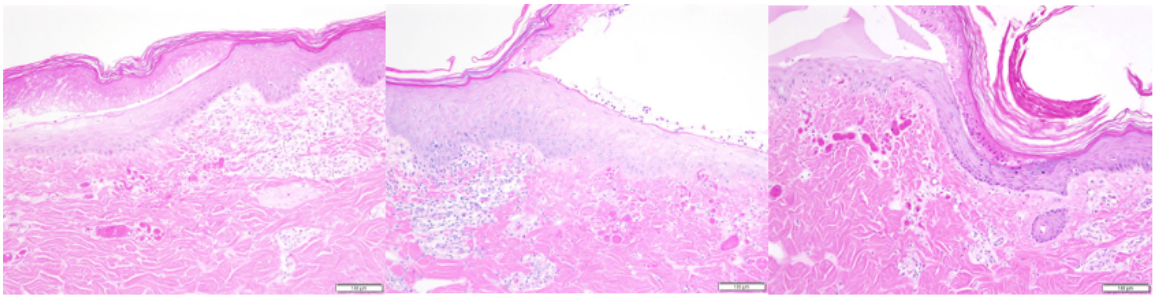

Figure 2.18. H&E of Group 1 for gauze (left), no dressing (middle), and hydrogel dressing (right).

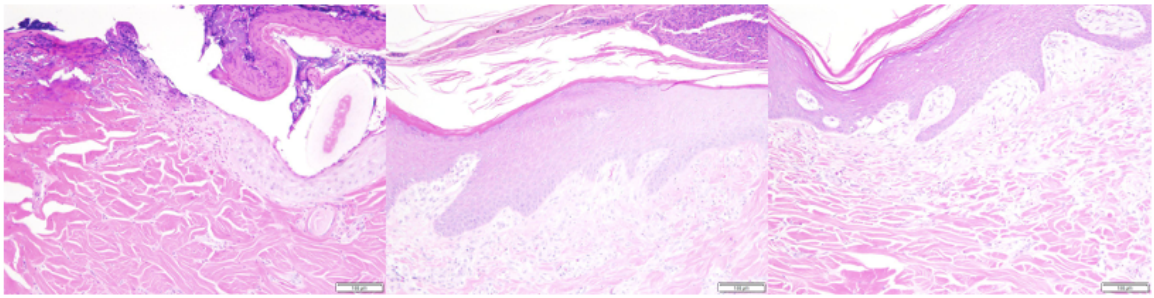

Figure 2.19. H&E of Group 2 for gauze (left), no dressing (middle), and hydrogel dressing (right).

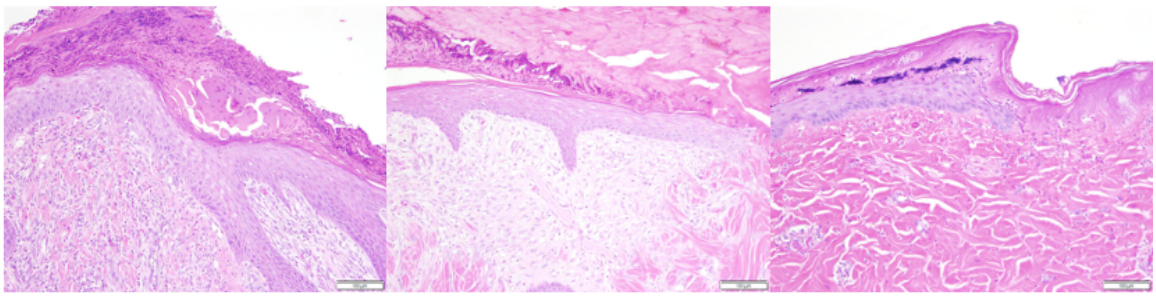

Figure 2.20. H&E of Group 4 for gauze (left), no dressing (middle), and hydrogel dressing (right).

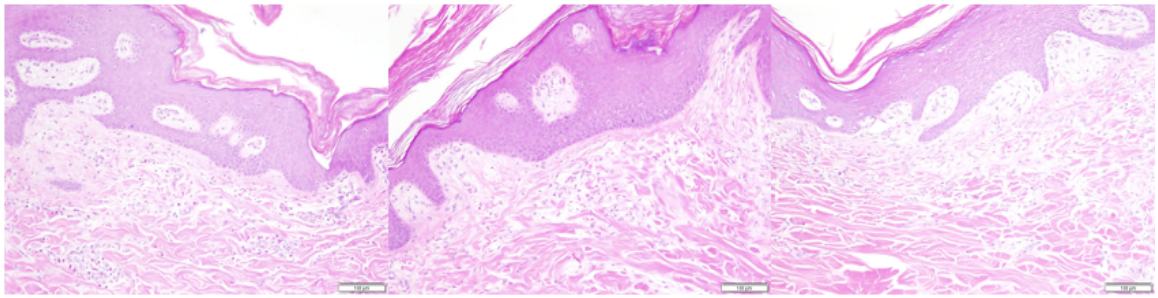

Figure 2.21. H&E of Group 5 for gauze (left), no dressing (middle), and hydrogel dressing (right).

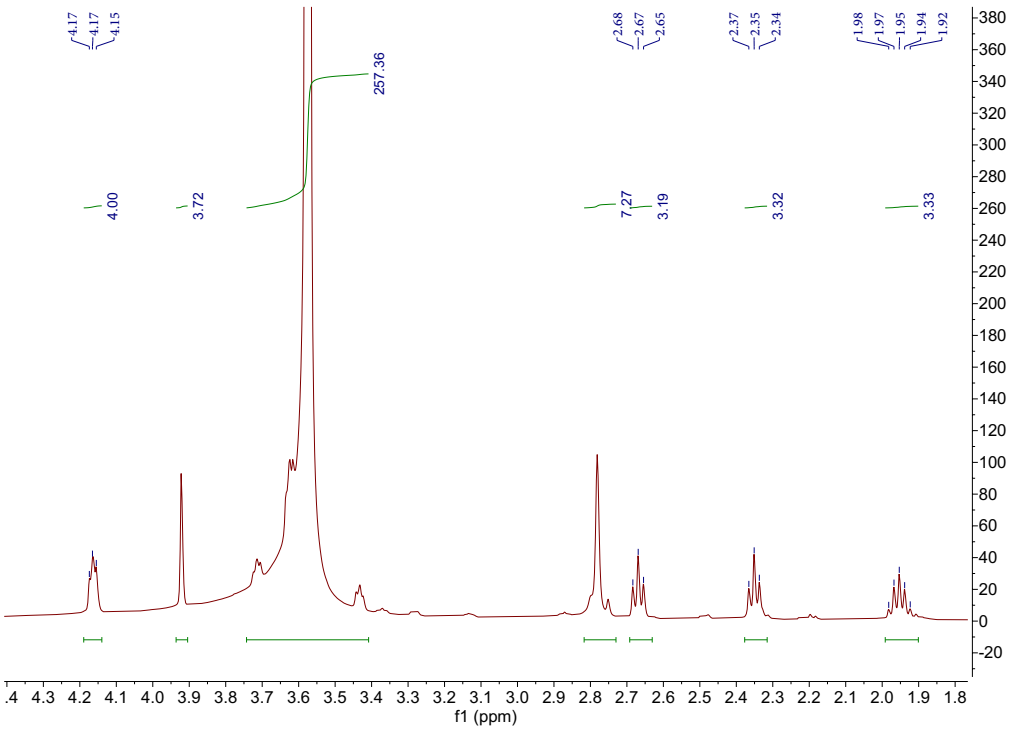

Figure 2.22. Representative ^{1}H NMR spectrum of crosslinker **5**

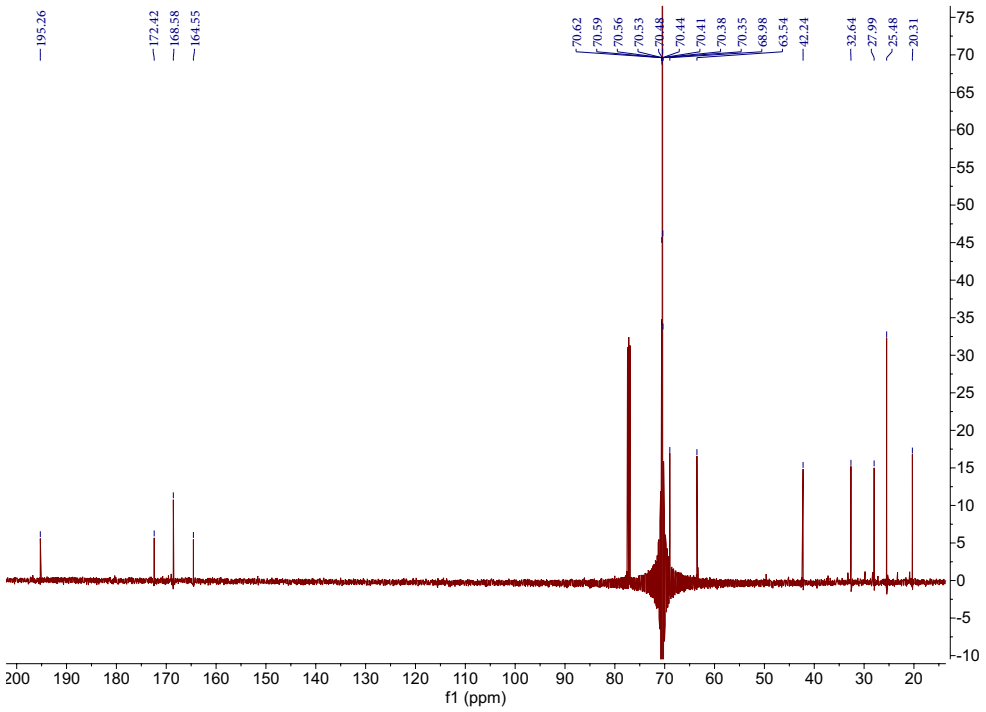

Figure 2.23. Representative ^{13}C NMR spectrum of crosslinker **5**

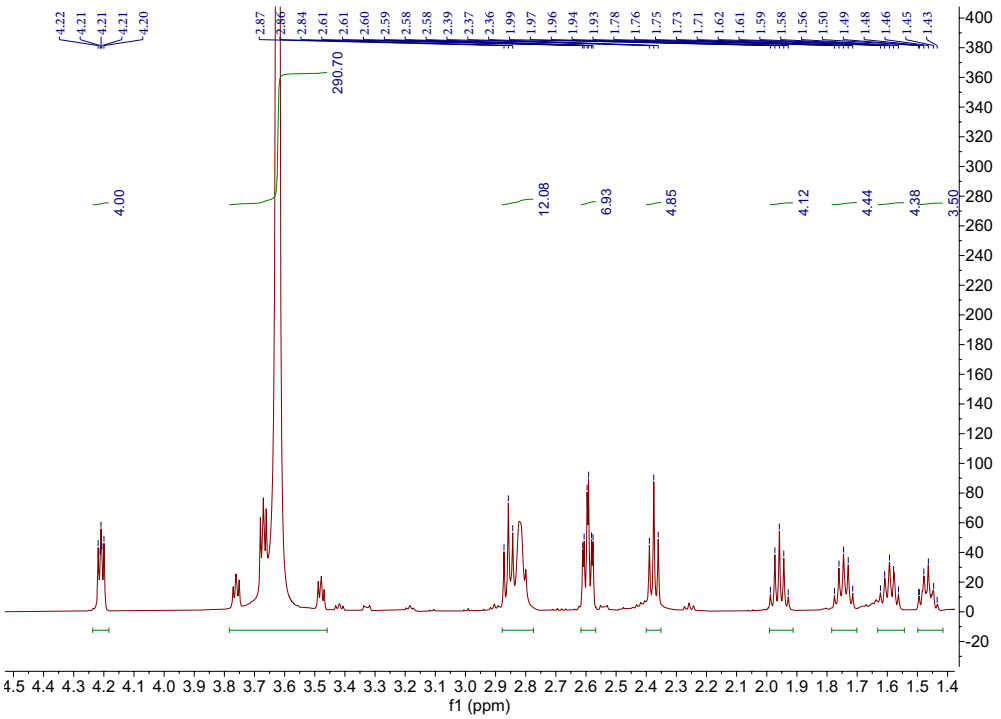

Figure 2.24. Representative ^{1}H NMR spectrum of crosslinker **6**

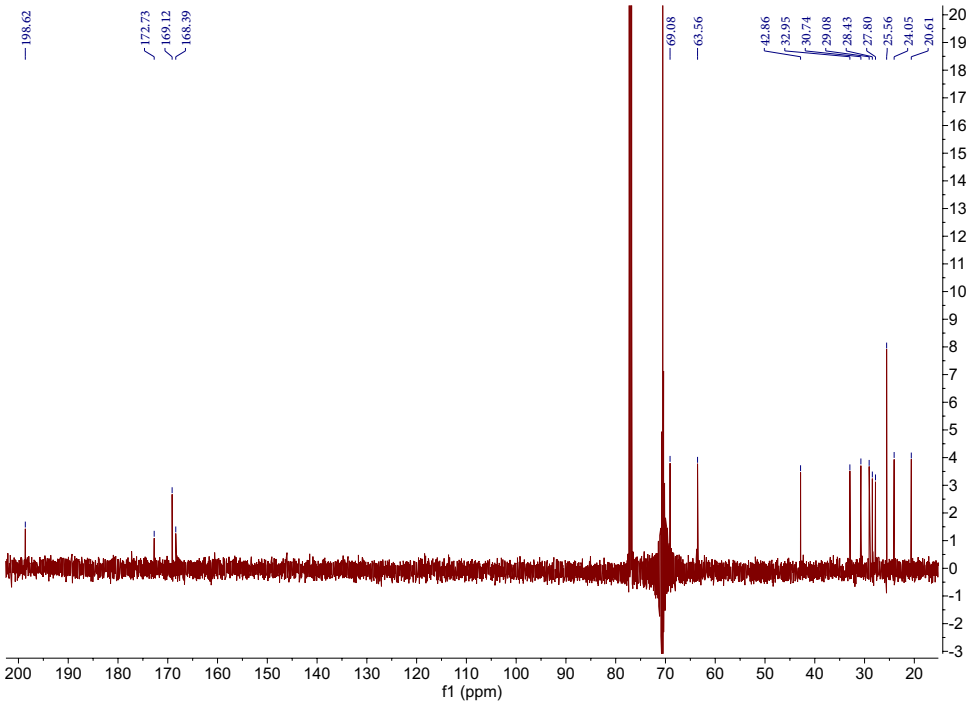

Figure 2.25. Representative ^{13}C NMR spectrum of crosslinker **6**

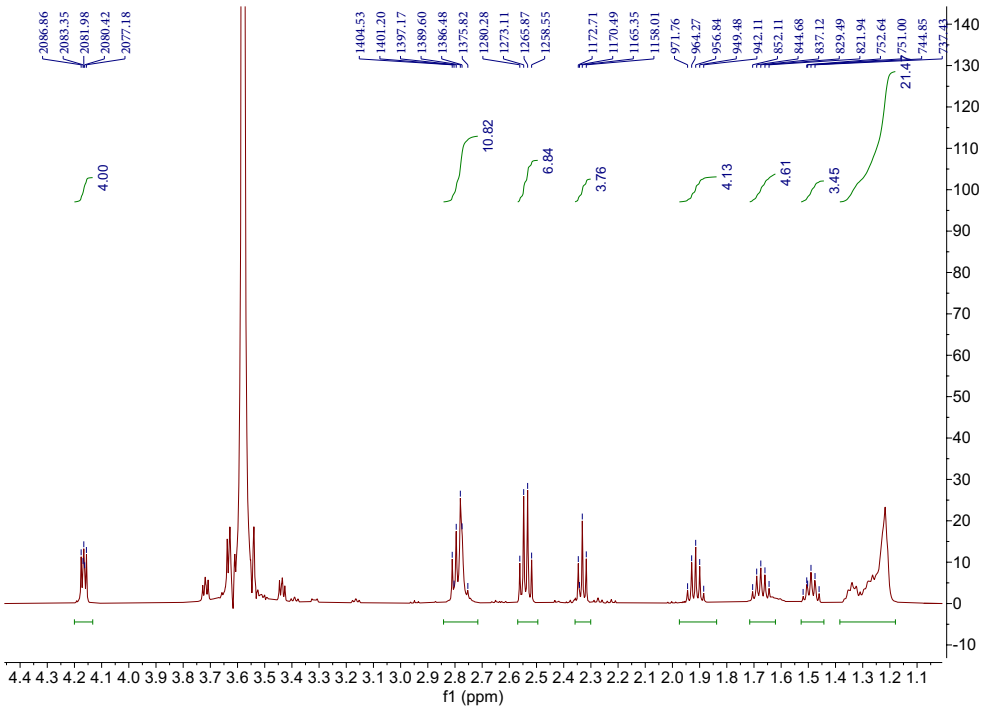

Figure 2.26. Representative ^{1}H NMR spectrum of crosslinker **7**

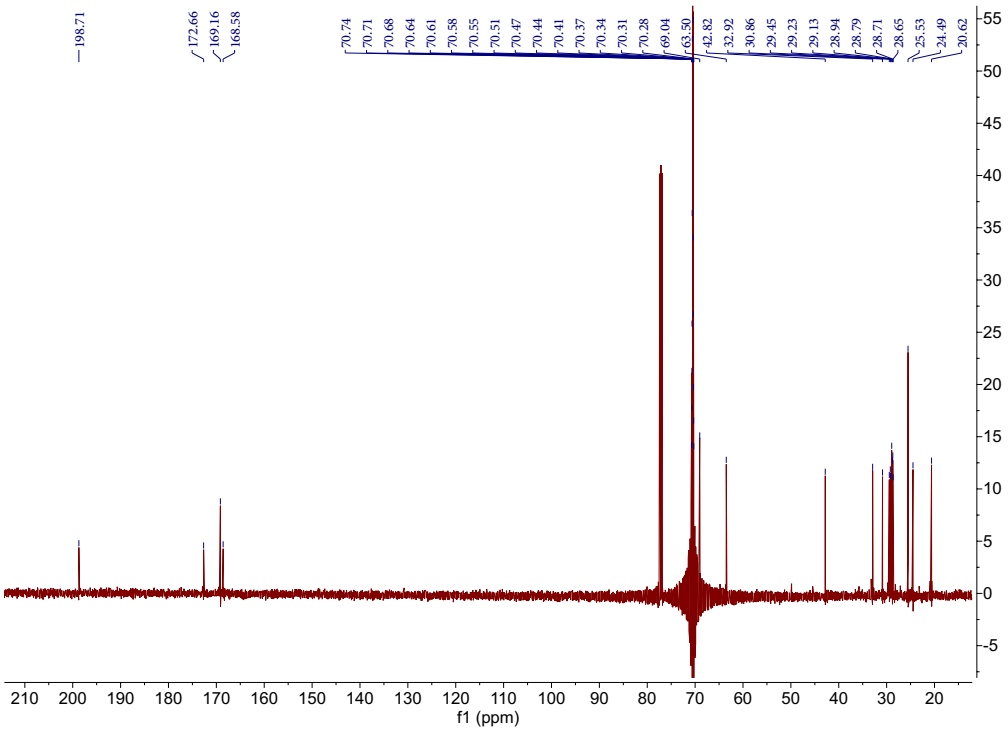

Figure 2.27. Representative ^{13}C NMR spectrum of crosslinker **7**

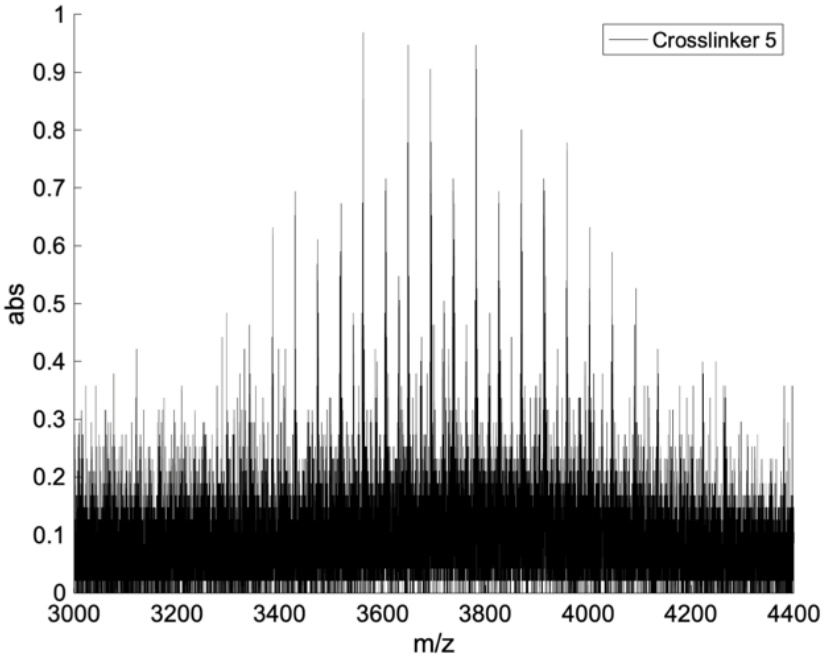

Figure 2.28. Representative MALDI spectrum of crosslinker **5**

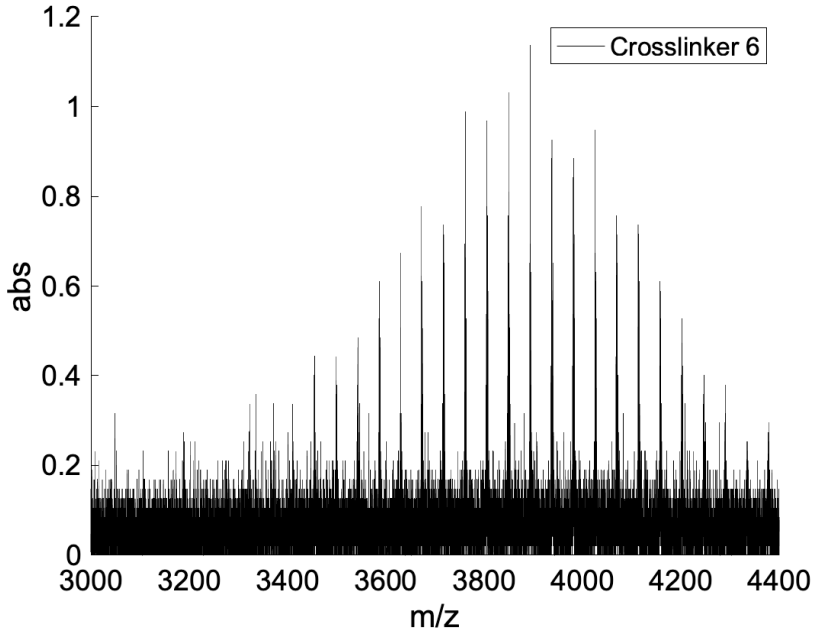

Figure 2.29. Representative MALDI spectrum of crosslinker **6**

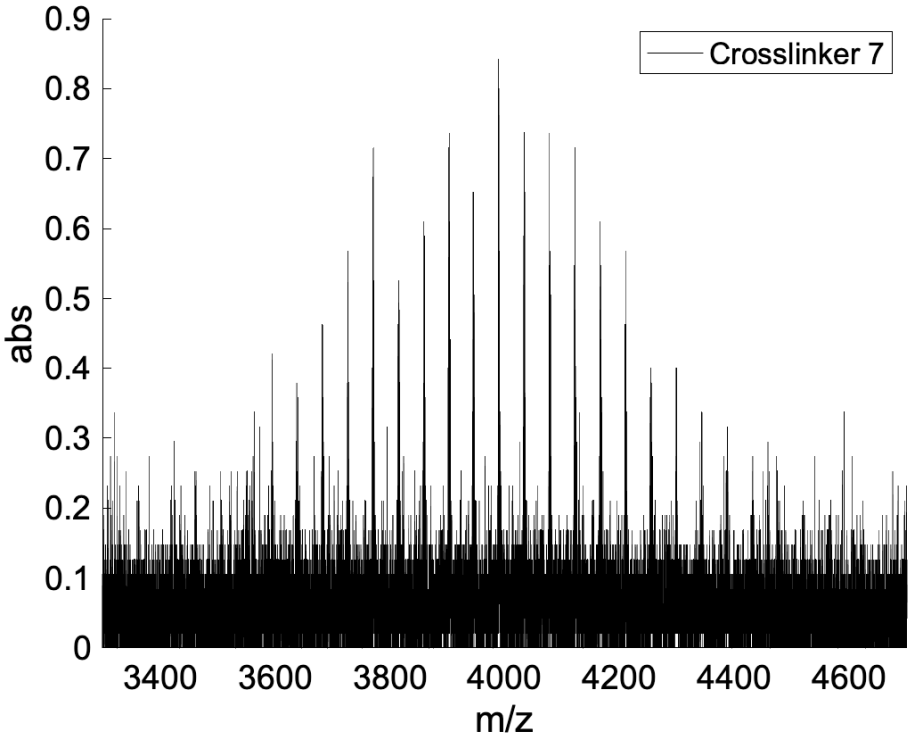

Figure 2.30. Representative MALDI spectrum of crosslinker **7**

Parameter	Ionic Hydrogel Dissolving (n=3)	Gauze Sponge (Sterile) (n=3)	No Material Used (n=3)
Inflammation	1.00 ± 0.00	1.00 ± 0.00	1.33 ± 0.58
	1.00	1.00	1.00
Neutrophils	0.33 ± 0.58	0.00 ± 0.00	1.00 ± 1.00
	0.00	0.00	1.00
Histiocytes	0.00 ± 0.00	0.00 ± 0.00	0.00 ± 0.00
	0.00	0.00	0.00
Lymphocytes	1.00 ± 0.00	1.00 ± 0.00	1.00 ± 0.00
	1.00	1.00	1.00
Multinucleated Giant Cells	0.00 ± 0.00	0.00 ± 0.00	0.00 ± 0.00
	0.00	0.00	0.00
Plasma Cells	0.00 ± 0.00	0.00 ± 0.00	0.00 ± 0.00
	0.00	0.00	0.00
Eosinophils	1.00 ± 0.00	1.00 ± 0.00	1.00 ± 0.00
	1.00	1.00	1.00

Table 2.1. Mean ± SD and median of inflammation and inflammatory cell types. Day 3, Group 1, no dressing changes.

Parameter	Ionic Hydrogel Dissolving (n=3)	Gauze Sponge (Sterile) (n=3)	No Material Used (n=3)
Inflammation	1.33 ± 0.58	1.33 ± 0.58	1.33 ± 0.58
	1.00	1.00	1.00
Neutrophils	1.33 ± 0.58	1.33 ± 0.58	1.33 ± 0.58
	1.00	1.00	1.00
Histiocytes	1.00 ± 0.00	1.00 ± 0.00	1.00 ± 0.00
	1.00	1.00	1.00
Lymphocytes	1.00 ± 0.00	1.00 ± 0.00	1.00 ± 0.00
	1.00	1.00	1.00
Multinucleated Giant Cells	0.00 ± 0.00	0.00 ± 0.00	0.00 ± 0.00
	0.00	0.00	0.00
Plasma Cells	0.00 ± 0.00	0.00 ± 0.00	0.00 ± 0.00
	0.00	0.00	0.00
Eosinophils	1.00 ± 0.00	1.00 ± 0.00	1.00 ± 0.00
	1.00	1.00	1.00

Table 2.2. Mean ± SD, median and incidence of inflammation and inflammatory cell types. Day 7, Group 3, no dressing changes.

Parameter	Ionic Hydrogel Dissolving (n=3)	Gauze Sponge (Sterile) (n=3)	No Material Used (n=3)
Inflammation	1.67 ± 0.58	1.67 ± 0.58	2.00 ± 0.00
	2.00	2.00	2.00
Neutrophils	1.33 ± 0.58	1.33 ± 0.58	2.00 ± 0.00
	1.00	1.00	2.00
Histiocytes	1.00 ± 0.00	1.00 ± 0.00	1.00 ± 0.00
	1.00	1.00	1.00
Lymphocytes	1.00 ± 0.00	1.00 ± 0.00	1.00 ± 0.00
	1.00	1.00	1.00
Multinucleated Giant Cells	0.00 ± 0.00	0.00 ± 0.00	0.00 ± 0.00
	0.00	0.00	0.00
Plasma Cells	0.00 ± 0.00	0.00 ± 0.00	0.00 ± 0.00
	0.00	0.00	0.00
Eosinophils	1.00 ± 0.00	1.00 ± 0.00	1.00 ± 0.00
	1.00	1.00	1.00

Table 2.3. Mean ± SD and median of inflammation and inflammatory cell types. Day 7, Group 2, 1 dressing changes.

Parameter	Ionic Hydrogel Dissolving (n=3)	Gauze Sponge (Sterile) (n=3)	No Material Used (n=3)
Inflammation	1.33 ± 0.58	2.00 ± 0.00	1.00 ± 0.00
	1.00	2.00	1.00
Neutrophils	1.33 ± 0.58	2.00 ± 0.00	1.00 ± 0.00
	1.00	2.00	1.00
Histiocytes	1.00 ± 0.00	1.00 ± 0.00	1.00 ± 0.00
	1.00	1.00	1.00
Lymphocytes	1.00 ± 0.00	1.00 ± 0.00	1.00 ± 0.00
	1.00	1.00	1.00
Multinucleated Giant Cells	0.00 ± 0.00	0.00 ± 0.00	0.00 ± 0.00
	0.00	0.00	0.00
Plasma Cells	0.00 ± 0.00	0.00 ± 0.00	0.00 ± 0.00
	0.00	0.00	0.00
Eosinophils	1.00 ± 0.00	1.00 ± 0.00	1.00 ± 0.00
	1.00	1.00	1.00

Table 2.4. Mean ± SD, median and incidence of inflammation and inflammatory cell types. Day 14, Group 4, 1 dressing changes.

Parameter	Ionic Hydrogel Dissolving (n=3)	Gauze Sponge (Sterile) (n=3)	No Material Used (n=3)
Inflammation	1.33 ± 0.58	2.00 ± 0.00	1.00 ± 0.00
	1.00	2.00	1.00
Neutrophils	1.33 ± 0.58	2.00 ± 0.00	1.00 ± 0.00
	1.00	2.00	1.00
Histiocytes	1.00 ± 0.00	1.00 ± 0.00	1.00 ± 0.00
	1.00	1.00	1.00
Lymphocytes	1.00 ± 0.00	1.00 ± 0.00	1.00 ± 0.00
	1.00	1.00	1.00
Multinucleated Giant Cells	0.00 ± 0.00	0.00 ± 0.00	0.00 ± 0.00
	0.00	0.00	0.00
Plasma Cells	0.00 ± 0.00	0.00 ± 0.00	0.00 ± 0.00
	0.00	0.00	0.00
Eosinophils	1.00 ± 0.00	1.00 ± 0.00	1.00 ± 0.00
	1.00	1.00	1.00

Table 2.5. Mean ± SD, median and incidence of inflammation and inflammatory cell types. Day 14, Group 4, 2 dressing changes.

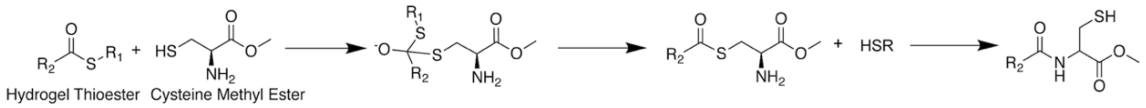

Scheme 2.1: Controlled dissolution through thiol-thioester exchange.

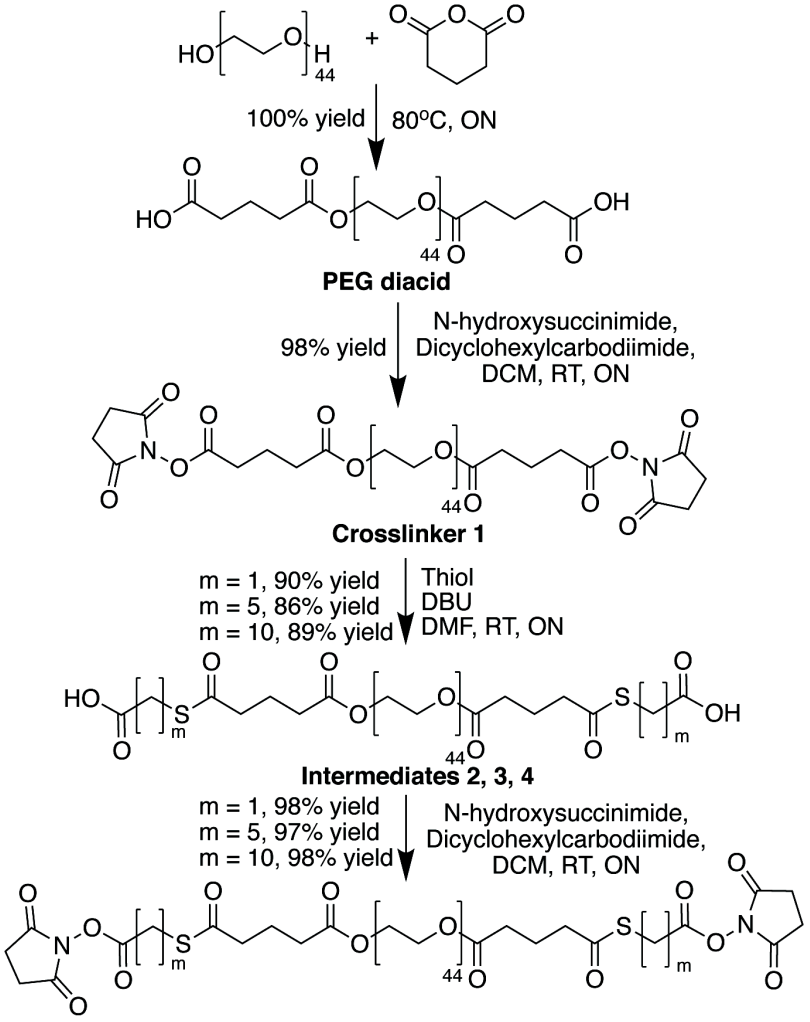

Scheme 2.2: Synthetic scheme of crosslinkers **1-7**.

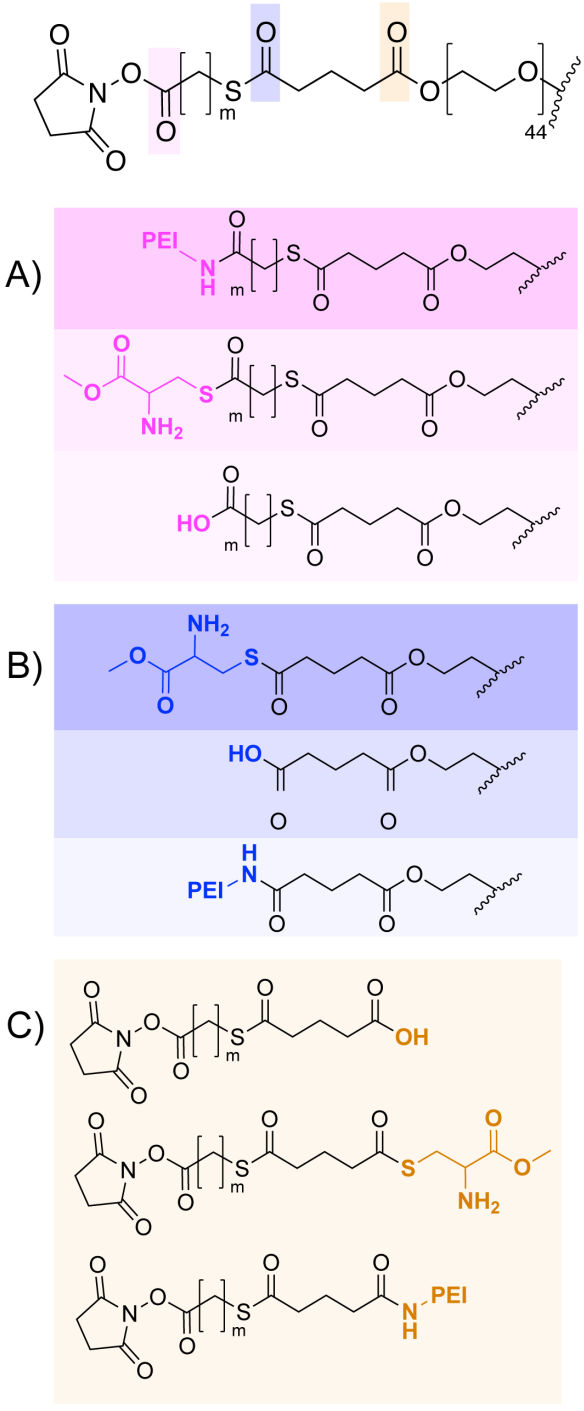

Scheme 2.3. Selective conjugation of the crosslinker with PEI, cysteine methyl ester, and water at various sites of reactivity, respectively. A) Reaction with the NHS ester. B) Reaction with the internal thioester. C) Reaction with the internal ester. Darker colored regions correlate with greater preference for that specific reaction over others.

CHAPTER 3. Temporary *in situ* hydrogel dressing for colon polypectomies

3.1 Introduction

Colorectal cancer (CRC) is among the leading causes of cancer death in the developed countries.[112–115] Standard preventative care for patients over 50 years old involves a colonoscopy to biopsy and remove polyps, known as a polypectomy, to assess for CRC.[113–115] As of 2019, approximately 60% of the US population age 50-75 years has undergone a colonoscopy.[116] Practically, a physician inserts an endoscope into the patient's colon while under anesthesia, examines the colon, and then removes the polyps. After removal, the wound is either left open to the internal colon environment or thermally sealed using electrocoagulation. Open wounds after a polypectomy can result in bleeding (12.3 out of 10,000 procedures in the US), hemorrhaging, and sepsis, while electrocoagulation can result in perfusion (9.0 out of 10,000 procedures in the US) or post polypectomy coagulation syndrome (PPCS), an electrocoagulation-based thermal injury to the tissue (25 out of 10,000 procedures in the US).[99,112–114,117–119] Three days after polypectomy, colon tissue regains 60% of its strength, however these complications continue to persist, sometimes beyond this period.[99,113,117,120] When complications arise, additional colonoscopies and invasive techniques are required to diagnose and treat.[99,120,121] Today, there is a clear unmet need to prevent colon bleeding, perfusion, PPCS, and sepsis after a polypectomy.

We envision a temporary *in situ* hydrogel dressing, applied at the time of

polypectomy, may prevent or reduce the likelihood of these complications by covering and protecting the wound. Hydrogels are three-dimensional, hydrophilic, polymeric networks used for a variety of biomedical applications, including as wound dressings, adhesives, or sealants.[51,52,110,111,122–124]From a biomaterials design perspective, the polypectomy dressing will: 1) form rapidly *in situ*; 2) adhere to colon tissue; 3) be non-cytotoxic; 4) naturally dissolve over 3-5 days; 5) swell up to 200% to absorb wound exudate; 6) prevent the spread or migration of bacteria; and, 7) conform to the malleable shape of a colon lumen. As a first step towards this goal, we report a small library of hydrogels and assess variations in gelation rate, adhesion strength, swelling, cytotoxicity, and degradation as a function of hydrogel composition. Further, we evaluate the delivery of the hydrogel via a dual lumen catheter inserted through an endoscope and the barrier properties of the hydrogel to prevent bacterial migration.

3.2 Hydrogel synthesis

We synthesized the SA crosslinker starting from PEG (M_W 3000) as shown in scheme 3.1A. Briefly, we heated the PEG to 120^{o}C and dried it under vacuum for thirty minutes in a round bottom flask with a magnetic stir bar. While the PEG dried, the temperature was decreased to 80 ^{o}C. After 30 minutes, succinic anhydride (4eq) was added to the round bottom flask containing PEG. The reaction was stirred overnight. The resultant mixture was subsequently cooled to room temperature, dissolved in methylene chloride, and precipitated in diethyl ether. The

precipitate was dried under vacuum to afford a white PEG diacid product (yield = 99%). The PEG diacid was then dissolved in methylene chloride, and reacted with dicyclohexylcarbodiimide, and N-hydroxysuccinimide at room temperature, overnight. The precipitate was filtered off, and the filtrate was concentrated under vacuum. The concentrated filtrate was precipitated in diethyl ether, and dried under vacuum to afford a white powder (yield = 98%). The SA crosslinker was characterized via ^{1}H NMR, ^{13}C NMR, DSC, and GPC. The final product is completely soluble in water. The SVA crosslinker was commercially purchased from Laysan Bio with M_n of 4635 g/mol (PDI = 1.03). The SVA crosslinker is a water-soluble white powder.

3.3 Hydrogel gelation

Given the dynamic nature of the colon, the two liquid hydrogel pre-cursors, the crosslinker and PEI or 4-arm PEG-NH_2 must be quickly applied, gel, and adhere to the colon tissue before washing down the sides of the colon. We dissolved the PEG crosslinkers and amine-terminal macromers in 0.1M phosphate buffer pH 6.5 and 0.3M borate buffer pH 8.5, respectively, and measured the gelation times after mixing according to previously published protocols.[95,110,125,126] The SA+PEI hydrogels gel faster with increasing weight percents from 10 to 20 wt% (**Fig 3.3B**). The increase of gelation time results from a higher concentration of reactive groups therefore favoring quicker gelation. Next, we compared the gelation times between the SA crosslinker and either the PEI or 4-arm PEG-NH_2

macromer at 15 wt%. The gelation times are similar at approximately 1.5 minutes suggesting that gelation is independent of the amine macromer. The SVA+PEI hydrogels gel at a similar rate to SA+4-arm PEG-NH_2 and SA+PEI hydrogels. However, the SVA+4-arm PEG-NH_2 hydrogel gels faster. We attribute this increase in gelation time to two factors. The 4-arm PEG-NH_2 macromer contains four, long, amine-terminal arms and has a molecular weight of 5kDa. PEI is a more condensed branched macromer with a molecular weight of 2.0 kDa. The long PEG arms 4-arm PEG -NH_2 favor a faster gelation time for the SVA+4-arm PEG-NH_2 hydrogel due to increased steric freedom relative to PEI, a branched polymer with short arms containing terminal amines and low molecular weight. The steric hindrance observed in the PEI structure reduces the ability to readily react with NHS reactive groups in the hydrogel network. With regards to defects in the hydrogel network, terminal amines favor conjugation at the NHS-ester, however SA crosslinkers contain an internal ester that is also susceptible to macromer amidation and hydrolysis. The preferred site for amidation in the SA crosslinker is at the NHS ester as observed via ^{1}H NMR. While unlikely, amidation may occur at the internal ester, resulting in defects in the hydrogel network. Additionally, hydrolysis at the ester linkage has a half-life of $t_{1/2}$ = <5 minutes at pH 8.0 further providing defects in the hydrogel network as observed in ^{1}H NMR. Defects in the network disassemble the hydrogel network, countering the amidation reaction, and therefore slowing the time to gelation relative to the SVA+4-arm PEG-NH_2 hydrogel. Furthermore, we evaluated the effect of pH on gelation time. We observe

an increase in gelation kinetics due to an increased pH (**Fig 3C**).[127–130] A fast gelation time (<3 seconds) is an important criterion in developing an *in situ* forming polypectomy hydrogel wound dressing. The location of a polypectomy, for example, may require dressing application against gravity, such that a quick gelling hydrogel will be necessary for *in situ* delivery and gelation.

3.4 Rheological and swelling measurements

After gelation, we measured the rheological and swelling properties over 30 days or until the hydrogel dissolved in 100 uM PBS (pH 7.4). First, we assessed the storage modulus (G') as an indicator for strength as well as hydrogel swelling (**Fig 3.2**). Increased hydrogel weight percent affords greater G' and longer sustained mechanical strength as shown in SA+PEI hydrogels (**Fig 3.2A**). Additionally, the G' decreases over time for each hydrogel comprised of SA + PEI due to hydrolysis at the internal ester linkage, while G' remains unchanged for the SVA + PEI hydrogels over 30 days of swelling due to a lack of degradable linkage within the SVA crosslinker structure. To assess the effects of a degradable ester linkage in the crosslinker relative to mechanical strength, we prepared hydrogels using the SA or SVA crosslinker and a 4-arm PEG-NH_2 (**Fig 3.2B**). The degradable hydrogel, SA+4-arm PEG-NH_2, maintains mechanical integrity with the G' being unchanged (3591 Pa) over 48 hours, and sustained mechanical strength during hydrolysis over 7 days of swelling, while the non-degradable hydrogel (SVA+4-arm PEG-NH_2) maintains mechanical strength over 30 days of swelling (13766 Pa). A

similar trend is observed for SA and SVA hydrogels prepared with PEI, however the degradable hydrogel, SA+PEI, maintains G' over 48 hours (1380 Pa). We attribute the increased degradation rate in SA+PEI hydrogels relative to SA+4-arm PEG-NH_2 hydrogels a local basic pH within the hydrogel network due to the presence of the PEI. We evaluated the effects of pH by swelling SA+PEI hydrogels in dH_2O, pH 5.0, and the SA+4-arm PEG-NH_2 in an aqueous TEA solution (a tertiary amine; comparable [M] to that present in the PEI-based hydrogels), pH 8.0. The SA+PEI hydrogels swell in pH 5.0 and hydrolyze in 48h, similar to swelling in PBS pH 7.4. The similar degradation rates are a result of the strong, basic nature of PEI, and inability to buffer it locally. However, swelling SA+4-arm PEG-NH_2 gels in a solution containing TEA increase hydrolysis of the hydrogel, such that hydrogels degrade in 24h relative to 7d in PBS pH 7.4 (**Fig 3.4B**). We confirmed hydrolysis at the ester linkage via following a shift in the methylene peak adjacent to the ester from 4.71ppm to 4.25ppm on ^1H NMR. We determine the half-life ($t_{1/2}$) to be 19.8 minutes for the ester linkage at pH 8.0 in D_2O with TEA present (again, comparable [M] to that present in the PEI-based hydrogels), whereas no ester linkage hydrolysis occurs when TEA is not present (at pH 5 or 6) via ^1H NMR over 24 hrs. Lastly, we evaluated the hydrolysis of the SA+PEI hydrogels at 37 ^oC to mimic the colon environment.[127] The SA+PEI hydrogel degrades within 24 h at 37 ^oC, whereas the SA+4-arm PEG-NH_2 hydrogel degrades at the same rate regardless of temperature (RT or 37 ^oC). The increase in temperature further accelerates the PEI catalyzed hydrolysis of the hydrogel.

Regardless of the hydrogel composition, an initial increase in storage moduli and swelling occurs after the first four hours when the hydrogels are immersed in 100mM PBS. (**Fig 3.3A**). The hydrogels swell until they reach equilibrium at 24h or degrade. All the hydrogels swell to at least 200% of its initial weight in buffer, addressing our absorption requirement of wound exudates for a polypectomy dressing.

3.5 Hydrogel cell viability

We also assessed cell viability of the hydrogels against NIH3T3 mouse embryo fibroblasts. All the hydrogels are non-cytotoxic (>88% viability) (Fig 3.17).

3.6 Hydrogel adhesion on colon tissue

Next, we measured the adhesive strength of the SA+PEI, SVA+PEI, and SA+4-arm PEG-NH_2 hydrogels (15 wt%) on intact porcine colon tissue with and without the mucosa layer. We selected the SA+PEI, SVA+PEI, and SA+4-arm PEG-NH_2 hydrogels to determine whether the presence of the PEI vs 4-arm PEG-NH_2 in the hydrogel alters the adhesion, and if the hydrolysable SA vs non-hydrolyzable SVA crosslinkers affects the adhesion. Additionally, we removed the mucosa layer to better model the tissue after a polypectomy. The SA + PEI and SVA+PEI hydrogels adhere the greatest to the tissue with an intact mucosa layer with an adhesivity value of 0.18 N and 0.36 N, respectively. While the SA+4-arm PEG-NH_2 hydrogel adheres the strongest to the tissue without the mucosa layer

(0.64 N) (Fig 3.6). We attribute this difference in adhesion as a consequence of hydrogen bonding and charge-charge interactions between the mucosa layer and the cationic PEI compared to the neutral PEG. Mucus is an anionic, hydrophobic, and viscoelastic network with glycoproteins available for hydrogen bonding and electrostatic interactions to molecules such as PEI.[131,132] PEG, on the other hand, is an uncharged, hydrophilic, and nonfouling molecule that resists adhesion to mucus.[131,133,134] The SA+4-arm PEG-NH_2 hydrogel adheres the strongest to the colon tissue, without the mucosa layer, likely due to the absence of electrostatic interactions with the tissue substrate.

3.7 Bacterial migration through hydrogels

For the bacterial migration studies, we chose isolates of *E. coli* and *B. fragilis* because these microbes are both commonly found in the intestine and are known to cause infections. *E. coli* is highly motile and thus may easily cross the hydrogel, whereas *B. fragilis* isolates frequently display multi-drug resistance and are known to opportunistically cause sepsis. *In vitro* testing on agar plates and microscopy studies show that these microbes do not transverse across the SA + 4-arm PEG-NH_2 hydrogel, indicating its potential for preventing sepsis *in vivo* (**Fig 3.7**). In contrast, the SA + PEI hydrogel hydrolyzes under these laboratory conditions of 37 ºC, and is not a suitable for this application.

3.8 Handleability of hydrogels

Lastly, we qualitatively evaluated the application and handleability of the crosslinker and macromer by administering the hydrogel pre-cursors components through a dual lumen catheter for subsequent hydrogel formation upon exit at the tissue site (Figure 3.9). We utilized a dual lumen catheter, to deliver our two-part hydrogel formulation on *ex vivo* colon tissue. All 12 hydrogel formulations were injected through the dual lumen catheter and exhibit gelation and adhesion to colon tissue both with and against gravity, suggesting ease of application for future *in vivo* studies (Fig 3.20).

3.9 Conclusions

We describe a series of new hydrogels which conform to any shape, possesses tunable G' from 100–16,000 Pa, adsorb and swell in aqueous buffer 200+%, adhere to colon tissue (0.1–0.4N), degrade over various time frames via hydrolysis of an internal ester linkages (4h-7d), are non-cytotoxicity (>88% viability), and exhibit capability for immediate gelation *in situ* (<3s gelation time), a requirement for application to the lumen of the colon.

3.10 Materials and methods

Materials

Poly(ethylene glycol) (PEG; average Mn 3000 g/mol; Sigma Aldrich), succinic anhydride (99%; Aldrich), dicyclohexylcarbodiimide (DCC; 99%; Sigma

Aldrich), *N*-hydroxysuccinimide (NHS; 99%, Sigma Aldrich), anhydrous methylene chloride (DCM; 99%; anhydrous; Sigma Aldrich), branched poly(ethyleneimine) (PEI; average Mn 2000 g/mol; Polysciences), 4-arm PEG-NH_2 HCl salt (4-arm PEG-NH_2; Mn 5000 g/mol; JenKem), SVA-PEG-SVA (SVA; average Mn 3400; Laysan Bio) were all used as received.

Characterization

Proton and carbon nuclear magnetic resonance (^{1}H-NMR, ^{13}C-NMR) spectra were obtained on an Agilent 500MHz spectrometer in $CDCl_3$. The molecular weight and polymeric distribution were determined using gel permeation chromatography (GPC) in tetrahydrofuran (THF) as the mobile phase with flow rate of 1.0 mL/min. GPC analyses were performed on an OptiLab DSP Interferometric Refractometer (Wyatt Technology) fitted with two identical Jordi Gel DVB columns (Jordi Labs, 250 mm x 10 mm, 10^5 Å pore size). Matrix-assisted laser desorption/ionization (MALDI-TOF) was performed on a Bruker autoflex Speed spectrometer equipped with a SMART-beam II and a flash detector. Differential scanning calorimeter (DSC) spectra was taken on Q100 TA instrument calorimeter and used to determine melting point (mp).

Synthesis of the SA crosslinker (NHS-SA-PEG-SA-NHS)

Synthesis of SA-PEG-SA. PEG (5 g, 1.6 mmol) was melted in a tri-neck round bottom flask at 120 ^{o}C with a stirring mechanism. Once melted, the flask was put under vacuum and the temperature was then decreased to 80 ^{o}C and allowed to stir for 30 minutes. The flask was purged with nitrogen three times.

Succinic anhydride (SA) (0.75 g, 7.5 mmol) was added to the flask. The reaction was stirred under nitrogen for 18 hours. The contents were then dissolved in minimal DCM, and precipitated in diethyl ether. Finally, the product was filtered and dried under vacuum for 1 day (white solid, 99 % yield).

^{1}H NMR (500MHz), $CDCl_3$: δ 2.62 (m, 8H), 3.64 (overlap, 288H), 4.24 (m, *J*=4.6 Hz, 4H) ppm;

^{13}C NMR (500 MHz), $CDCl_3$: 174.0, 172.1, 70.5, 63.8, 29.3, 28.3 ppm;

Synthesis of NHS-SA-PEG-SA-NHS. SA-PEG-SA (4 g, 1.3 mmol) was added to a dry, round bottom flask and dissolved in dry DCM. NHS (0.4 g, 3.8 mmol) and DCC (0.8 g, 3.8 mmol) were added and the flask was purged with argon. The mixture was stirred for 18 hours at room temperature. Dicyclohexylurea was filtered, the solution was concentrated, and precipitated in diethyl ether. The resulting product was collected through filtration and dried on vacuum overnight (white solid, 98 %).

^{1}H NMR (500MHz), $CDCl_3$: δ 2.70 (t, *J*=1.0 Hz, 4H), 2.77 (t, *J*= 1.0 Hz, 8H), 2.89 (t, *J*=1.0 Hz, 4H), 3.57 (overlap, 296H), 4.20 (t, *J*=1.0 Hz, 4H) ppm;

^{13}C NMR (500 MHz), $CDCl_3$: δ 170.9, 168.9, 167.6, 70.7, 64.1, 28.6, 26.2, 25.5 ppm;

MALDI-TOF (pos): M_w: 3600 m/z

GPC: M_n: 2893 g/mol; M_w: 2949 g/mol; PDI: 1.02

Mp (DSC): 43.5 ºC

SVA-PEG-SVA (Laysan bio)

SVA-PEG-SVA (3400) was commercially purchased from Laysan Bio and stored in the glove box.

^{1}H NMR (500MHz), $CDCl_3$: δ 1.69 (tt, *J*=7.3, 7.4 4H), 1.83 (tt, *J*=6.1, 7.3, 4H), 2.64 (t, *J*=7.3, 4H), 2.83 (b, 8H), 3.49 (t *J*=6.1, 4H), 3.63 (m, 300H) ppm;

^{13}C NMR (500 MHz), $CDCl_3$: δ 169.1, 168.6, 70.4, 30.6, 28.4, 25.5, 21.4 ppm;

MALDI-TOF (pos): M_w: 3700 m/z

GPC: M_n: 4635 g/mol; M_w: 4812 g/mol; PDI: 1.03

Mp (DSC): 47.6 °C

Preparation of hydrogels

PEG crosslinkers were dissolved in 0.1 M phosphate buffer, pH 6.5. The hyperbranched polyethyleneimine (PEI; Mn 2000 g/mol) or 4-arm PEG-NH_2 (Mn 5000 g/mol) was dissolved in 0.3 M borate buffer, pH 8.6. Solutions were mixed and placed in an 8 mm width x 2.5 mm height round Teflon mold, in a humid chamber, at room temperature for 1 hour to allow for complete gelation. The molar ratio of amine to NHS was 1:15 and hydrogels were prepared at either 10, 15 or 20 weight percent (wt %).

Rheological measurements

Rheological measurements were obtained from TA instruments DHR-2 Rheometer. Rheological 8 mm parallel plates were used to perform rheological measurements at 22°C. Oscillatory strain sweeps were performed at a frequency of 0.1 Hz. Frequency sweeps were subsequently performed at all time points over

30 days. Strain was set to 3 %, and the frequency ran from 0.1 Hz to 10 Hz. Data are expressed as mean ± standard deviation (n = 3).

Gelation measurements

The crosslinker and dendron solutions were mixed and put in a 2 mL glass vial. Gelation was tested using the inverted tube test mechanism. Every 10 seconds the tube was inverted. Gelation was defined by the time at which the solution remained at the bottom of the vial when inverted.

Adhesion

Adhesion of hydrogels on *ex vivo* porcine colon tissue was performed on an Instron 5944 Micro-tester. Hydrogels were mixed and placed between two pieces of colon tissue. After allowing gelation for one hour in a humid chamber, a lap shear test following ASTM D3165 protocol for adhesion of the hydrogels on colon tissue was administered.[106] Tissue pieces were pulled apart at a rate of 5mm/min at room temperature until failure in adhesion was detected. Data is expressed as mean ± standard deviation (n = 3).

Hydrolysis kinetics

Dissolution of hydrogel kinetics was observed using ^{1}H-NMR. The SA crosslinker was dissolved in a 0.3M sodium bicarbonate buffered solution in D_2O, pH 8.0. ^{1}H-NMR spectra were obtained at various time points over 6 hours to determine the hydrolysis rate of the crosslinker.

In Vitro Cell Viability

Crosslinker and PEI solutions were passed through a 0.22 μm PVDF filter

prior to mixing and gelation under aseptic conditions. 50 mg, 25 mg, and 10 mg (± 2.5 mg) portions of hydrogel (15 wt%) were placed into permeable cell culture inserts (PES, 3 μm pore)(Cell Treat, 230637). Permeable cell culture inserts containing hydrogel samples were incubated in sterile DI H_2O at 4 ^oC for 16 hours to allow for swelling. NIH3T3 (ATCC, CRL-1658) were cultured in DMEM + 10% BCS + 1% PS at 37^oC in 5% CO_2 and 95% humidified air. All cells were passage 4-8 for the experiments. Cells were seeded at 1.25 X 10^4 cells/cm^2 in 24 well plates and allowed to adhere for 16 hours. Media was exchanged and cell culture inserts with swelled hydrogel were transferred into the wells containing adhered cells. Hydrogel samples were briefly equilibrated to 37^oC prior to transfer. Hydrogels were incubated for 24 hours in the presence of cells. Cell culture inserts were removed and a 1:9 dilution of MTS reagent (Promega, G5421) in media was added to each well. Absorbance (490 nm) was measured after 4 hours. Relative cell viability was determined by normalizing absorbance of cells exposed to hydrogel vs a non-exposed control. All experiments were completed in triplicate and error bars represent 1 standard deviation from the mean.

Microbial culture.

Clinical isolates *Escherichia coli* ADR129Q and *Bacteroides fragilis* CFPLTA004_1B were obtained from children with cystic fibrosis. Prior to inoculation of hydrogels, *E. coli* isolates were cultured aerobically overnight in LB (lysogeny broth) and *B. fragilis* isolates were cultured anaerobically for 48 hours on blood agar (TSA + 5% sheep's blood) using the GasPak system. After growth,

the *B. fragilis* isolate was scraped into 1mL PBS and homogenized. 1mL each of *B. fragilis* and *E. coli* were centrifuged for 30s at 16,000 x g and resuspended in PBS. Each isolate was then normalized to OD600 of 1.0 in PBS for agar plate experiments and OD600 of 0.1 in minimal medium, as reported (bioproject accession number PRJNA557692), for microscopy experiments.

Agar plate experiments.

Hydrogel discs (8 mm diameter x 2.5 mm height) were placed onto LB agar (for *E. coli*) or TSA + 5% sheep's blood agar (for *B. fragilis*), and 5uL of bacteria or PBS was added to the top of each hydrogel. Plates where then incubated at 37^{o}C for 24 hours aerobically (*E. coli*) or anaerobically (*B. fragilis*). After 24 hours, hydrogels were removed, and the agar plates were incubated for an additional 24 hours under the appropriate conditions for each organism to test for bacterial growth below the hydrogel as a measure as to whether the microbes could transit through the hydrogel.

Microscopy.

300uL of SA + 4-arm PEG-NH2 was inoculated into each well of an 8-well plate for microscopy (Cellvis, catalog #C8-1.5H-N). To visualize bacteria, Syto9 was added to each culture prior to hydrogel inoculation. Bacterial cultures were inoculated either on top of the hydrogel, or below hydrogels that had first been perforated with a pipette tip. Plates where then incubated at 37^{o}C for 24 hours aerobically (*E. coli*) or anaerobically (*B. fragilis*) using the GasPak system. Plates were imaged both before and after incubation to determine whether top-inoculated

bacteria were able to cross the hydrogel.

Image acquisition and data analysis.

Microscopy was conducted on a Nikon Eclipse Ti inverted microscope equipped with a Hamamatsu ORCA-Flash 4.0 camera running on Nikon Elements AR. Fast scan mode and 2X2 binning was used and Images were acquired through a Plan Fluor 40x DIC M N2 objective. Images were processed in ImageJ in which background was subtracted and signal strength quantified by measuring mean signal intensity/pixel through the Integrated Density (IntDen) function.

Statistical analysis.

Data were analyzed with Graph Pad Prism 8. Wells treated with medium-only served to determine background fluorescence, which was subtracted from each sample before analysis. Error bars represent standard deviation of the results from three biological replicates each performed with three technical replicates or more. A student's T-test was used to compare results and to assess significance and a $p < 0.05$ is significant.

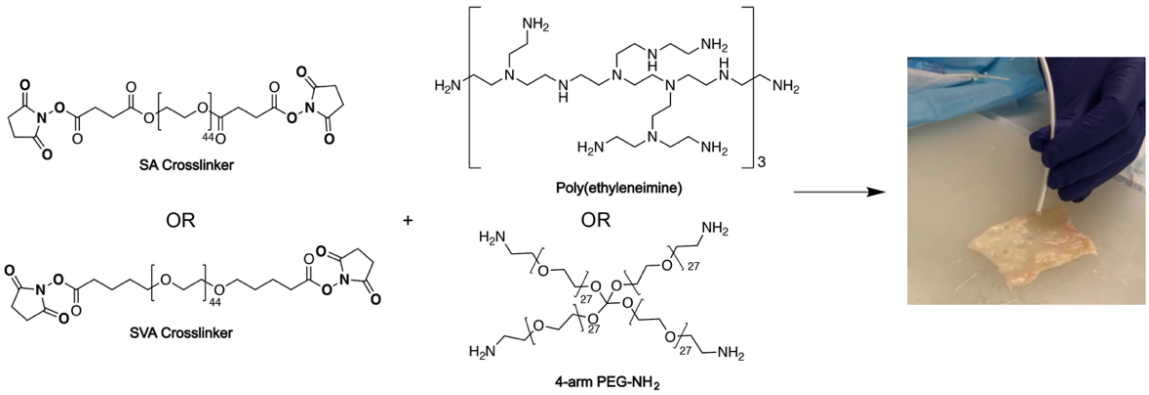

Figure 3.1: Hydrogel formation on *ex vivo* colon tissue.

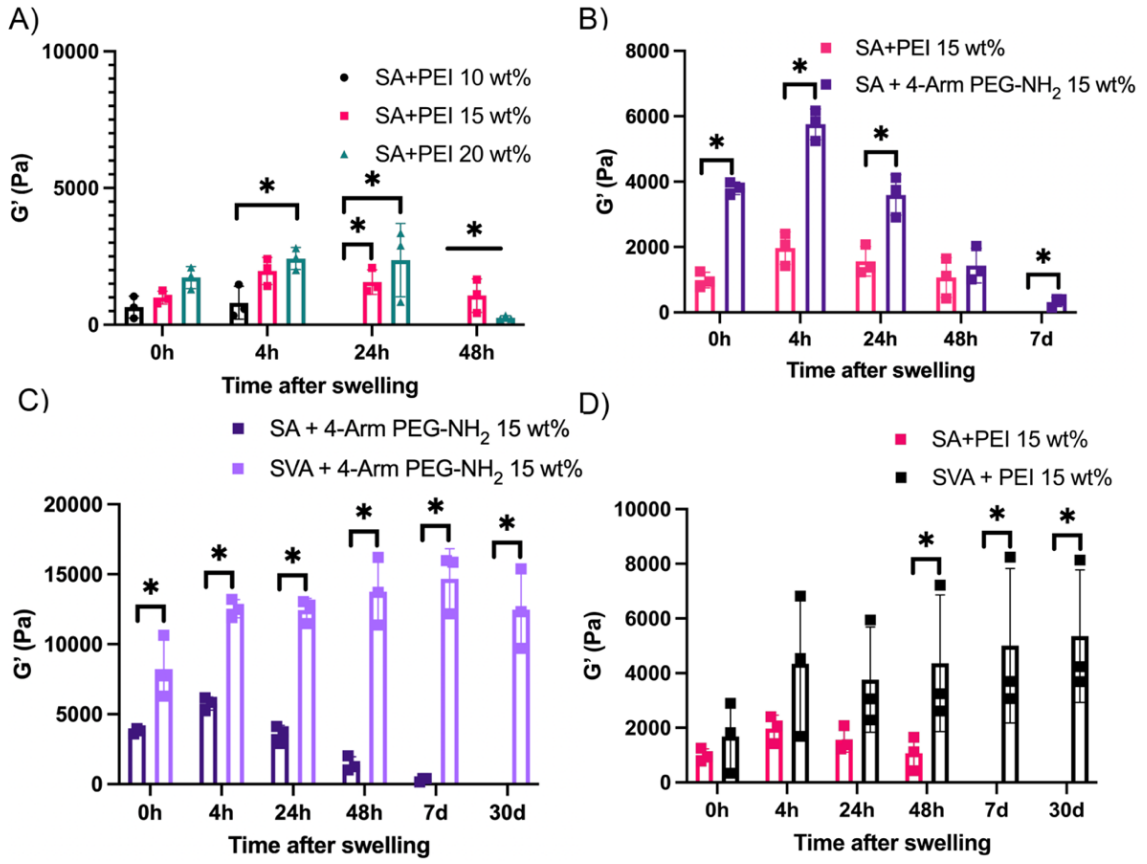

Figure 3.2: A. Strength (G') of hydrogels comprised of SA crosslinker (with ester) + PEI dendron at varying weight percents. B. G' of SA crosslinkers (with ester) with either PEI or 4-arm PEG-NH_2 dendrons. C. G' of SA (with ester) and SVA (without ester) crosslinkers with 4-arm PEG-NH_2 dendrons. D. G' of SA (with ester) and SVA (without ester) crosslinkers with PEI. All rheometry is recorded over time after swelling.

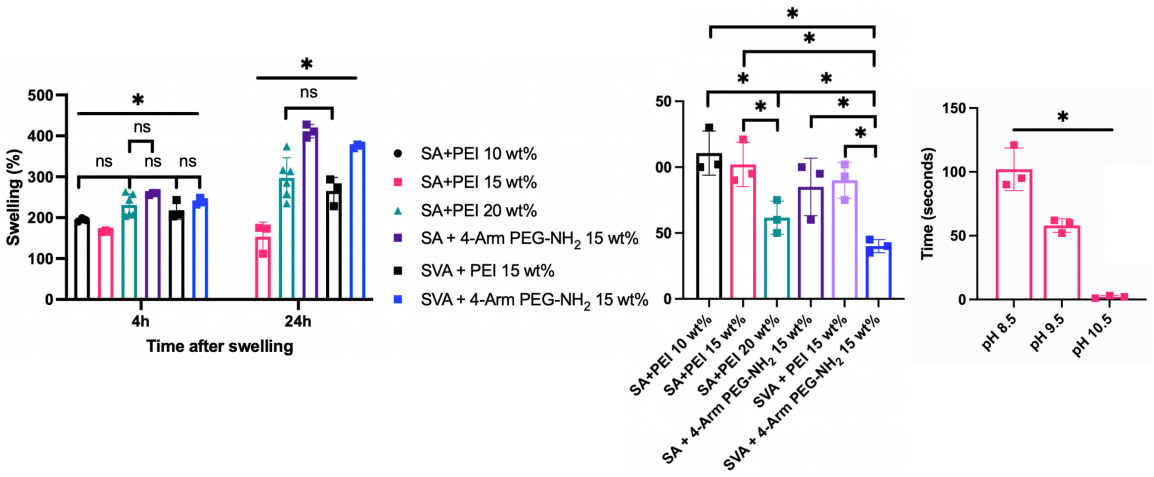

Figure 3.3: A. Swelling of hydrogels over time B. Gelation time of hydrogels C. pH dependent gelation.

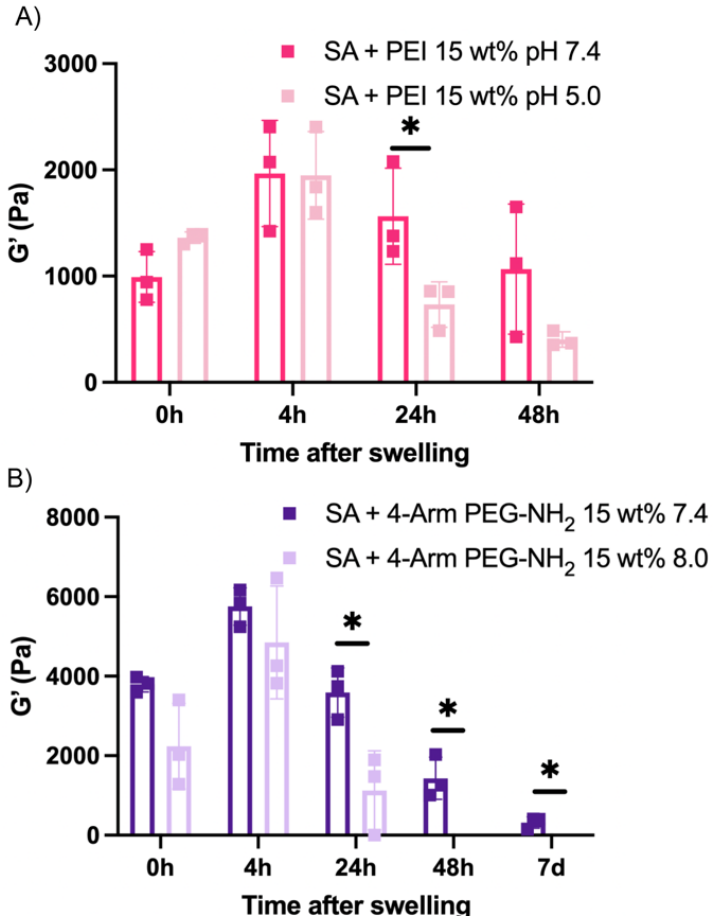

Figure 3.4. Storage modulus of hydrogels swelled in A. SA + PEI pH 7.4 and pH 5.0. B. SA + 4-arm PEG-NH_2 pH 7.4 and pH 8.0

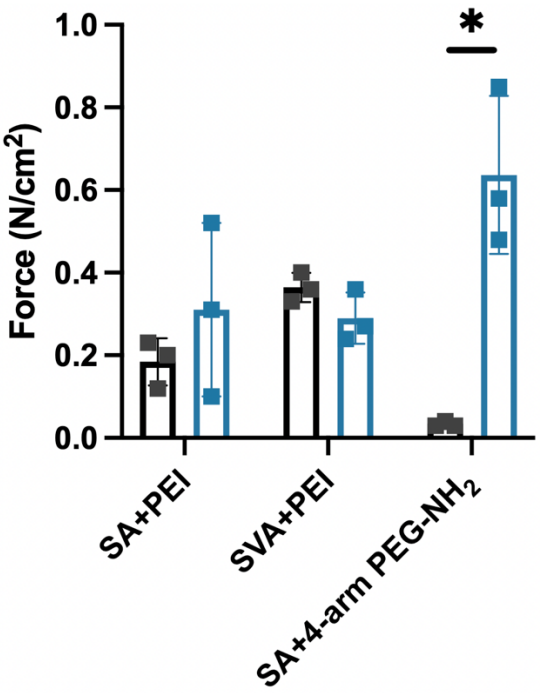

Figure 3.5. Adhesion of hydrogels on colon tissue with mucosa layer intact (black) and without mucosa layer (blue).

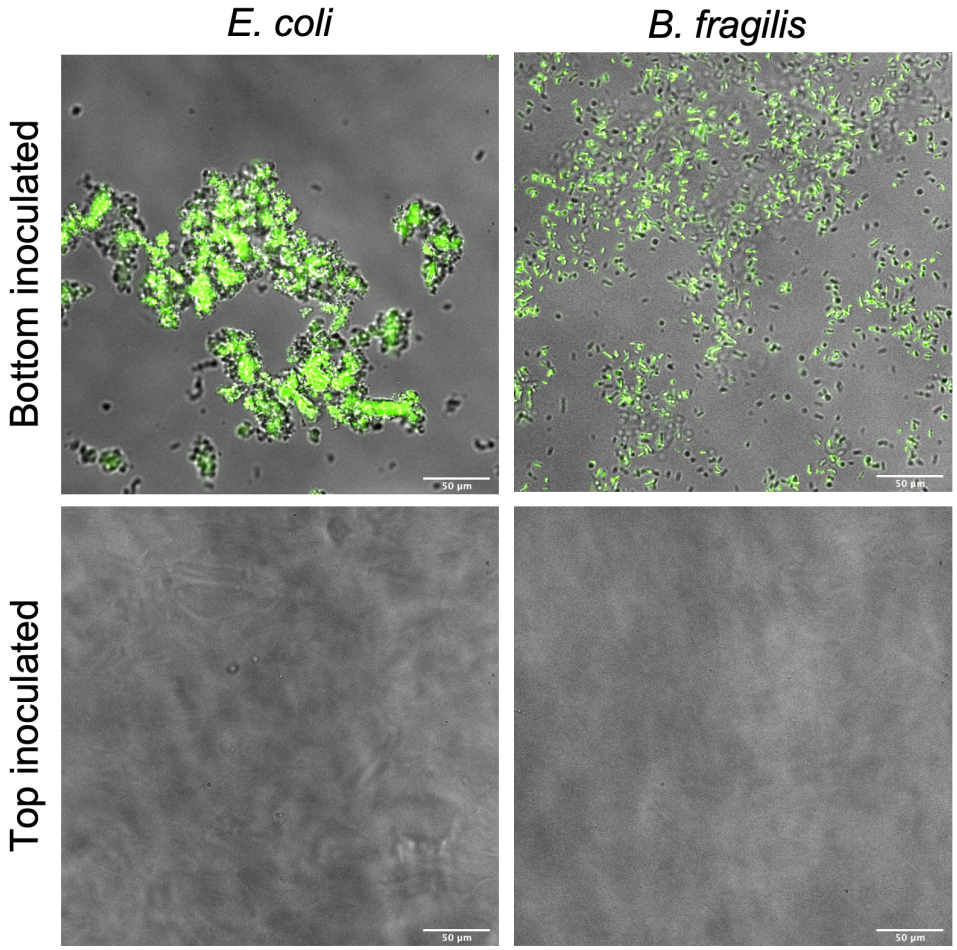

Figure 3.6. Bacterial mitigation by SA + 4-arm PEG-NH_2. The presence of *E. coli* (left) and *B. fragilis* (right) was assessed in perforated hydrogels where bacteria were inoculated into the bottom of the well (top two panels) and non-perforated hydrogels in which bacteria where onto the surface (bottom two panels). Three independent experiments were performed, each with three technical replicates. Representative images of merged brightfield and Syto9 staining are shown here.

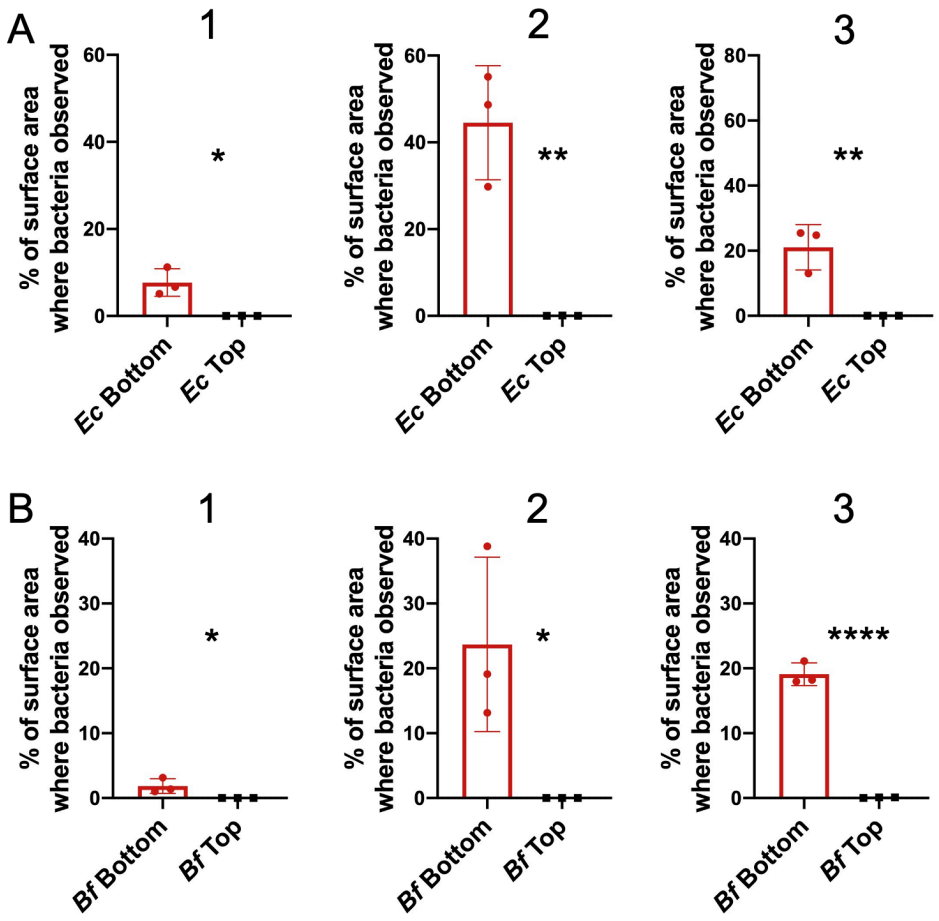

Figure 3.7. Surface area of Syto9-stained bacteria in glass bottom plates containing and SA + 4-arm PEG-NH2 24h after the inoculation of *E. coli* (A) and *B. fragilis* (B). The presence of bacteria was measured in three independent experiments. The surface area occupied by bacteria was compared between perforated hydrogels where bacteria were inoculated into the bottom of the well and non-perforated hydrogels in which bacteria where inoculated onto the surface. Each independent experiment was performed with three technical replicates. Error bars represent standard deviation, *,** and **** indicate a difference of bacterial surface area that is significant at a P value of less than 0.05, 0.01 and 0.0001, respectively.

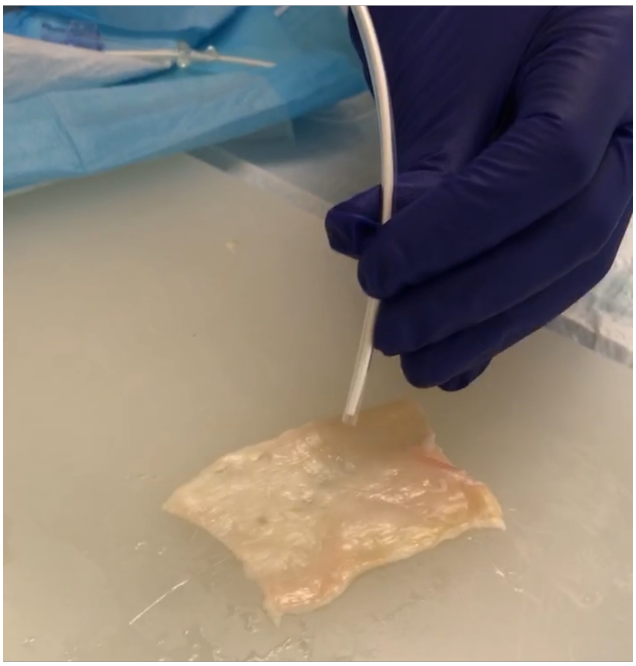

Figure 3.8. *ex* vivo hydrogel application on colon tissue via a dual lumen catheter.

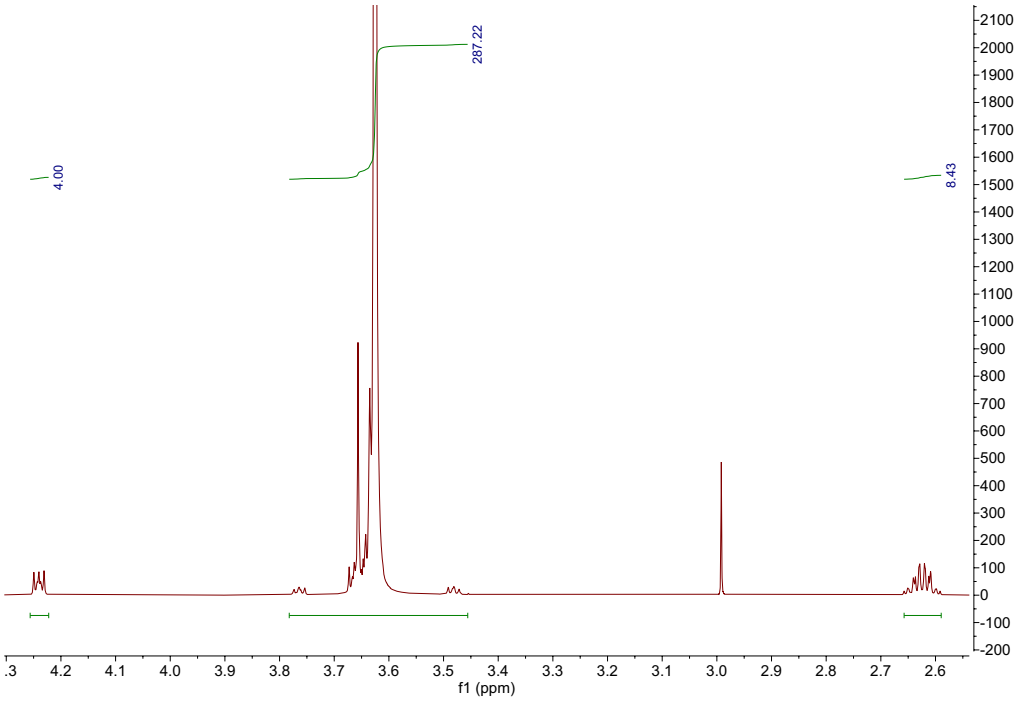

Figure 3.9. ^{1}H-NMR of SA-PEG-SA.

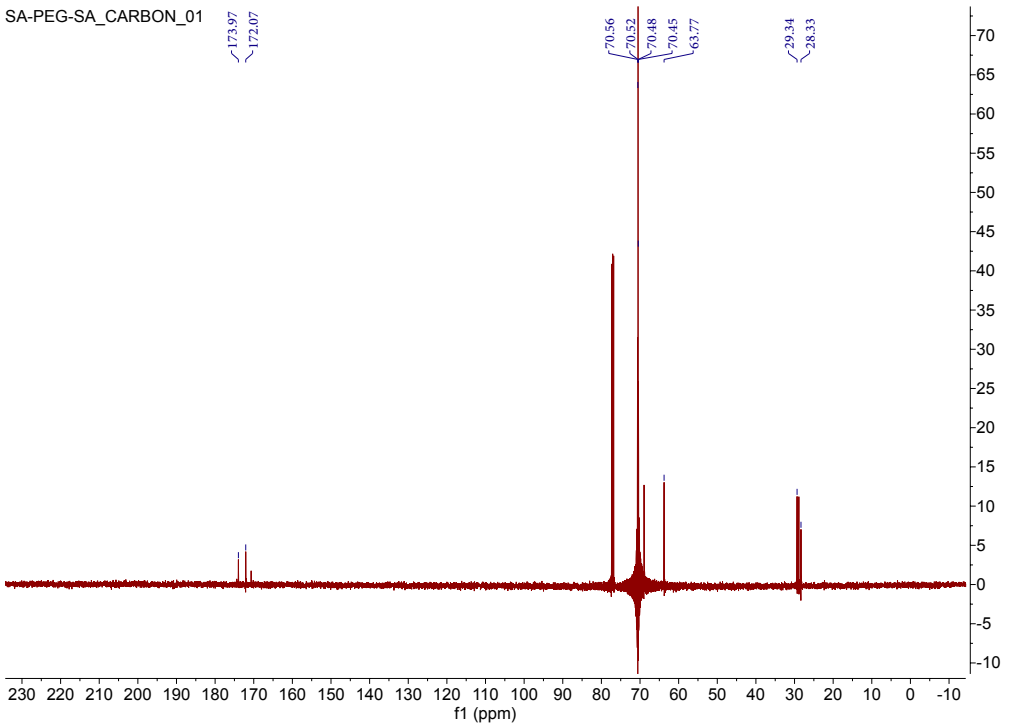

Figure 3.10 ^{13}C NMR of SA-PEG-SA.

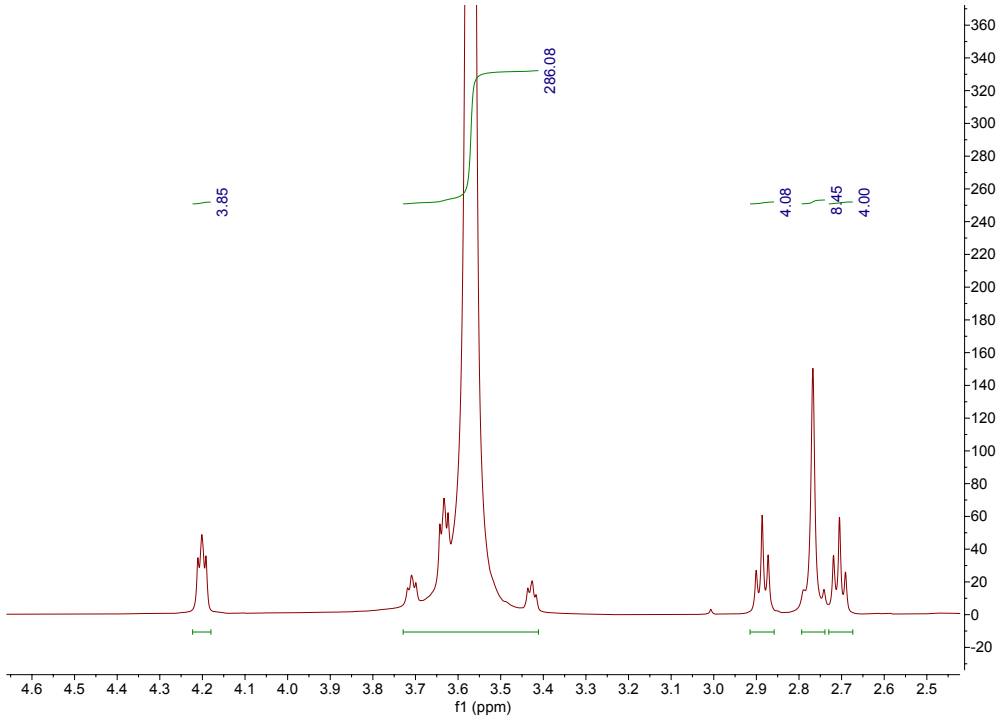

Figure 3.11. ^{1}H-NMR of SA Crosslinker

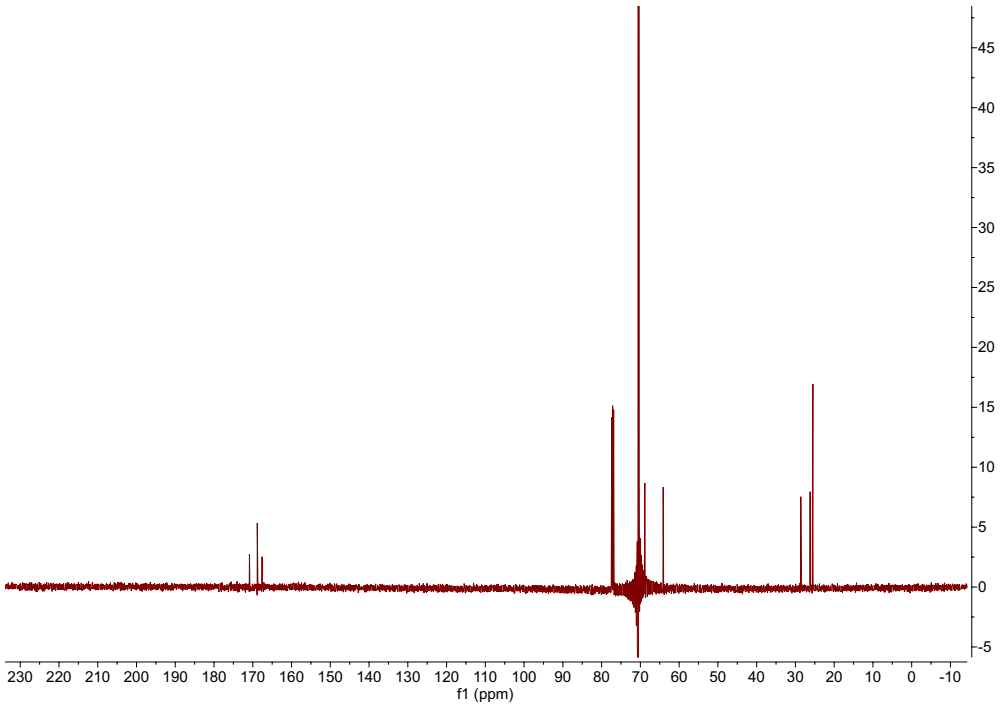

Figure 3.12. ^{13}C-NMR of SA Crosslinker.

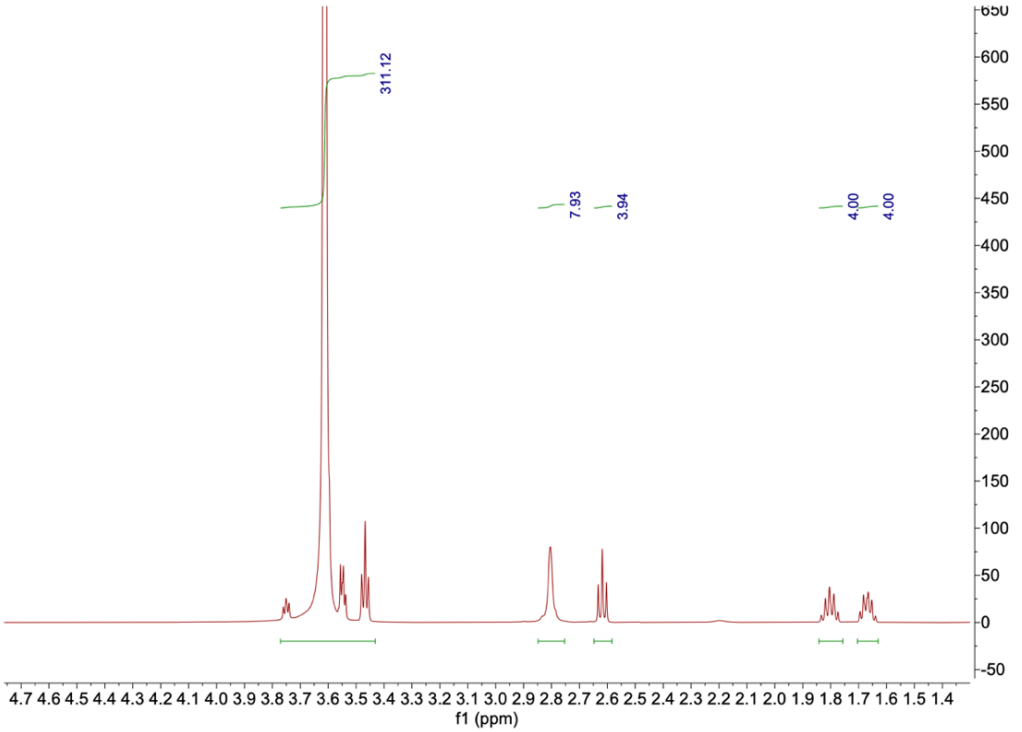

Figure 3.13. ^{1}H-NMR of SVA crosslinker.

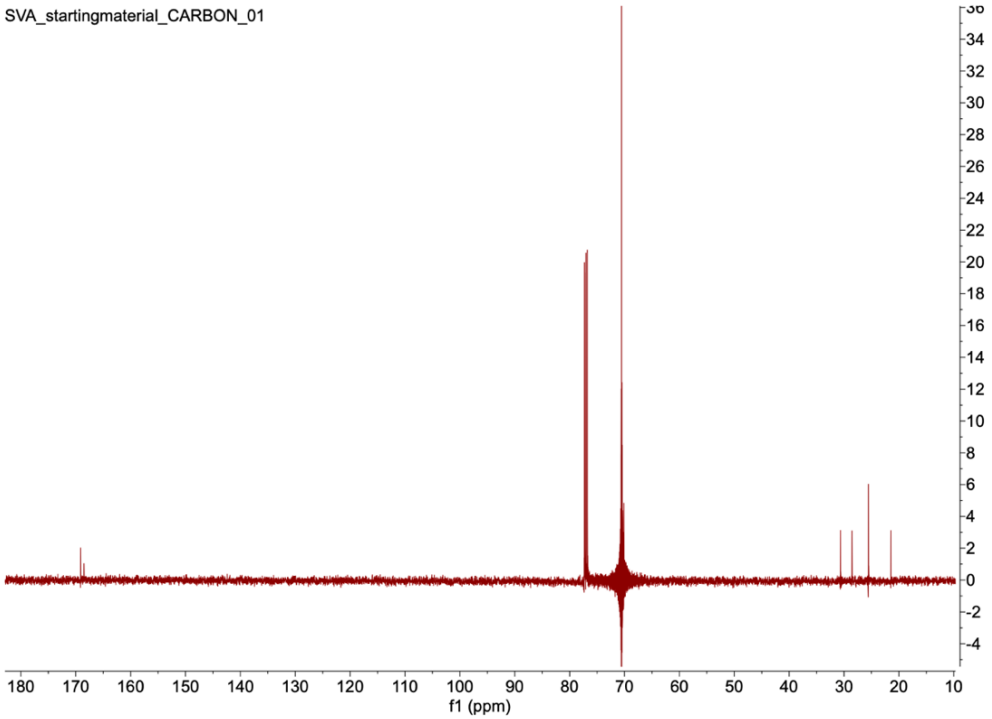

Figure 3.14. ^{13}C-NMR of SVA crosslinker.

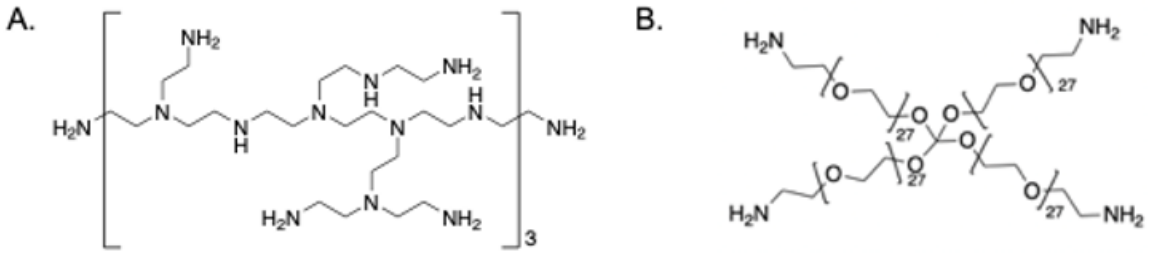

Figure 3.15. A. PEI. **B.**4-arm PEG-NH_2.

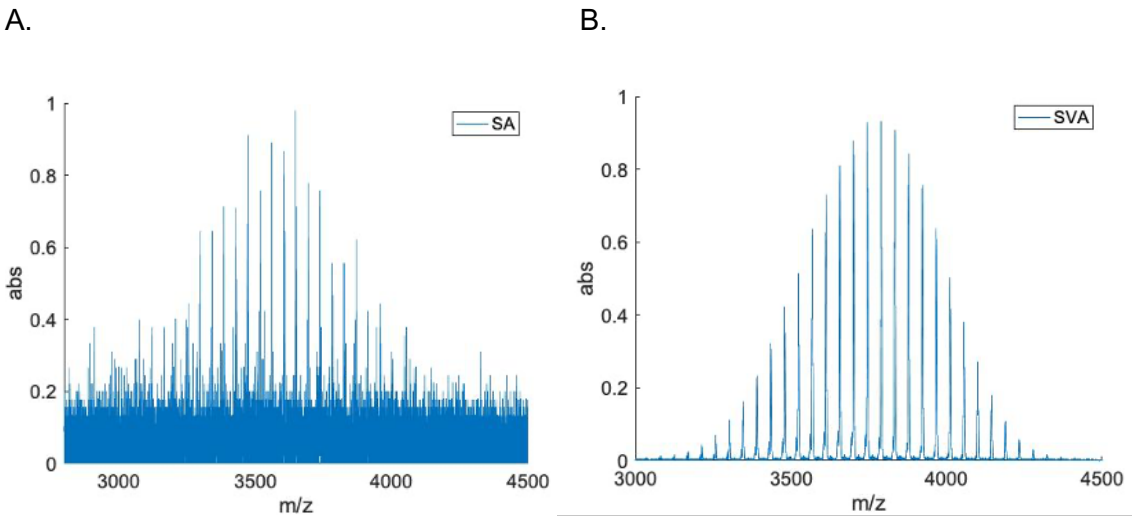

Figure 3.16. MALDI spectrum of A) SA crosslinker and B) SVA crosslinker.

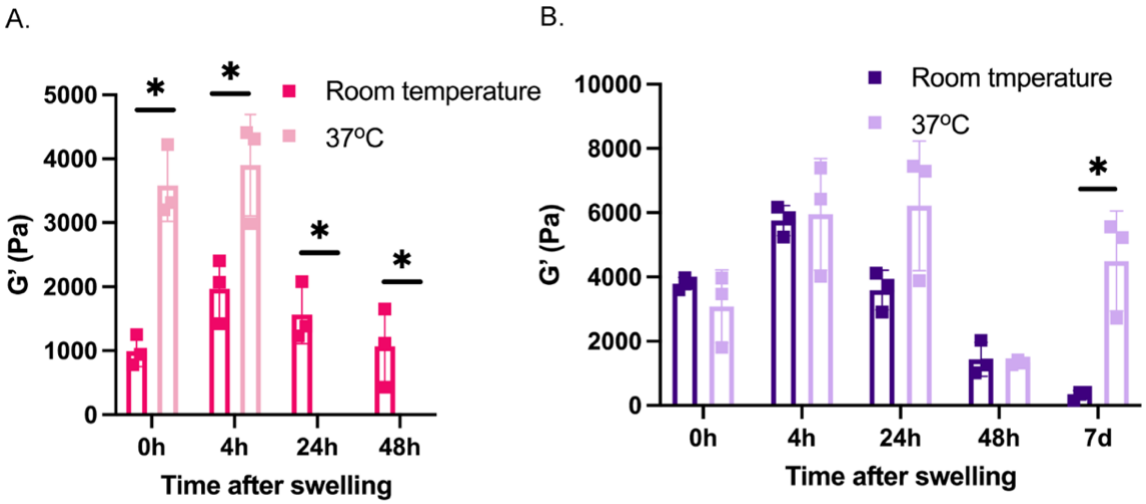

Figure 3.17. A) G' of SA + PEI hydrogels B) SA + 4-arm PEG-NH_1 at room temperature as compared to 37°C.

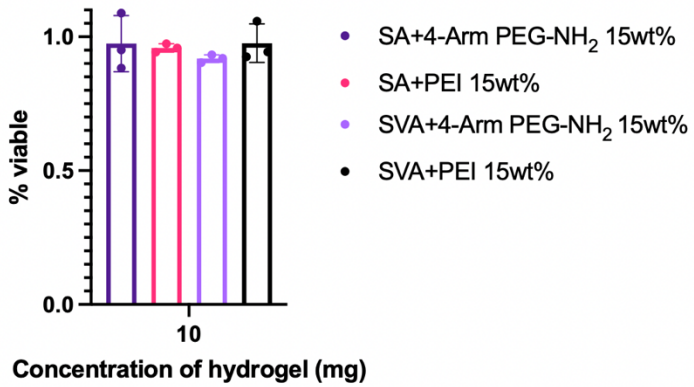

Figure 3.18. Cytotoxicity of 10mg hydrogels against NIH3T3 fibroblasts.

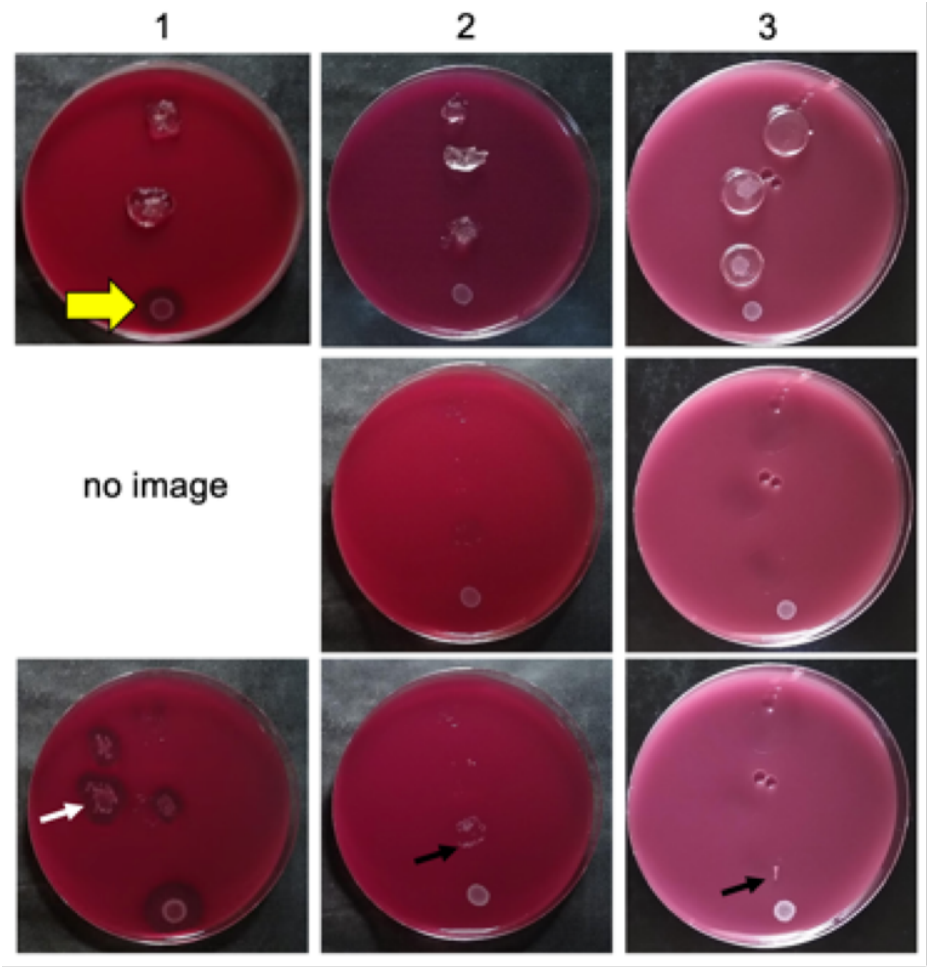

Figure 3.19. This agar plate assay tests whether *B. fragilis* can cross SA + 4-arm PEG-NH_2 hydrogel b placing hydrogels on a TSA + 5% sheep's blood agar, applying the bacteria to the surface of the hydrogel and assessing for subsequent *B. fragilis* growth on the agar after 24 and 48 hours total incubation time. Three independent experiments

were performed, with n = 3 control and n = 4—5 *Bacteroides*-inoculated hydrogel discs per experiment. For each plate, bacteria was spotted directly onto the plate as a positive control (yellow arrow). One representative plate is displayed for each independent replicate. The apical side of each hydrogel was inoculated with either 10uL sterile PBS or 10 uL *B. fragilis* culture in PBS at 1 OD_{600}/mL. Plates were incubated anaerobically for 24 hours at 37^{o}C (top row). After 24 hours, hydrogels were removed (middle row), and plates were incubated for an additional 24 hours under the same conditions (bottom row). After 24 hours, *B. fragilis* growth was apparent on the apical side of the hydrogels but not on the agar, indicating that *B. fragilis* did not cross the hydrogel in high abundance. After 48 hours, contamination was visible in 11/14 total technical replicates. Of these, 10/11 were most likely edge contamination that occurred while the hydrogel was being removed from the plate (black arrows). In experiment 1, hydrogels were flipped over onto the plate after 24 hours to confirm viability of *B. fragili* on the apical side of the hydrogel. Growth derived from the apical side of the hydrogel at 48 hours indicates the *B. fragilis* was still viable (white arrow).

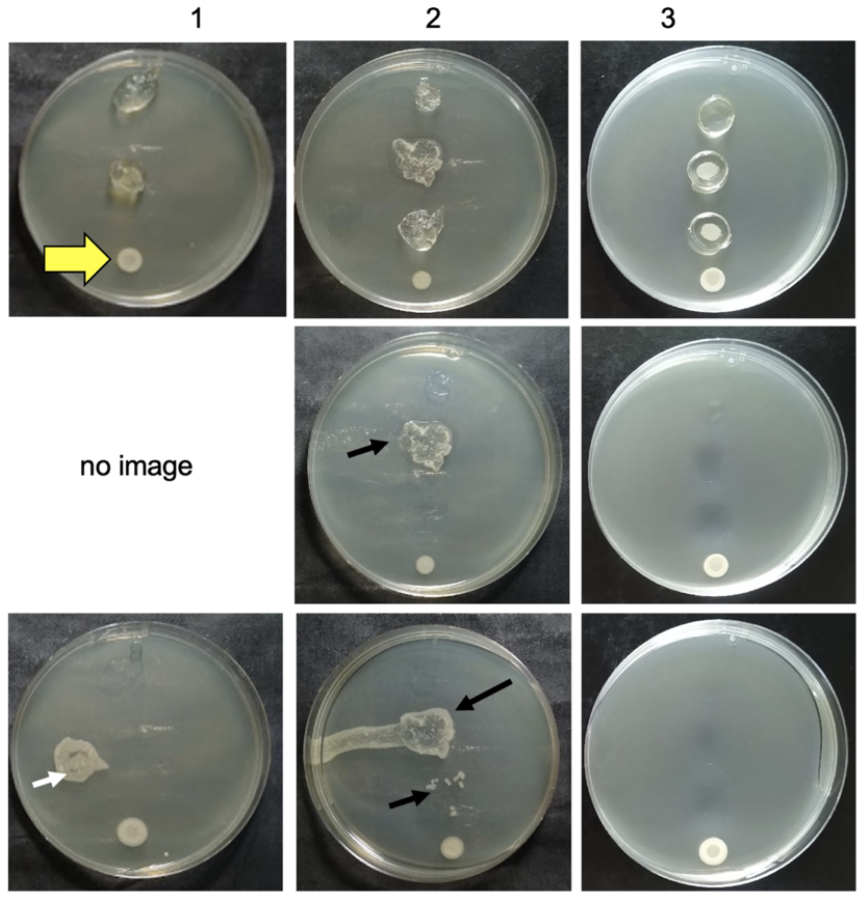

Figure 3.20. This assay tests whether *E. coli* can cross SA + 4-arm PEG-NH_2 hydrogel by placing hydrogels on a LB agar plate, applying the bacteria to the surface of the hydrogel and assessing for subsequent *E. coli* growth on the agar plate after 24 and 48 hours total incubation time. Three independent experiments were performed, with n = 3 control and n = 4-5 *E. coli*-inoculatd hydrogel discs per experiment. One representative plate is displayed for each independent replicate. For each plate, bacteria was spotted directly onto the plate as a positive control (yellow arrow). The apical side of each hydrogel was inoculated with either 10uL sterile PBS or 10uL *E. coli* culture in PBS at 1 OD_{600}/mL. Plates were incubated aerobically for 24 hours at 37°C (top row). After 24 hours, hydrogels were removed (middle row), and plates were incubated for an additional 24 hours under the same conditions (bottom row). After 24 hours, *E. coli* growth was apparent on the apical side of the hydrogels but not on the agar for those *E. coli*-inoculated hydrogels that remained intact (n = 11/15), indicating that *E. coli* did not cross the hydrogel in high abundance. At 48 hours, plate contamination was visible for n = 8/15 discs (black arrows). All of the 24 hour and the majority of the 48 hour contamination occurred during experiment 2. These hydrogels were slightly thinner than in other experiments and some had melted at 24 hours, which si the most likely cause of contamination. In experiment 1, hydrogels were flipped over onto the plate after 24 hours to confirm viability of *E. coli* on the apical side of the hydrogel. Growth from the apical side at 48 hours indicates that *E. coli* was still viable (white arrow).

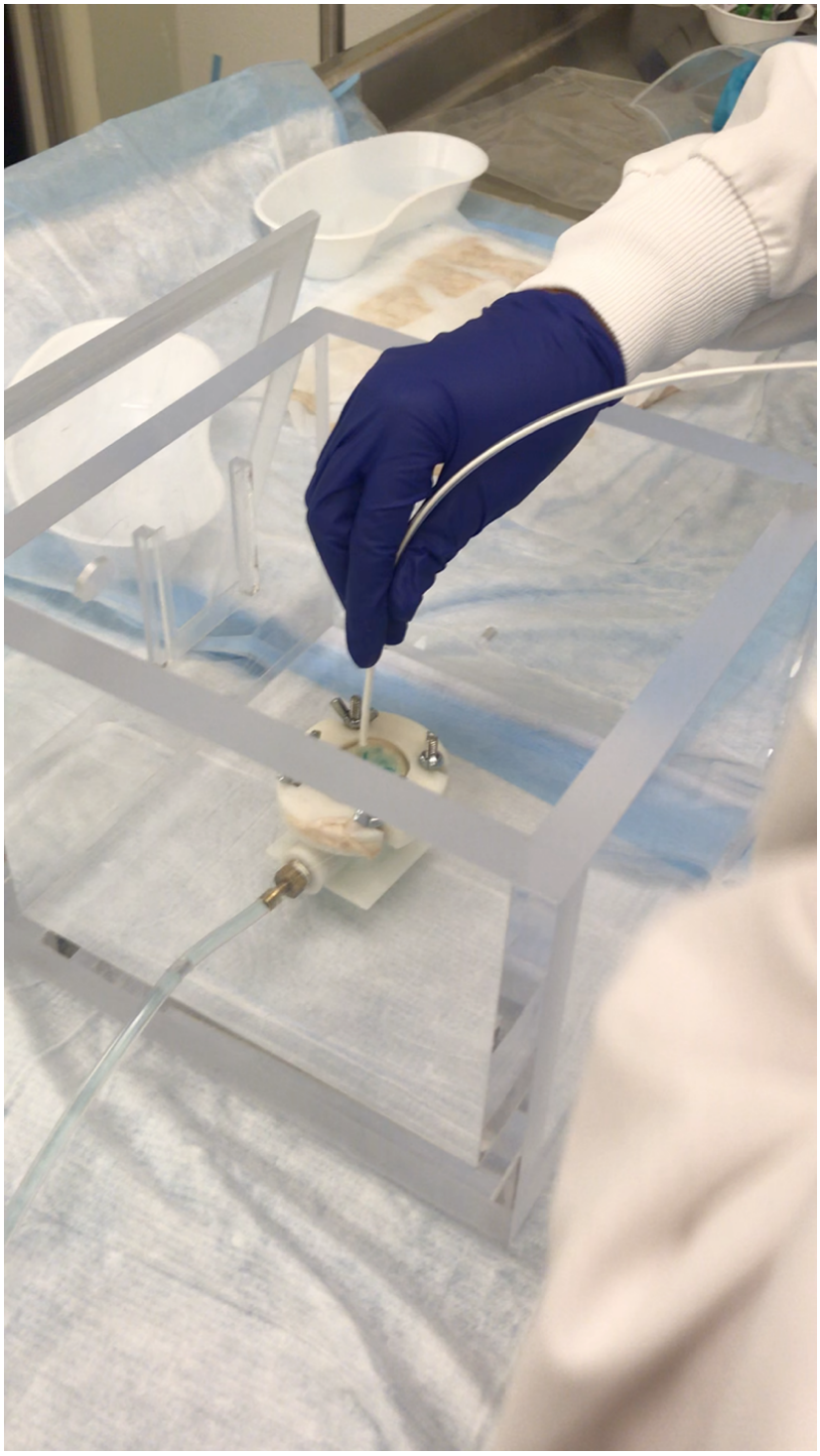

Figure 3.21. Photograph of the SA+PEI hydrogel application on *ex vivo* colon tissue using the dual lumen catheter.

CHAPTER 4. *In situ* forming and dissolvable hydrogel based vascular occlusion devices: An alternative to cross-clamps

4.1 Introduction

Coronary-artery bypass grafting (CABG) is the most common, major surgical procedure performed with > 400,000 procedures annually in the US and > 800,000, globally.[135–137] During this procedure, cross-clamps compress the vessel and provide temporary occlusion of the vessel, removing blood from the surgical field of interest.[138–143] These clamps, also known as vascular occlusion clamps, damage endothelial cells, promote thrombus formation, cause graft failure and incite embolisms.[138–145] Materially, vascular occlusion clamps are metal or plastic, and possess flat or jagged edges like “teeth” to pinch and occlude the vessel, namely the hydrajaw, softjaw, safejaw and tractionjaw.[139,140,143,146] The average cross-clamp time during CABG surgery is 55.1 ± 23.6 minutes, and studies show that any duration longer than 30 minutes results in vessel damage due to cross-clamp use.[139–141,143,144,146,147] During this time, cross-clamped vessels sustain external pressures anywhere from 411-811 mmHg, ten-fold higher than internal vessel pressure, in order to prevent leakage of blood into the surgical field.[139–141,143,144,146,147] Greater than 50% of local endothelial cells are damaged after 30 minutes of applied cross-clamp pressure.[140,143,146,147] Regeneration of this tissue requires 5-14 days post injury leaving the patient with compromised tissue and sub-optimal vessel performance.[138–141,143,146,147] Damage remains

unavoidable regardless of metal or plastic cross-clamp usage.[140,143,148]

With regards to cross-clamp design and function, we propose an alternative vascular occlusion device: a compliant, adhesive hydrogel which *in situ* polymerizes to form a plug and dissolves on demand within the interior of a vessel to stop and start blood flow, respectively. The device is injected directly into the lumen of the vessel that immediately gels (Figure 4.1). Optimal characteristics of the hydrogel plug, we envision, includes: 1) immediate gelation, 2) dissolution within 10 minutes, 3) mechanical integrity lasting >4 hours, 4) non-cytotoxic with cell viability >85%, 5) sustained burst pressure greater than 180 mmHg, and 6) conforming to the shape of and filling the vessel lumen. We hypothesize that these characteristics will minimize endothelial cell damage, maintain occlusion of the surgical area, and minimize embolism and thrombosis risk from manipulating the vessel with high external pressures, therefore outperforming a conventional, externally applied metal or plastic clamp. Herein, we describe a small library of new, *in situ* polymerizable, and dissolvable hydrogel plugs, their mechanical, swelling, and adhesive properties as a function of composition, as well as their performance as a vascular occlusion clamp alternative in an *ex vivo* vessel model and large animal porcine model.

4.2 Hydrogel synthesis

Hydrogels are three-dimensional, hydrophilic networks used for a variety of applications such as sealants, wound dressings, drug delivery devices, and

adhesives among others.[51,84,146,149–153] Hydrogels are an ideal cross-clamp alternative because of their biocompatibility, adhesivity, ease of administration and use as a liquid precursor prior to gelation, and pliable morphology with strong, tunable mechanical properties capable of withstanding a burst pressure greater than that of an arterial vessel. Specifically, we are investigating a small library of synthetic hydrogels that form *in situ* via a Michael addition reaction between a branched PEI-thiol and a bifunctional maleimide-activated, PEG crosslinker. Within this crosslinker is an internal thioester linkage, susceptible to dissolution via thiol-thioester exchange with a cysteine methyl ester (CME) solution.[61,95,126] After thiol-thioester exchange, the primary amine on CME rearranges to form an irreversible amide bond, preventing reformation of the hydrogel after the polymeric network disassembles (**Scheme 4.1**). We describe the mechanical properties, swelling capabilities, dissolution times, and burst pressure strengths of hydrogels with varying methylene chain lengths of 2, 3, and 4, to identify an adhesive hydrogel suitable as a cross-clamp alternative.

We synthesized a small library of PEG crosslinkers with methylene chain lengths of 2, 3, or 4, for use as hydrogel cross-clamp alternatives (**Scheme 4.2**). We varied the methylene chain lengths to determine its dependence on hydrogel mechanical properties, swelling, dissolution time, and burst pressure. The hydrogels contain an internal thioester for dissolution via thiol-thioester exchange, and maleimide end groups for conjugation with the hyperbranched, poly(ethyleneimine)-thiol (PEI-SH). Briefly, we reacted PEG-diol, and the

respective anhydride (succinic anhydride, glutaric anhydride, or adipic anhydride), to obtain our PEG diacid crosslinker. Next, we functionalized the PEG-diacid with N-hydroxysuccinimide (NHS) end groups, via DCC coupling to afford the crosslinkers 1, 2, and 3. From there, in a flame-dried, round bottom flask, we reacted crosslinkers 1, 2, or 3, with thioglycolic acid, and diisopropylethylamine (DIPEA), in dry dimethylformamide to afford intermediates 1, 2, and 3. We selected thioglycolic acid because of its hydrophilicity adjacent to the thioester, allowing for fast dissolution times, necessary for a hydrogel vascular occlusion device.[61,95,125,154] Following the previous step, we functionalized intermediates 1, 2, and 3 with maleimide reactive end groups via a peptide coupling method using maleimide trifluoroacetic acid, PyBOP, DIPEA, in dry DCM to obtain the final crosslinkers **4, 5, and 6** with methylene chain lengths of 2, 3, and 4, respectively.. All yields for the above reactions were above 80%. We characterized these crosslinkers by ^{1}H NMR, ^{13}C NMR, GPC, and DSC, and the data is found in the materials and methods section.

Next, we synthesized a thiol-terminated polyethyleneimine (PEI-SH) hyperbranched polymer (**Scheme 4.1B**) to react with the maleimide terminated PEG crosslinkers. The synthesis of PEI-SH involved reacting a pentafluorophenyl-functionalized, 3-(tritylthio)propionic acid with PEI overnight to obtain a trityl-protected PEI-thiol hyperbranched polymer (yield = 68%). The trityl groups were then deprotected using TFA and Et_3Si, resulting in the final, PEI-SH hyperbranched polymer (yield = 96%). The characterization data, which include ^{1}H

NMR, ^{13}C NMR, GPC, and DSC, are found in the materials and methods.

Initially in the PEI-SH synthesis, we reacted 15 equivalents of thiol per PEI molecule to fully thiolate PEI. However, due to the high concentration of thiols per polymer, intra- as well as inter-molecular disulfide bonds formed, as observed visually via a pink solution of PEI-SH in borate buffer, pH 8.6. This minimized the number of available free thiols for a Michael addition reaction with our maleimide-functionalized crosslinkers. Therefore, we reduced the equivalents of thiol reacted with PEI to minimizing the number of inter- and intra-molecular disulfide bonds. Specifically, we determined the number of free amines via a colorimetric TNBS assay (**Figure 2**). We prepared a standard curve based on varying concentrations of PEI and fully thiolated PEI-SH where, specifically, the slope of the RFU vs concentration (ug/mL) graph correlates with the number of free amines on a particular molecule. (**Figure 2**). PEI (MW 1800) has on average 15 free amines, with a TNBS assay slope of 0.007. Fully thiolated PEI-SH, exhibits a slope of 0.000, as expected, signifying zero primary amines on the molecule. Next, we assessed the slope of the line representing the PEI-SH we prepared with 4 equivalents of tritylthiopropionic acid. The slope of that line is 0.002, one third of the slope of unfunctionalized PEI. These data confirm, we thiolated approximately 2/3 of our PEI polymer, or 5-6 primary amines remain. This partial functionalization of PEI will minimize intramolecular and intermolecular disulfide bonds and enable formation a hydrogel with our maleimide-functionalized crosslinkers.

4.3 Hydrogel preparation

Next, we prepared our hydrogels at a ratio of 2:1, crosslinker:$PEI(SH)_4$. The crosslinkers and PEI-SH were dissolved in 0.1M phosphate buffer pH 6.5 and 0.3M borate buffer pH 8.6, respectively. We then loaded each solution into a dual-lumen syringe with a mixing tip and injected into a cylindrical mold to form one, solid hydrogel.

4.4 Gelation

We assessed the gelation kinetics by following the disappearance of the maleimide alkene peak upon mixing the maleimide crosslinkers with mercaptopropionic acid, a PEI-SH mimetic, at 6.70 ppm on ^1H NMR. An NMR spectrum was recorded every 0.4s for approximately 20 seconds after injecting 2 equivalents of mercaptopropionic acid, used as a PEI-SH mimetic *in situ*. We observe no alkene peak at 6.70ppm immediately following injection of PEI-SH mimetic, exhibiting gelation kinetics faster than 0.4s (Fig 4.3). Fast hydrogel gelation is a vital cross-clamp alternative characteristic. Fast gelation allows for quick, *in situ*, application of the hydrogel for vascular occlusion, resulting in a similar prep time as placing standard practice cross-clamps for patients undergoing vessel replacement or CABG procedures.

4.5 Rheological and swelling measurements

After gelation, we determined storage modulus of the hydrogel as an

assessment of its mechanical strength by first performed strain and frequency sweeps to determine the linear viscoelastic region (LVER). The LVER exists to 10 strain %, and is the maximum strain that can be applied to these hydrogels before plastic deformation occurs. Next, we performed a frequency sweep, within the LVER at 3% strain, from 0.1-10Hz. The initial storage moduli of our hydrogels are between 2000-5000Pa. Upon hydrogel swelling in 50mM PBS, crosslinkers **4, 5,** and **6** exhibit decreasing storage moduli (Figure 4.4A). We attribute the declining G' overtime to degradation of the crosslinker via hydrolysis. To estimate the rates of degradation and confirm the location of hydrolysis at the internal thioester instead of the ester, we monitored the ^{1}H NMR crosslinker spectrum over 20 minutes in 0.3M sodium bicarbonate buffer, pH 8.0. The methylene adjacent to the internal thiol shifts from 3.41ppm to 3.17ppm, while the methylene peak adjacent to the ester linkage at 4.15ppm, corresponding to the other terminal methylene on the diacid linkage in the crosslinker (succinic acid, glutaric acid, adipic acid), does not shift during base-catalyzed hydrolysis. This ^{1}H NMR shift confirms selective hydrolysis of the thioester (Figure 4.5). Varying degradation rates, of >4h, >24h, and >7d, for crosslinkers **4, 5,** and **6**, increase relative to the hydrophobic methylene chain lengths of the internal diacid linkage protecting the internal thioesters from hydrolysis. Crosslinker **4** contains an internal succinic acid linkage with two methylenes, while crosslinkers **5** and **6** contain glutaric acid and adipic acid linkages of three and four methylenes, respectively. The longer and more hydrophobic methylene chain length in the crosslinker, the more stable the

thioester is against hydrolytic cleavage, resulting in slower degradation rates.[155] The varying degradation rates, relative to the methylene chain length within crosslinkers **4, 5,** and **6,** allows us to tune the hydrogel mechanical properties through crosslinker structure in order to maintain mechanical integrity for vascular occlusion over 3-4 hours, the average duration with which cross-clamps are in place.[138] Furthermore, we observe swelling of our hydrogels between 200-400% (Figure 4.4B). Swelling reaches its maximum at 24h after submersion in 50mM PBS. Swelling in aqueous solution is advantageous for a hydrogel vascular occlusion device due to its ability to expand in size as it absorbs aqueous fluid from the surrounding environment ensuring the hydrogel continues to occlude the vessel from the surgical field.

4.6 Hydrogel dissolution

Additionally, we assessed the rapid and on-demand dissolution time of our hydrogels via thiol-thioester exchange when submerged in a 0.3M cysteine methyl ester (CME) solution (Scheme 4.2). We performed frequency sweeps at ten-minute intervals, to allow sufficient CME exposure, until the hydrogel network completely disassembles or degrades (G'<300Pa). Upon thiol-thioester exchange, the hydrogel network disassembles and the amine on the CME rearranges to form an irreversible amide bond, preventing reformation of the hydrogel. Dissolution occurs within 10 minutes or less for all three hydrogel formulations (Figure 4.4C). While the acid linkages (succinic acid, glutaric acid and adipic acid) retard

hydrolysis under neutral conditions, the basic conditions of CME solution catalyze the thiol-thioester exchange reaction. Fast dissolution of the hydrogel network via thiol-thioester exchange will minimize the patient's time under anesthesia as well as minimize for the likelihood for an embolism. Furthermore, based on the molecular weights of our hydrogel dissolution components, approximately 11.0 kDa, 3.0 kDa, and 0.2 kDa relative to dextran standards on GPC, below 500kDa – the lower limit for biliary excretion (data in materials and methods), after thiol-thioester exchange, we predict excretion of our adhesive hydrogel vascular occlusion device through the kidneys.[156–158]

4.7 Hydrogel cytotoxicity

Prior to *ex vivo* studies, we assessed the cytotoxicity of our hydrogels against NIH3T3 fibroblasts over 24 hours of exposure. Hydrogels 4 and 5 exhibit a mean cell viability of 60%, while hydrogel 6 shows a mean cell viability of 98% (**Figure 4.6**). We attribute the low cell viability in hydrogels **4** and **5** to the rapid release of succinic and glutaric acid, due to disassembly of the hydrogel network, increases the local acidity in the confined environment of a trans-well plate

4.8 Burst pressure

We then determined the hydrogel burst pressure when applied as a vascular occlusion device in *ex vivo* porcine carotid artery. We injected the macromers into one end of an ex vivo 2 cm porcine carotid artery at a total volume

of 1mL to form the hydrogel. The hydrogel fills the vessels and remains in place. After storing the plugged artery in a humid environment for 30 minutes, mirroring the time during a surgical procedure, we attached the vessel to our in-house burst pressure system with a pressure transducer connected to a computer, and a syringe pump (Figure 4.7). Deionized H_2O was pumped through the vessel at 1mL/min until a leak was observed and we recorded the pressure until failure. The burst pressures for the hydrogels composed of crosslinkers **4, 5**, and **6** are 382 mmHg, 440 mmHg, and 231 mmHg respectively, up to 4x greater than arterial pressure (120/60) (Figure 4.8). A burst pressure of 200-600mmHg is more than sufficient for a hydrogel vascular occlusion device.

4.9 Conclusions

Overall, we describe of a library of hydrogels for use as vascular occlusion devices. The hydrogels possess tunable mechanical properties, swelling, selective dissolution at the thioester, cell viability, and *ex vivo* burst pressure capable of withstanding arterial pressure. In particular, we have exhibited that hydrogel **4:** 1) is stable over 4 hours when submerged in aqueous solution, 2) swells in aqueous environments up to 200%, 3) can be injected *in situ*, 4) sustains a burst pressure greater than 3x that of arterial pressure, 5) is non-cytotoxic, and 6) dissolves on-demand, in less than 10 minutes. This work highlights the variability and tunability of hydrogels for *in situ* application of vascular occlusion and provides further motivation for continued work to assess the *in vivo* efficacy.

4.10 Materials and methods

Materials

NMR spectra were recorded on Varian 500MHz VNMRs; chemical shifts, quoted in parts per million (ppm) calibrated to residual non-deuterated solvent. (^{1}H NMR: $CDCl_3$ at 7.26ppm; ^{13}C NMR: $CDCl_3$ at 77.16ppm.) Coupling constants (*J*) are quoted in Hertz. Multiplicities are reported as: singlet (s), doublet (d), triplet (t), quartet (q), multiplet (m), broad (br), or doublet of triplets (dt). Gel permeability chromatography (GPC) analyses were performed on an OptiLab DSP Interferometric Refractometer (Wyatt Technology) fitted with two identical Jordi Gel DVB columns (Jordi Labs, 250 mm x 10 mm, 10^5Å pore size). Samples were dissolved in THF (2 mg/mL) and passed through a 0.45 μm syringe filter immediately prior to injection. Measurements were taken using a flow rate of 1.0 mL/min at 25˚C with THF as the eluent. The resulting chromatograms were calibrated against polystyrene standards (EasiCal calibration kit, Agilent). Differential scanning calorimetry (DSC) of crosslinkers were recorded on a DSCQ100TA instrument and heated between -50^{o}C and 50^{o}C.

All anhydrous solvents were purchased from Sigma Aldrich. All reagents were purchased from commercial sources and used without further purication. All reactions were carried out under Argon with magnetic stirring. Polyethyleneimine, molecular weight 2000 was purchased from Polysciences Inc.

Synthesis and characterization of compounds

PEG diacid. This polymer was prepared from a previously published protocol (**Scheme 1A**).[159] ^{1}H NMR and ^{13}C NMR spectra were similar to literature.[159]

Crosslinker 1, 2, 3. The synthesis of crosslinkers **1**, **2**, and **3** were based off of a previously published protocol.[97,159–161] ^{1}H NMR and ^{13}C NMR spectra were similar to literature.[159]

Intermediate 1, 2, 3. In a flame-dried, roundbottom flask with a magnetic stir bar, crosslinker **1**, **2**, or **3** (1g) were dissolved in dimethylformamide (DMF). Thioglycolic acid (68.8μL) and diisopropylethylamine (DIPEA) (279μL) were added in that order. The reaction was stirred at room temperature, overnight. The organic phase was extracted with a 1N HCl solution, water and then brine. The organic phase was dried with sodium sulfate, filtered through filter paper, and precipitated in diethyl ether to obtain a white powder (98% yield).

^{1}H NMR (500MHz), $CDCl_3$:

Intermediate 1 - δ 4.22 (tt, *J* = 4.7Hz, 4H), 3.62 (m, 310H), 2.93 (t, *J* = 6.8Hz, 4H), 2.68 (t, *J* = 6.8Hz, 4H) ppm;

Intermediate 2 - δ 4.22 (tt, *J* = 4.8Hz, 4H), 3.63 (m, 308H), 2.86 (t, *J* = 7.2Hz, 4H), 2.61 (t, *J* = 7.3Hz, 4H), 2.38 (t, *J* = 7.4Hz, 4H), 2.30 (t, *J* = 7.4Hz, 4H), 1.97 (t, *J* = 7.3Hz, 4H), 1.60 (m, 8H), 1.39 (m, 4H) ppm;

Intermediate 3 – δ 4.21 (tt, *J* = 4.4, 4.9Hz, 4H), 3.63 (m, 277H), 2.62 (t, *J* = 6.7, 7.2Hz, 4H), 2.34 (t, *J* = 6.7, 7.2Hz, 4H), 1.69 (m, 8H) ppm;

^{13}C NMR (500 MHz), $CDCl_3$:

Intermediate 1 – 195.9, 171.5, 70.5, 64.1, 30.9, 29.1 ppm;

Intermediate 2 - 198.6, 172.7, 70.7, 69.0, 33.5, 32.9, 20.6 ppm;

Intermediate 3 – 197.0, 173.0, 70.5, 63.5, 33.7, 31.0, 24.7, 24.0 ppm

Crosslinker 4, 5, 6. In a flame-dried, round bottom flask with a magnetic stir bar, intermediate **1**, **2**, or **3**, was dissolved in dry methylene chloride. Maleimide-ethylamine trifluoroacetic acid, DIPEA, and PyBOP were added to the reaction. The solution was stirred at room temperature, overnight. The organic phase was extracted using a saturated citric acid solution, water, and brine. The organic phase was then dried with sodium sulfate, filtered through filter paper, and precipitated in diethyl ether to obtain an off-white solid. The solid was dried under vacuum overnight. The solid was then dissolved in water, filtered through a 0.22μm syringe filter, and lyophilized to obtain an off-white solid (80-90% yield).

^{1}H NMR:

Crosslinker 4 – δ 6.71 (s, 2H), 6.55 (b, 1H), 4.23 (tt, *J* = 4.2, 4.9Hz, 4H), 3.62 (m, 322H), 2.96 (t, *J* = 6.8Hz, 4H), 2.74 (t, *J* = 6.8Hz, 4H) ppm;

Crosslinker 5 –δ 6.72 (s, 2H), 6.51 (b, 1H), 4.23 (tt, *J* = 4.8Hz, 4H), 3.63 (m, 297H), 2.73 (t, *J* = 7.3Hz, 4H), 2.42 (t, *J* = 7.2Hz, 4H), 2.01 (m, *J* = 7.2, 7.3Hz, 4H) ppm;

Crosslinker 6 – δ 6.71 (s, 2H), 6.50 (b, 1H), 4.21 (tt, *J* = , 4H), 2.67 (t, 3H), 2.36 (t, *J* = , 4H), 1.67 (m, 8H) ppm;

^{13}C NMR:

Crosslinker 4 – 197.5, 171.9, 134.2, 70.5, 64.0, 32.3, 29.1 ppm;

Crosslinker 5 – 198.2, 172.6, 134.2, 70.4, 63.6, 32.8, 32.3, 20.2 ppm;

Crosslinker 6 – 198.6, 173.1, 134.2, 70.5, 63.5, 33.5, 32.4, 24.6, 24.0 ppm;

M_w (GPC, THF): **4** – 2868 Da, **5** – 3028 Da, **6** – 3351 Da

M_n (GPC, THF): **4** – 2801 Da, **5** – 2955 Da, **6** – 3162 Da

PDI (GPC, THF): **4** – 1.02, **5** – 1.02, **6** – 1.06

Melting point (DSC): **4 –** 41.78°C, **5 –** 40.22°C, **6 –** 45.04°C

Crystallization point (DSC): **4 –** 39.9°C, **5 –** 21.3°C, **6 –** 33.5°C

PEI-STr. PEI (3g) was dissolved in DMF. 3-(tritylthio)propionic-pentofluorophenol (3.4g), HOBt (3.2g), and DIPEA (4.7mL) were added. The reaction was stirred at room temperature, overnight. The reaction was dissolved in methylene chloride, and the organic phase was extracted from sodium bicarbonate, water, and brine. The organic solution was dried over sodium sulfate, filtered through filter paper, and concentrated. The organic solution was precipitated in diethyl ether and dried under vacuum to obtain a light yellow, solid (68% yield).

^{1}H NMR: δ 8.00 (s, 1H), 7.49-7.10 (m, 48H), 3.65-2.01 (m, 60H) ppm;

^{13}C NMR: 162.5, 144.6, 129.5, 127.9, 126.7, 36.5, 35.1, 27.7 ppm;

PEI-SH. In a round bottom flask with a magnetic stir bar, PEI-STr (2g) was solubilized in a minimal amount of methylene chloride. Trifluoroacetic acid (TFA) (12.3mL) and triethylsilane (2.7mL) were added to the stirring solution dropwise, simultaneously. The reaction was stirred for 3 hours at room temperature. Methylene chloride and TFA were removed under vacuum, and redissolved in a

minimal amount of methylene chloride. The solution was precipitated in diethyl ether and the product was dried under vacuum overnight. The product was dissolved in 1N HCl, filtered through a 0.22μm syringe filter, and lyophilized to afford a light-yellow solid (96% yield).

^{1}H NMR: 7.9 (s, 1H), 3.61-2.49 (m, 217.13H) ppm;

^{13}C NMR: 163.1, 162.8, 117.6, 115.3, 39.5, 22.7 ppm;

M_w (GPC, Aqueous): 5660 Da

M_n (GPC, Aqueous): 6994 Da

PDI (GPC, Aqueous): 1.12

Mp (DSC): 15.6^{o}C

Dissolution components of:

4 –

M_w (GPC, Aqueous): 12570, 1400, 247 Da

M_n (GPC, Aqueous): 10611, 1370, 209 Da

PDI (GPC, Aqueous): 1.18, 1.02, 1.18

5 –

M_w (GPC, Aqueous): 11601, 1426, 262 Da

M_n (GPC, Aqueous): 9517, 1397, 255 Da

PDI (GPC, Aqueous): 1.22, 1.02, 1.16

6 –

M_w (GPC, Aqueous): 10707, 2281, 264 Da

M_n (GPC, Aqueous): 11408, 2858, 325 Da

PDI (GPC, Aqueous): 1.10, 1.09, 1.14

Methods

TNBS assay

We reacted 0.01% (w/v) solution of 2,4,6-trinitrobenzene sulfonic acid (TNBS) with PEI-SH in 0.1M sodium bicarbonate buffer, pH 8.5. After incubating the solution at 37 ^{o}C for 2 hours, we diluted the resulting yellow solution with 10% SDS and 1N HCl to stop the reaction. The absorbance was read at 335nm and correlates to the number of primary amines present on solution.

Rheological measurements

Rheological data was obtained from a TA Instruments DHR-2 Rheometer. Crosslinkers and PEI(SH), at a ratio of 2:1 Maleimide:SH, at 25 wt%, were dissolved in 0.1M phosphate buffer, pH 6.5 and 0.3M borate buffer, pH 8.5, respectively. The hydrogel components were reacted together in a cylindrical tube and formed instantaneously. Hydrogels were left in a humid chamber at room temperature for 1 hour to ensure complete gelation. Frequency sweeps were measured between 0.1Hz and 10Hz, at room temperature and 3% oscillatory strain between 8mm parallel plates. Data are expressed as a mean ± standard deviation with n = 3.

Swelling

Hydrogels were swollen in 50mM PBS buffer, pH 7.4 over 30 days or until dissolution. The swelling ratjo was determined according to the following equation:

$$Swelling\ ratio = \frac{final\ mass}{initial\ mass} X\ 100$$

where the initial mass refers to the mass of the hydrogel prior to submerging in PBS. The final mass is the mass of the hydrogel at specific time points after submersion in PBS.

Dissolution

Hydrogels were submerged in 0.3M Cysteine methyl ester (CME) solution, and a frequency sweep from 0.1 Hz – 10 Hz at 3% strain and room temperature on the rheometer was performed every 10 minutes until dissolution (G' < 300 Pa).

Kinetics

Reaction kinetics for hydrogel gelation and hydrolysis were followed via ^{1}H NMR in D_2O, pH 7.4 and 8.0, respectively. An initial ^{1}H NMR spectrum of the crosslinker was performed and subsequently a thiol mimetic, mercaptopropionic acid, was injected into the NMR tube. ^{1}H NMR spectra were taken ever 0.4s for 20 seconds and gelation was assessed via the disappearance of the maleimide alkene peak at 6.71 ppm.

Crosslinkers were dissolved in 0.3M sodium bicarbonate buffer, pH 8.0, and ^{1}H NMR spectra were obtained every minute until complete hydrolysis of the thioester from 3.41 to 3.18ppm.

Cytotoxicity

Hydrogels were placed on transwells and directly exposed to NIH3T3 mouse embryo fibroblasts through cell media for 24 hours. The hydrogels were

subsequently removed and an MTS cell viability assay was performed.

Burst pressure

Hydrogel components were dissolved in 0.5mL buffer each, at 25 wt% and loaded into a dual-lumen syringe with a mixing tip. The hydrogels were injected into *ex vivo* porcine carotid arteries, 4-6mm in diameter, and left at room temperature for 30 minutes to allow for complete gelation. Hydrogel-injected carotid arteries were loaded onto our in-house burst pressure system with a syringe pump and pressure transducer. D_2O was pumped through the syringe pump at a rate of 1mL/min until a leak in the hydrogel-carotid artery sample was observed. The peak pressure detected from the pressure transducer was recorded as the burst pressure.

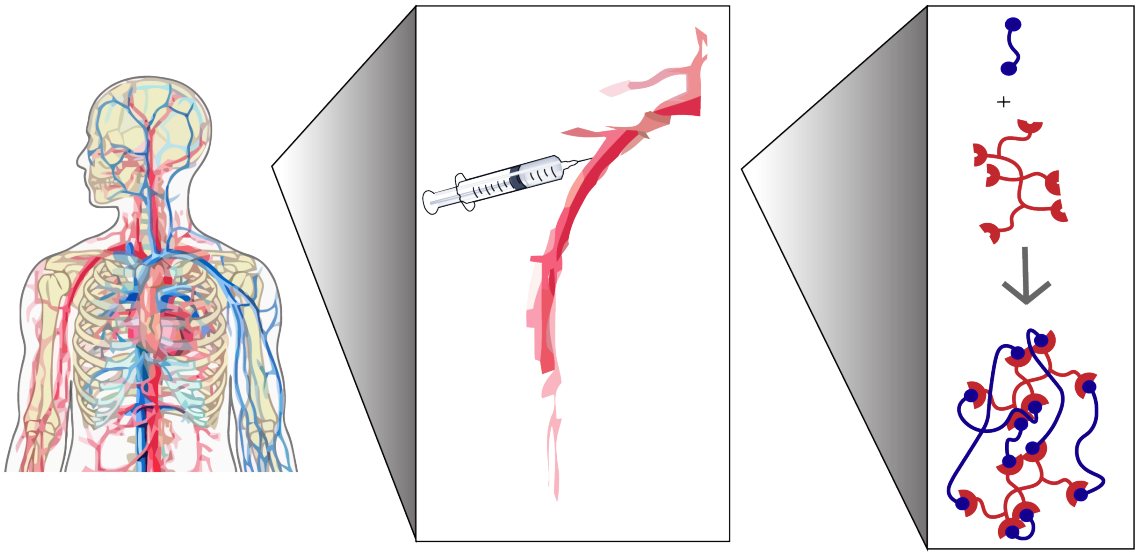

Figure 4.1. Injection of a dissolvable hydrogel as a cross-clamp alternative. Make an enlarge vein from the neck and then show the syringe.

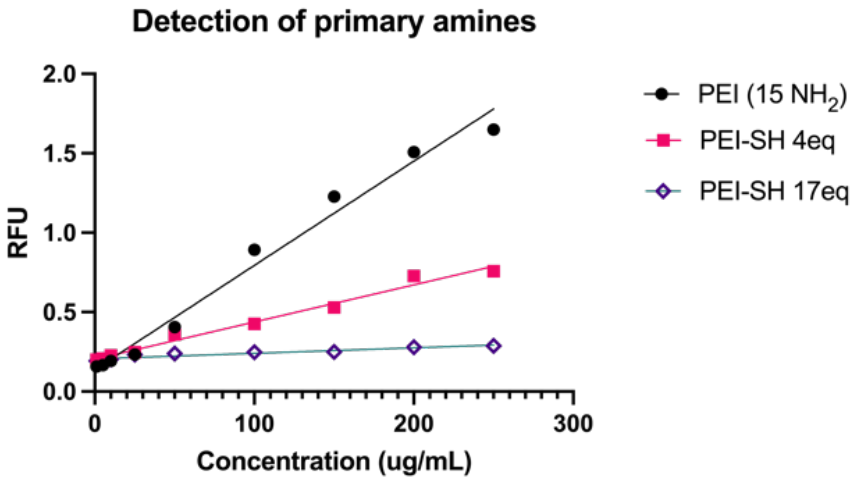

Figure 4.2. TNBS assay detecting primary amines on PEI and PEI-SH molecules.

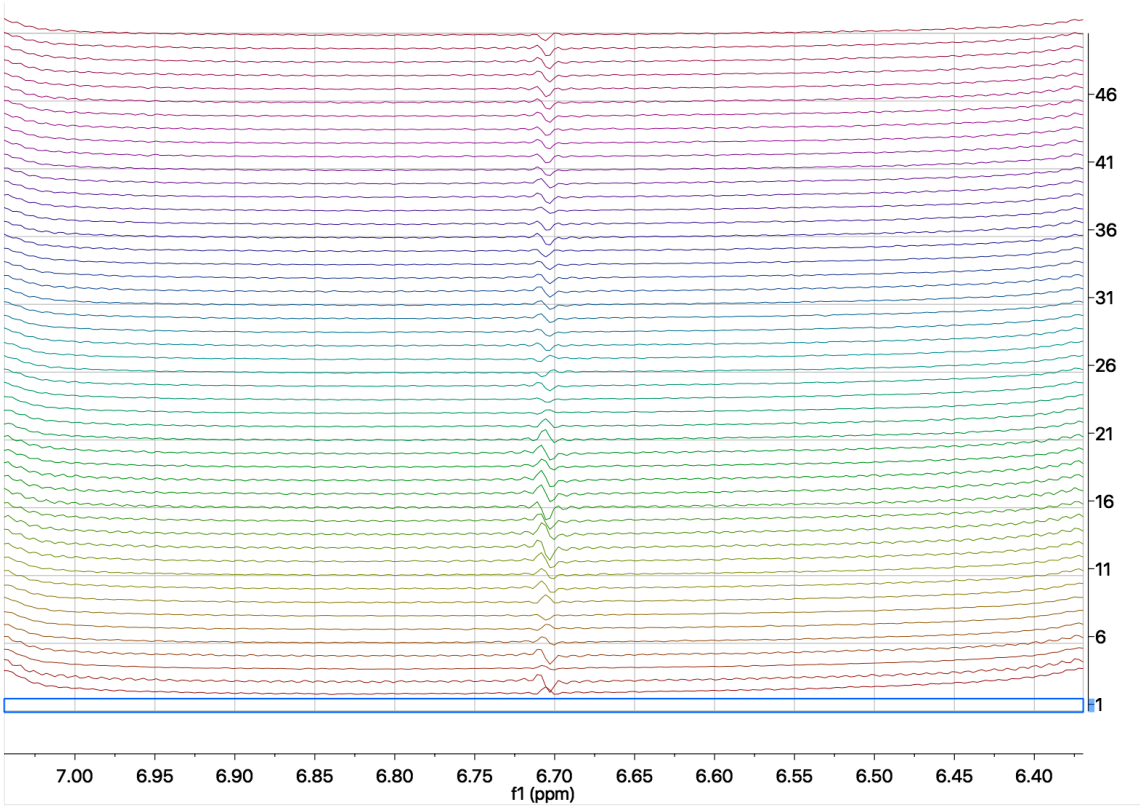

Figure 4.3. ^{1}H NMR spectra of maleimide-thiol reaction at pH 5.0 and pH 7.0 for the maleimide crosslinker and PEI-SH mimetic, respectively.

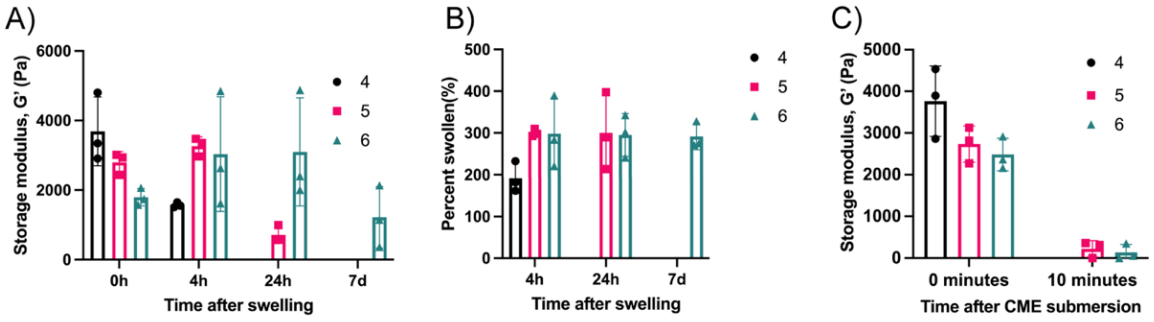

Figure 4.4. A) Rheological measurements for hydrogels; B) Swelling in 50mM PBS; C) Dissolution of hydrogels in 0.3M CME solution.

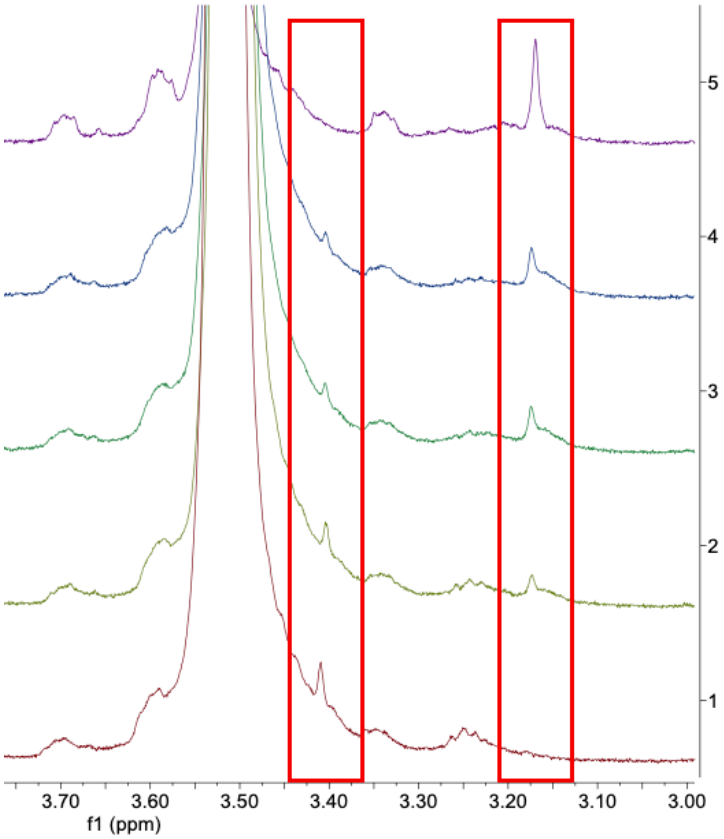

Figure 4.5. Hydrolysis of thioester, observed by shift in methylene adjacent to thiol, from 3.41ppm (conjugated), to 3.17ppm (hydrolyzed).

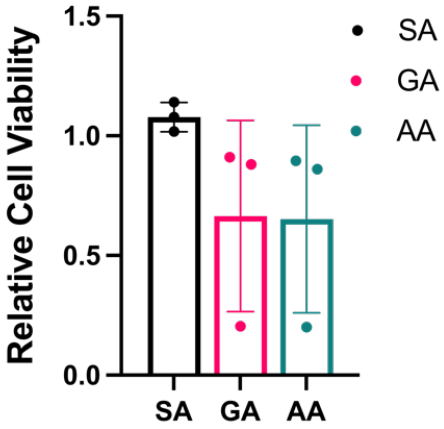

Figure 4.6. Cytotoxicity of hydrogels composed of crosslinkers **4**, **5**, and **6**.

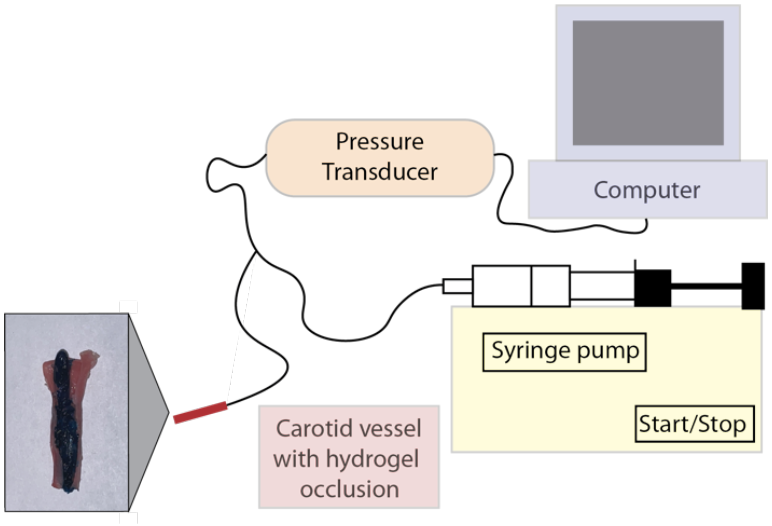

Figure 4.7. Burst pressure instrument setup and dissected *ex vivo* carotid artery with blue hydrogel occlusion

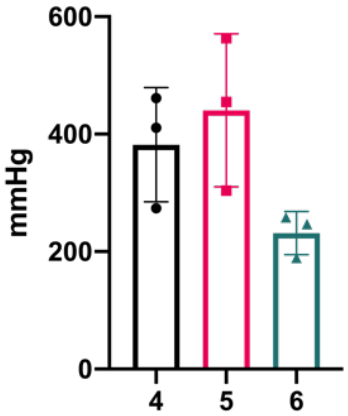

Figure 4.8. Burst pressure of hydrogels in healthy porcine carotid vessels.

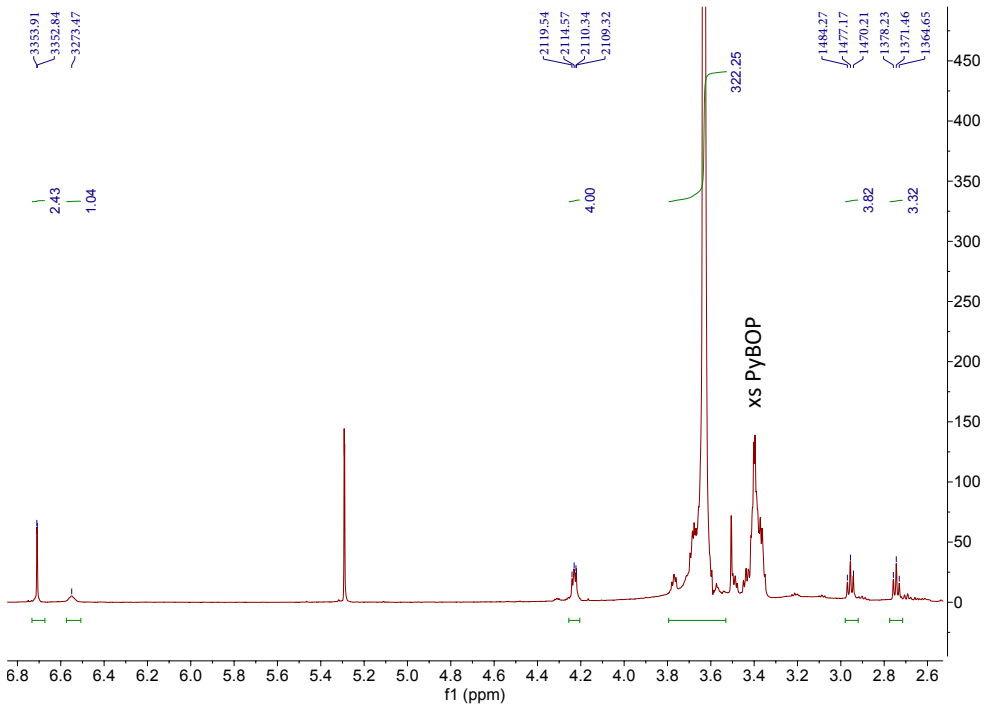

Figure 4.9. ^{1}H NMR spectrum of crosslinker **4**.

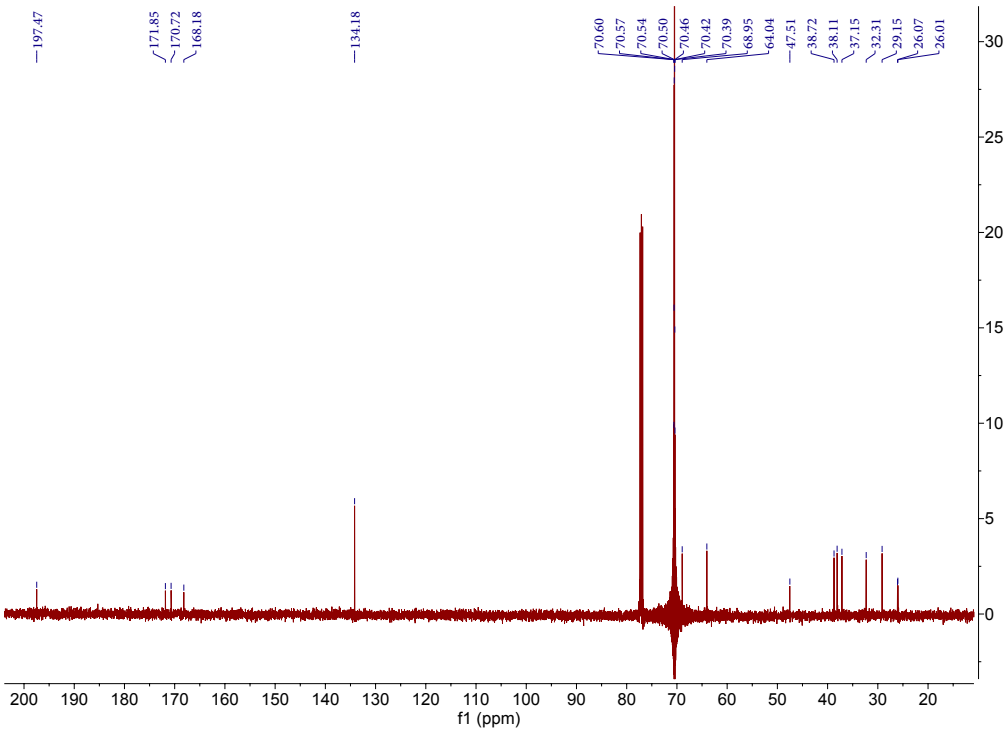

Figure 4.10. ^{13}C NMR spectrum of crosslinker **4**.

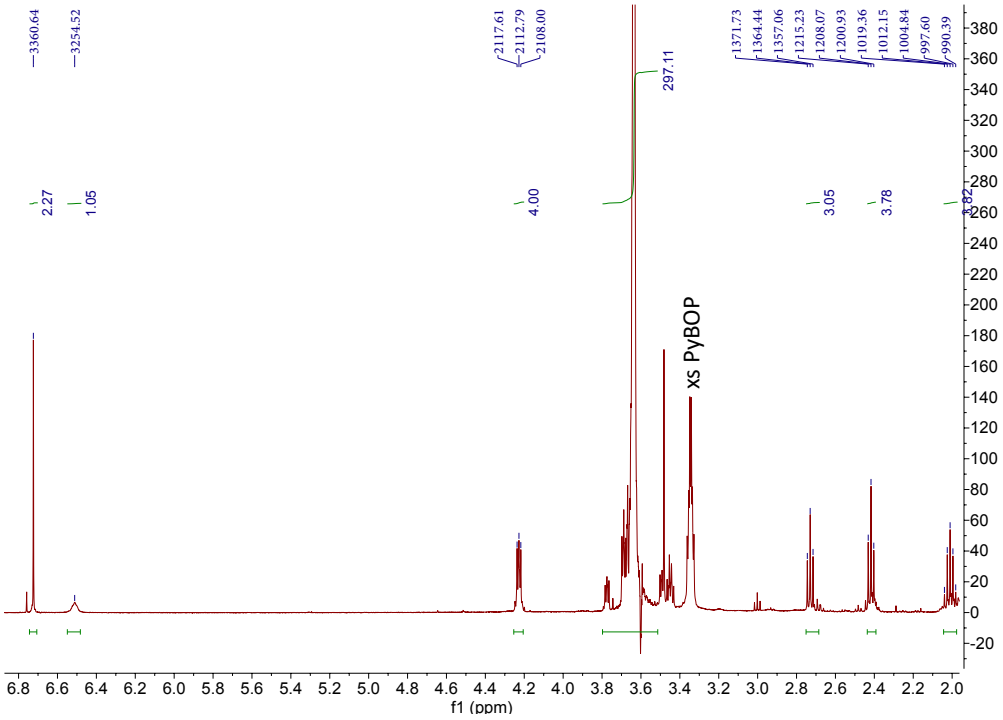

Figure 4.11. ^{1}H NMR spectrum of crosslinker **5**.

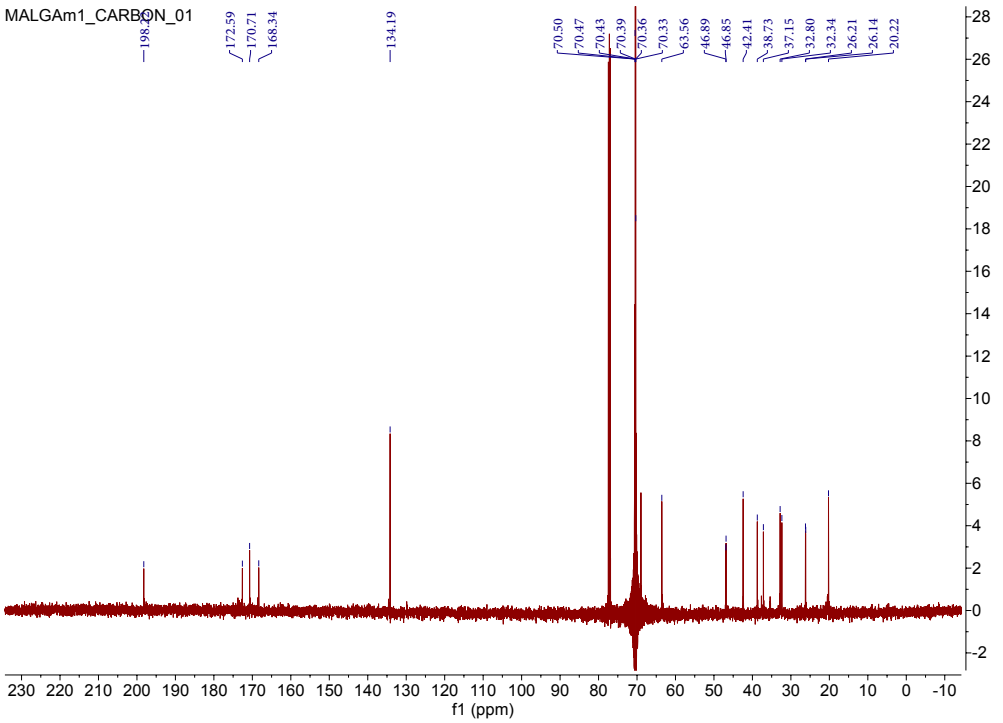

Figure 4.12. ^{13}C NMR spectrum of crosslinker **5**.

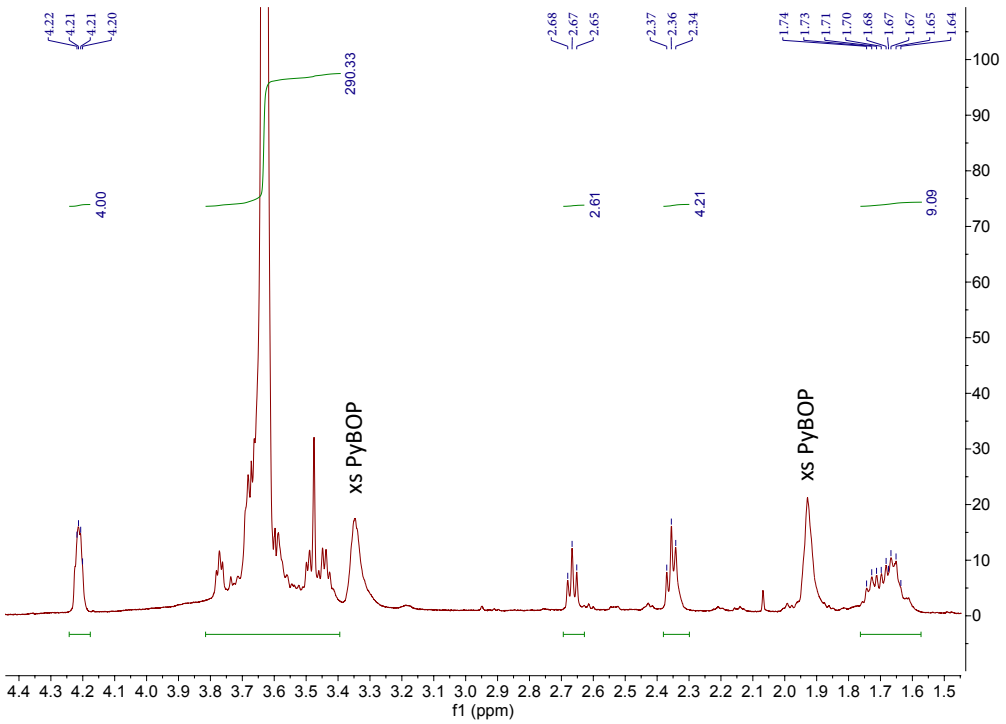

Figure 4.13. ^{1}H NMR spectrum of crosslinker **6**.

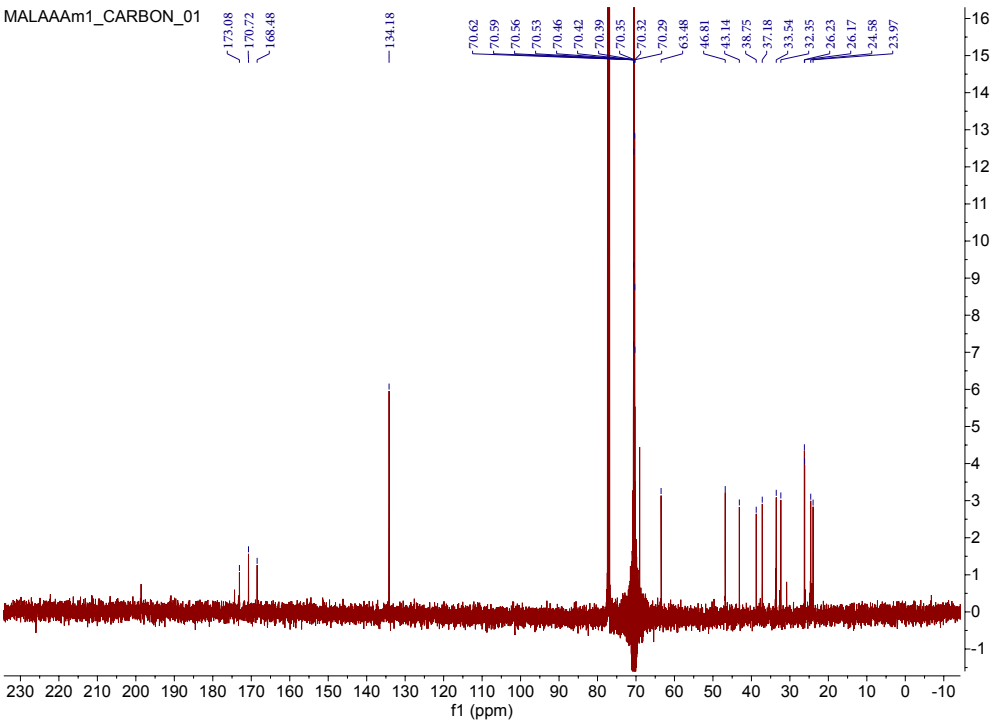

Figure 4.14. ^{13}C NMR spectrum of crosslinker **6**.

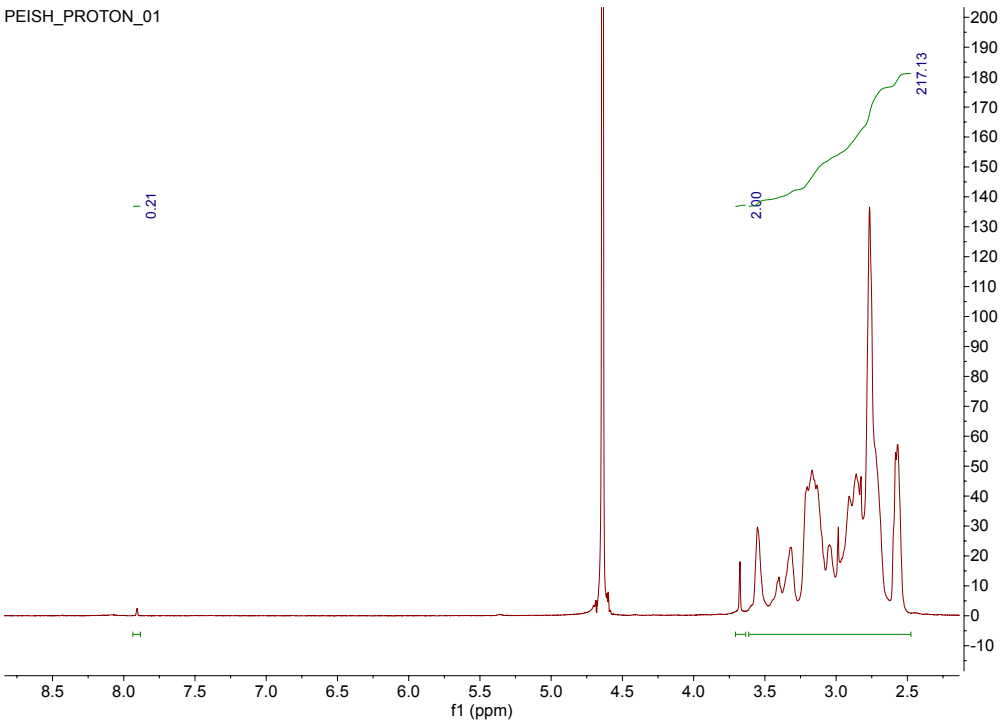

Figure 4.15. ^{1}H NMR spectrum of PEI-SH.

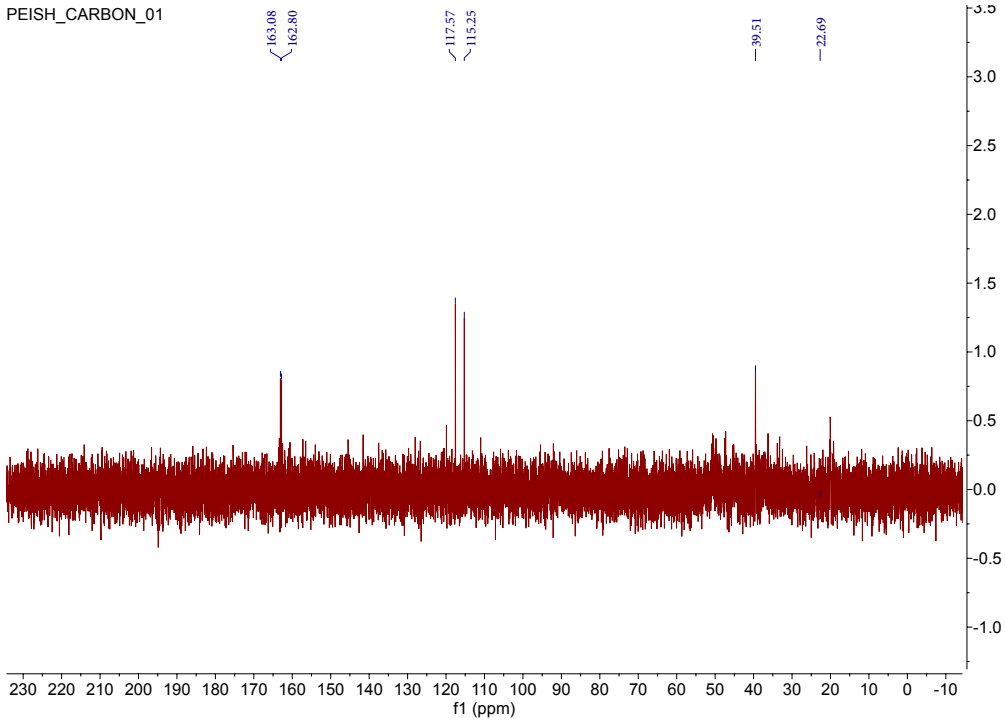

Figure 4.16. ^{13}C NMR spectrum of PEI-SH.

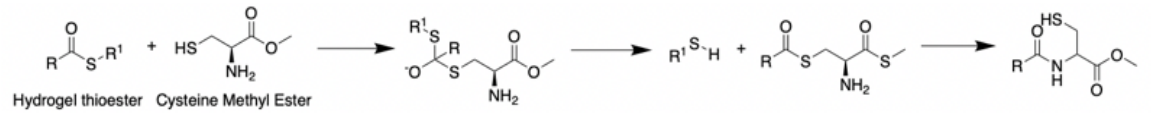

Scheme 4.1: Controlled dissolution through thiol-thioester exchange.

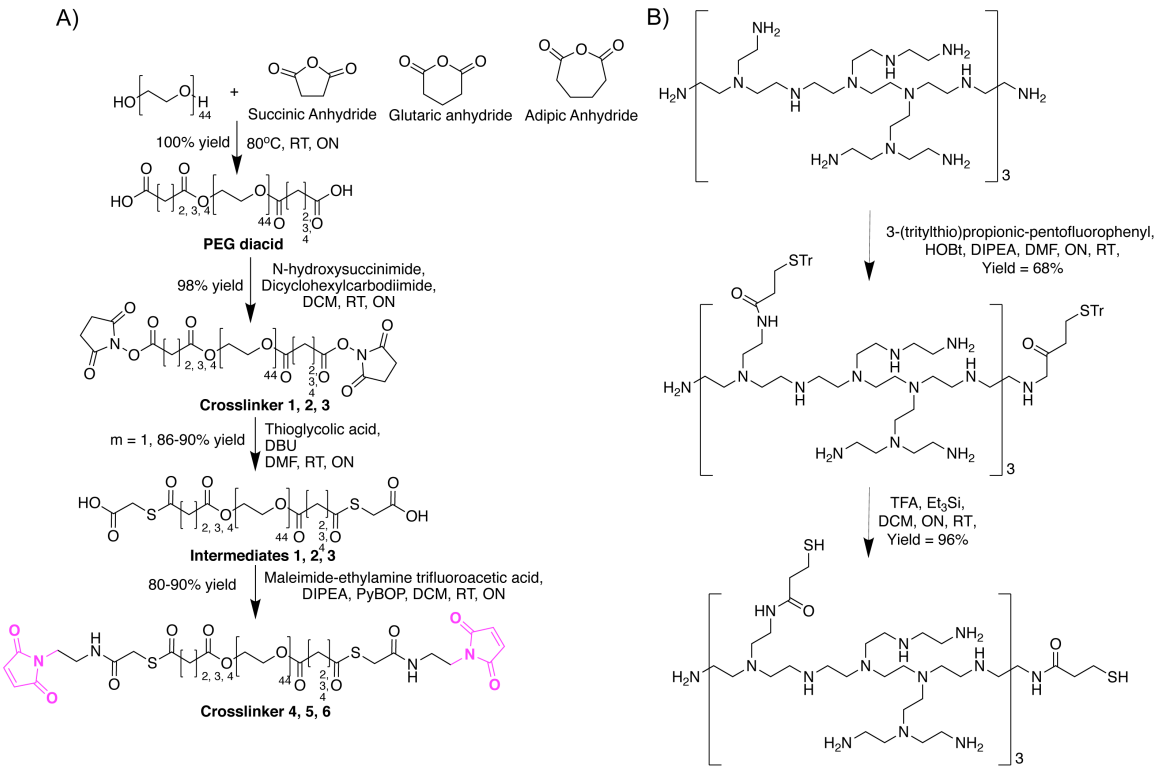

Scheme 4.2. A. Synthetic scheme of hydrogel crosslinkers, B. Synthetic Scheme of dendron.

CHAPTER 5. *In situ* kinetically controlled simultaneous interpenetrating network formation

5.1 Introduction

Interpenetrating networks (IPNs) encompass two or more intertwined polymeric networks. IPNs are widely used throughout industry sectors and in research settings as automotive parts, damping materials, energy storage materials, molding compounds, engineering plastics, drug delivery systems, and tissue engineering.[27,122,162–165] These three-dimensional networks are hydrophobic or hydrophilic, depending on the polymer compositions in use, and correspondingly may swell in organic solvents or water as an organogel or hydrogel, respectively.[122,166,167] The two synthetic strategies to prepare an IPN are: 1) sequential or stepwise, where one polymer network is formed first and then the second one is prepared within the existing structure; or 2) simultaneous, where both polymer networks are formed at the same time.[166–168] The latter is typically synthesized through orthogonal polymerization chemistry to synthesize the IPN.[166,167] For instance, the simultaneous free radical polymerization of a methacrylate/acrylate derivative and polymerization of a diisocyanate and diol affords such hydrophobic IPNs, and is a common synthetic strategy.[163,167] Examples of simultaneous hydrophilic IPNs are rarer.

Hydrophilic, simultaneous IPNs prepared through orthogonal chemistries include an IPN composed of collagen crosslinked with azide-alkyne cycloaddition

reaction, and hyaluronic acid crosslinked with a thiol via Michael click reaction for use as a corneal defect filler.[169] Furthermore, hydrophilic, simultaneous IPNs have also been prepared from photoinitiation and sol-gel processing of 2-acrylamido-2-methylpropane sulfonic acid (APMS) and inorganic silica precursors, respectively, for the use as fuel cells.[170]

One of the key advantages to using hydrophilic IPNs is the ability to 1) enhance the mechanical properties of each individual hydrogel, and/or 2) selectively tune hydrogels to respond to external stimuli such as pH, temperature, degradation, etc., known as a responsive hydrogel.[122,162,170–172] For example, a poly(2-crylamido-2-methylpropanesulfonic) acid and PAAm IPN displays strengths up to 17 times that of either individual network.[167,168] The hydrogen bonding between the two polymer networks affords enhanced mechanical strength of the IPN. On the other hand, a polyacrylamide(PAAm)/polyacrylic acid(PAA) IPN, formed through non-covalent interactions, elongates and contracts in response to changes in pH.[162] Additionally, a combined protein and polysaccharide IPN controllably degrades via enzymatic cleavage, by varying the protein and polysaccharide ratio and enzyme concentration.[166]

Herein, we report the synthesis and characterization of a simultaneous, hydrophilic, synthetic IPN using a four-component system. As discussed above, a simultaneous IPN typically requires two distinct polymerization chemistries and occurs in one step or *in situ*, while a sequential IPN employs orthogonal polymerization chemistry but occurs in two discreet steps. Our interest is lies in *in*

situ hydrogel formation, given the numerous applications in the biomedical arena, and the use of well-know, readily available, and widely used SN2 chemistry (e.g., amine with an activated ester). However, the challenge lies in obtaining orthoganality. Using kinetics to vary reaction rates, we synthesize and characterize an IPN through SN2 chemistry, to achieve selective reactivity between one set (two partners) of our four-component IPN. Further, we introduce an internal thioester linkage in one network to control dissolution through a thiol-thioester exchange mechanism. Controlled dissolution provides a supplemental, responsive characteristic resulting in a dissolvable IPN with controlled degradation, as a prime example. Specifically, we simultaneously crosslink a bifunctional N-hydroxysuccinimide (NHS) PEG-based crosslinker, containing an internal thioester linkage, with polyethyleneimine (PEI), and a bifunctional vinyl sulfone (VS) PEG-based crosslinker with thiolated PEI (PEI(SH)).

5.2 Interpenetrating network formation

Typically, two distinct reaction mechanisms are used to synthesize simultaneous IPNs. We report the synthesis of an IPN via selective SN2 reaction mechanisms, controlled through reaction kinetics. Secondary to the synthesis of the IPN, we report selective degradation of our IPN through thiol-thioester exchange upon exposure to a cysteine methyl ester (CME) solution. The simultaneous, hydrophilic IPN we discuss in this paper contains two crosslinkers: a commercially purchased, bifunctional vinyl sulfone (VS) crosslinker, which reacts

with PEI(SH), synthesized in-house, and a bifunctional N-hydroxysuccinimide (NHS) crosslinker synthesized with minimal modification from a previously published protocol, which reacts with commercially purchased PEI.[125,126,154]

We prepare our hydrogels by mixing the crosslinker, dissolved in 0.1M phosphate buffer pH 6.5 with PEI or PEI(SH) in 0.3M borate buffer pH 8.5. The IPN is prepared by mixing both crosslinkers with both PEI and PEI(SH) in the phosphate and borate buffers, respectively. The ratio of NHS:NH_2 and VS:thiol is 1:1, resulting in a 0.03 mol% hydrogel network. Our IPN network was prepared at a ratio of 1:1 NHS:VS. Upon mixing hydrogel components together, A transparent, solid hydrogel was formed within 60s for all hydrogel formulations.

5.3 IPN gelation kinetics

Gelation occurs through an SN2 reaction between the terminal amines on PEI and NHS, or the terminal thiols on PEI(SH) and VS. Reaction kinetics were studied through the inverted tube method, and ^{1}H NMR kinetics studies. The inverted tube test assesses gelation time qualitatively. Briefly, hydrogel components were mixed together in a scintillation vial, and the vial was inverted at various times to observe whether or not the hydrogel solution runs down the sides of the vial. Gelation is defined as the time at which the solution no longer runs down the sides of the scintillation vial upon inversion. We observe a gelation time of 6.3 seconds, 56.3 seconds, and 21.7 seconds, for VS, NHS, and IPN hydrogel networks, respectively. The increased gelation time of the IPN network results from

the combined kinetics of the VS and the NHS hydrogel networks.

To further investigate gelation kinetics of our IPN and its individual hydrogel components, we followed reaction kinetics via ^{1}H NMR. After mixing PEI and PEI(SH) mimetics, N-butylamine and thioglycolic acid, respectively, with our crosslinkers, we followed the disappearance of either the alkene peaks (3.80 ppm) on the vinyl sulfone moiety, or the NHS peak (2.81 ppm). We assessed both NHS:NH_2 and VS:SH kinetics, as well as the competitive reactions, NHS:SH and VS:NH_2. We identified selective reactivity between NHS:NH_2 and VS:SH reactive groups, with minimal reactivity between NHS:SH and VS:NH_2 functional groups (Figure 3, Table 1). Notably, the half-life of the NHS:NH_2 ^{1}H NMR reaction is faster than the half-life of the VS:SH reaction. We attribute this discrepancy between our ^{1}H NMR reaction and our *in situ* hydrogel reaction to the N-butylamine increasing the pH of the system and therefore catalyzing the reaction. Selective reactivity ensures that we are minimizing the number of defects in our IPN, in this system, through kinetics. Therefore, further assessment was required to determine the selectivity of NH_2 and SH in the presence of both crosslinker. In the presence of both crosslinkers, we observe selective reactivity between VS:SH ($t_{1/2}$ = 0.28 min^{-1}) and NHS:NH_2 ($t_{1/2}$ = 1.01 min^{-1}), with slow and no reaction kinetics between NHS:SH ($t_{1/2}$ = 4.80 min^{-1}) and VS:NH_2 ($t_{1/2}$ = N/A), respectively (Figure 4). The selective reactivity in the presence of both crosslinkers further ensures minimal crosslinking defects between NHS:SH or VS:NH_2 in our IPN.

5.4 Rheological and swelling measurements

Next, we assessed mechanical properties of our hydrogels. We performed strain and frequency sweeps at various time points after swelling in 50mM PBS. The strain sweep was performed to determine the linear viscoelastic region (LVER) of the hydrogel, and a strain % from within that LVER was used in the frequency sweep. Frequency sweeps were run from 0.1-10Hz at 3% strain, at time points 0h, 4h, 24h, 48h, 7d, 30d and 45d after swelling. Over 45 days of swelling, we observe a significant decrease in storage modulus (G') of NHS hydrogels, and a slight but insignificant decrease in G' in the IPN (Figure 5A). VS hydrogels maintain a stable storage modulus over 45 days of swelling. We attribute the loss of G' in our NHS hydrogels due to hydrolysis of the thioester and ester linkages in the crosslinker. In the IPN, however, we observe a sustained mechanical strength, accredited to the VS hydrogel stabilizing the hydrolysis of the NHS hydrogel. Over the same time span of 45 days, we observe similar swelling rates regardless of hydrogel formulation (Figure 5B).

5.5 Dissolution

Following rheological and swelling measurements, we assessed the effect of controlled dissolution through thiol-thioester exchange of 0.3M CME solution at pH 8.5 to G' of the hydrogels. Unique to our IPN is two degradable linkages in the NHS crosslinker, a thioester and an ester linkage. The thioester and ester linkages can be degraded through hydrolysis, while the thioester alone can undergo

dissolution through thiol-thioester exchange upon exposure to an external thiol such as cysteine methyl ester (CME). Introduction of CME to the IPN results in cleavage of the internal thioester of the NHS crosslinker. Subsequently, the CME rearranges to form an irreversible amide bond with the disassembled crosslinker structure. As expected, VS hydrogels did not dissolve after one hour exposure to CME due to the lack of degradable linkages in the structure. However, when exposed to 0.3M CME solution at pH 8.5, both the IPN and NHS hydrogels degrade in 60 minutes (Figure 6). When the NHS hydrogel degrades, the polymeric network is disassembled through thiol-thioester exchange. When the IPN network degrades through thiol-thioester exchange, the resulting VS hydrogel is too weak to maintain mechanical integrity and therefore disintegrates along with the cleaved NHS polymeric network.

5.6 Conclusions

We have synthesized and characterized a hydrophilic, simultaneous IPN based on selective reaction kinetics. Secondary to the chemistry utilized in forming this IPN, we developed an IPN with a controlled dissolution mechanism. We have demonstrated tunable mechanical strength, swelling, and dissolution based on hydrogel formulation. Specifically, our IPN promotes stabilization of hydrolysable moieties within our NHS crosslinker structure, while also sustaining similar on-demand dissolution kinetics via thiol-thioester exchange as compared to our NHS crosslinker. This work highlights the kinetically controlled IPN formation based on

SN2 reactions, and the secondary controlled dissolution properties of our hydrogel networks via a 50:50 NHS:VS IPN formulation.

5.7 Materials and methods

Materials

NMR spectra were recorded on a Varian 500MHz VNMR instrument with chemical shifts quoted in parts per million (ppm) and calibrated to non-deuterated solvent (^{1}H NMR: $CDCl_3$ at 7.26 ppm; ^{13}C NMR: $CDCl_3$ at 77.16 ppm). Coupling constants (J) from NMR spectra are quoted in Hertz, and multiplicities are reported as: singlet (s), doublet (d), triplet (t), quartet (q), multiplet (m), or broad (b). Gel permeation chromatography (GPC) analyses were performed on an OptiLab DSP Interferometric Refractometer (Wyatt Technology) fitted with two identical Jordi Gel DVB columns (Jordi Labs, 250mmx10mm, 10^5 Å pore size.) Samples were dissolved in tetrahydrofuran (THF) (2mg/mL) and passed through a 0.45μm filter immediately prior to injection. A flow rate of 1.0 mL/min was obtained at 25^{o}C with THF as the eluent and measurements were taken. Resulting chromatograms were calibrated against Agilent polystyrene standards (EasiCal calibration kit). Differential scanning calorimetry (DSC) of crosslinkers were recorded on a DSC Q100 TA instrument, and Thermogravimetric analysis (TGA) measurements were recorded on a Q series TA instrument.

Anhydrous solvents were purchased from Sigma Aldrich. Reagents were purchased from commercial sources and used without further purification. Reactions were performed under Argon with magnetic stirring. Polyethyleneimine, molecular weight 1800 was purchased from Polysciences, Inc, vinyl sulfone-poly(ethyleneglycol)-vinyl sulfone, molecular weight 5000 was purchased from JenKem.

Synthesis and characterization of compounds.

NHS GA m5 crosslinker.

PEG diacid. This polymer was prepared following previously published protocols. ^{1}H NMR and ^{13}C NMR were performed to confirm synthesis.

NHS-GA-PEG-GA-NHS. The synthesis of NHS-GA-PEG-GA-NHS was also based off of a previously published protocol; ^{1}H NMR and ^{13}C NMR confirmed synthesis.

Intermediate A (int A). In a flame dried, round bottom flask, NHS-GA-PEG-GA-NHS was dissolved in dimethylformamide (DMF). Subsequently, mercaptohexanoic acid and 1,8-Diazabicyclo[5.4.0]undec-7-ene (DBU) were added to the flask and stirred overnight. The next day, the reaction mixture was washed with 1N HCl, water, and brine, and the organic layer was collected after each wash. The organic layer was then dried over Na_2SO_4 and concentrated under vacuum. The solubilized product was precipitated in diethyl ether. The precipitate was collected and dried under vacuum to afford a white powder (yield = 96%).

^{1}H NMR:

^{13}C NMR:

NHS GA m5. The final crosslinker was synthesized via DCC coupling. In a round bottom, flame-dried flask, int A was dissolved in methylene chloride (DCM). Dicyclocarbodiimide and N-hydroxysuccinimide were added to the reaction and stirred overnight. The mixture was then filtered, to remove dicyclohexylurea (DCU) and concentrated under vacuum. The product was precipitated in diethyl ether and dried under vacuum to afford a white powder (yield = 98%).

^{1}H NMR: d 4.13 (tt, *J* = 4.5Hz, 4H), 3.54 (m, 404.36H), 2.77 (m, *J* = 7.1Hz, 12H), 2.51 (tt, *J* = 3.8, 3.5Hz, 8H), 2.29 (t, *J* =7.3Hz, 4H), 1.88 (m, *J* = 7.3Hz, 4H), 1.67 (m, *J* = 7.6Hz, 4H), 1.51 (m, *J* = 8.1, 7.6Hz, 4H), 1.39 (m, *J* = 8.1, 7.1Hz, 4H) ppm;

^{13}C NMR: 198.5, 172.6, 169.1, 168.3, 70.4, 69.0, 63.5, 42.8, 32.9, 30.7, 29.0, 27.7, 25.5, 24.0, 20.6 ppm;

Mp: 45.52^{o}C

Crystallization: 28.87^{o}C

Mn = 5044 g/mol,

Mw = 5660 g/mol,

PDI = 1.12;

PEI-SH. PEI was reacted with a pentafluorophenol functionalized (thiotrityl)mercaptopropionic acid, diisopropylethylamine, and hydroxybenzotriazole at room temperature, in DMF, overnight. The mixture was dissolved in methylene chloride and the organic layer was collected upon washing

with sodium bicarbonate, water, and brine. The organic layer was dried over Na_2SO_4, and concentrated under vacuum. The concentrated mixture was precipitated in diethyl ether. The precipitate was dried under vacuum to afford a yellow solid (yield = 66%). The yellow product was reacted with triethyl silane and trifluoroacetic acid to deprotect the trityl groups. The mixture was stirred at room temperature for 3 hours, concentrated under vacuum, and precipitated in diethyl ether to afford a yellow, viscous product. The yellow viscous product was then dissolved in 1N HCl, syringe filtered through a 0.22□m filter, and adjusted to neutral pH. The neutral aqueous solution was then lyophilized to afford a solid, pink product (yield = 90%).

Mechanical properties of the hydrogel

The rheological measurements of the hydrogels were obtained from a Discovery Hybrid Rheometer – 2 (DHR-2). To prepare the hydrogel samples, the hyperbranched Polyethyleneimine (PEI) and PEI-thiol (PEI(SH)) polymers were dissolved in 0.3M borate buffer, pH 8.5, and reacted with the respective crosslinkers: **NHS GA m5** and vinyl sulfone-PEG-vinyl sulfone (VS-PEG-VS), in 0.1M phosphate buffer, pH 6.5. The ratio of amine:NHS was 15:1, and the ratio of PEI(SH):VS was 2:1, and the total concentration of the hydrogels were 25 wt% for the amine:NHS gels, and 30 wt% for the PEI(SH):VS hydrogels. Hydrogels were prepared in a Teflon, cylindrical mold of 8mm in diameter and 2mm height. Gels formed spontaneously between 3 seconds - 5 minutes, and were left at room temperature in a humid chamber for 1 hour to ensure complete gelation. All

rheological measurements were taken at 22°C. Strain sweeps were performed at 1Hz, and frequency sweeps from 0.1-10Hz were performed at 3% strain. A normal force of 0.2N was applied to the hydrogel between two 8mm steel plate geometries. Data are expressed as a mean ± standard deviation (n = 6). The hydrogels exhibit viscoelastic properties where G'>G".

Swelling was determined by the following equation: $Swelling\ ratio = \frac{final\ mass}{initial\ mass} X\ 100$. Final mass is the mass of the hydrogel at a particular time point after swelling. The initial mass is the mass of the hydrogel at time t=0h, prior to swelling.

Gelation kinetics

Reaction kinetics were performed on a Varian 400MHz NMR in 0.1M sodium bicarbonate deuterated buffer, pH 8.0. Crosslinkers were dissolved in buffer at a concentration of 1mg/10μL. N-butylamine was used as a PEI mimetic, and thiopropionic acid was used as a PEI(SH) mimetic. ^{1}H NMR spectra were recorded at a rate of 1 spectrum every 26 seconds, and NHS or VS peak shifts were assessed.

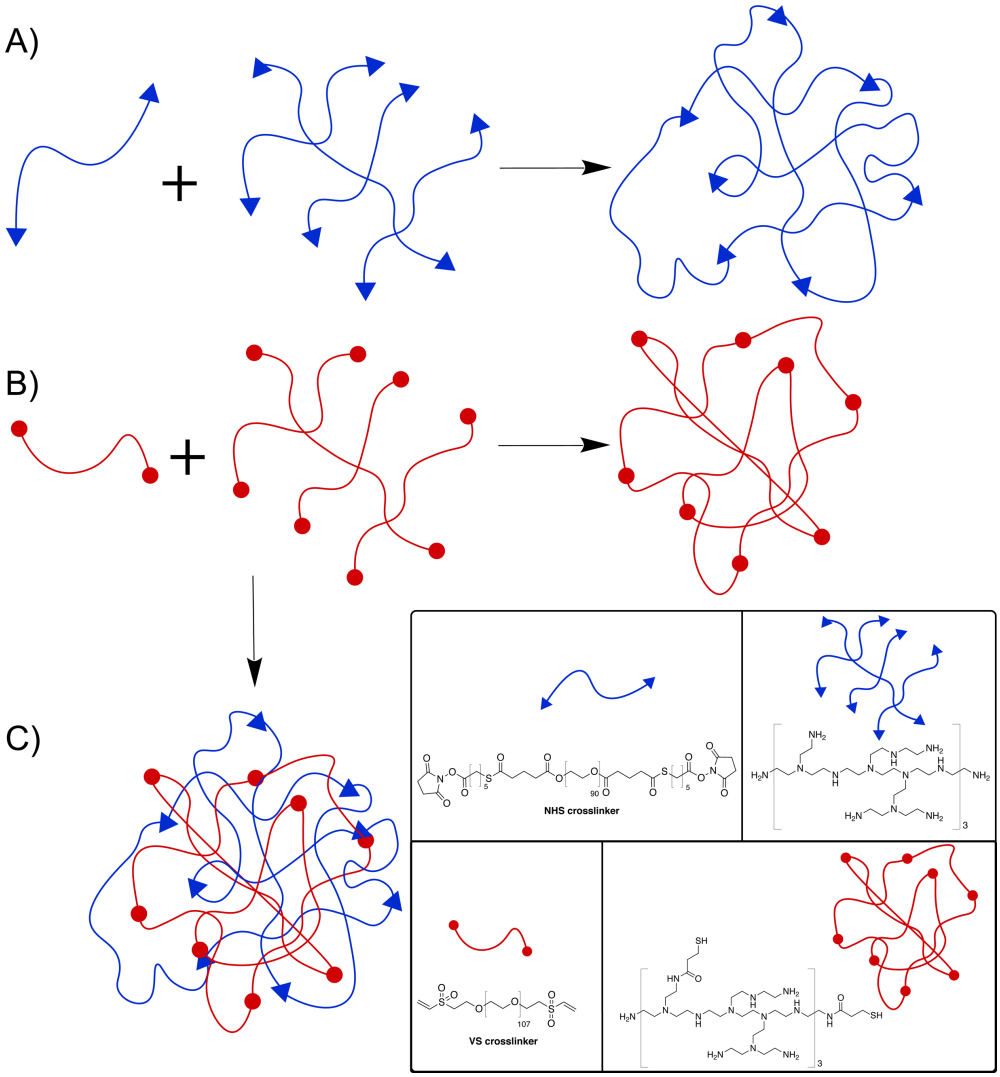

Figure 5.1. A) NHS/NH_2 hydrogel formation, B) VS/SH hydrogel formation, C) interpenetrating network composed of both networks A and B.

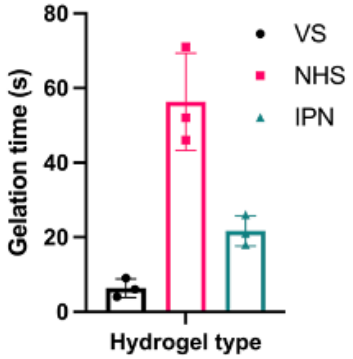

Figure 5.2. Gelation of hydrogels.

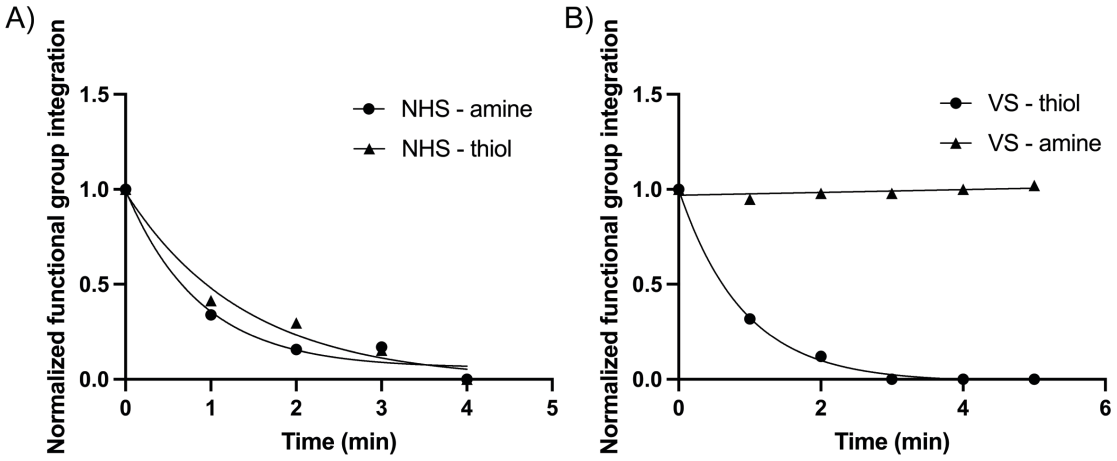

Figure 5.3. Kinetics reactions followed via ^{1}H NMR of A) NHS and amine or thiol, and B) VS and amine or thiol.

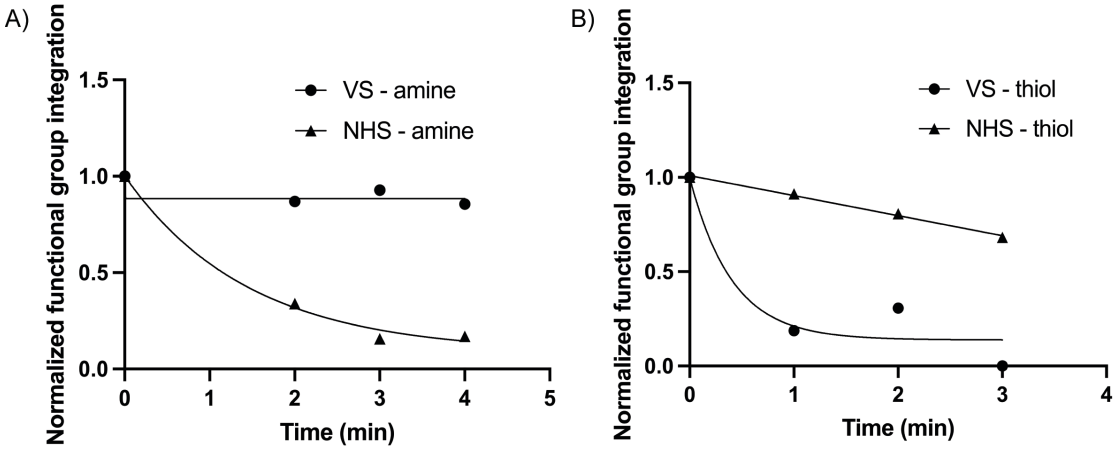

Figure 5.4. Kinetics reactions followed via ^{1}H NMR of NHS and VS crosslinkers in the presence of A) amine, and B) thiol.

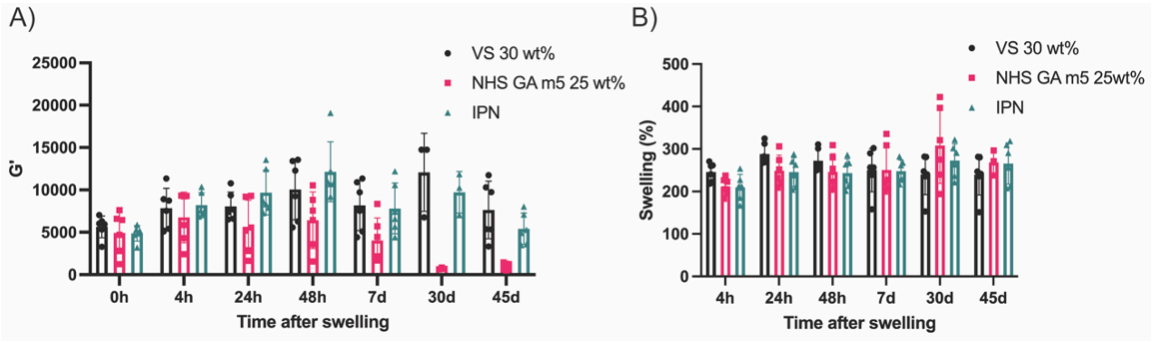

Figure 5.5. A) Rheometry of hydrogels over 45 days of swelling, B) swelling of hydrogels over time.

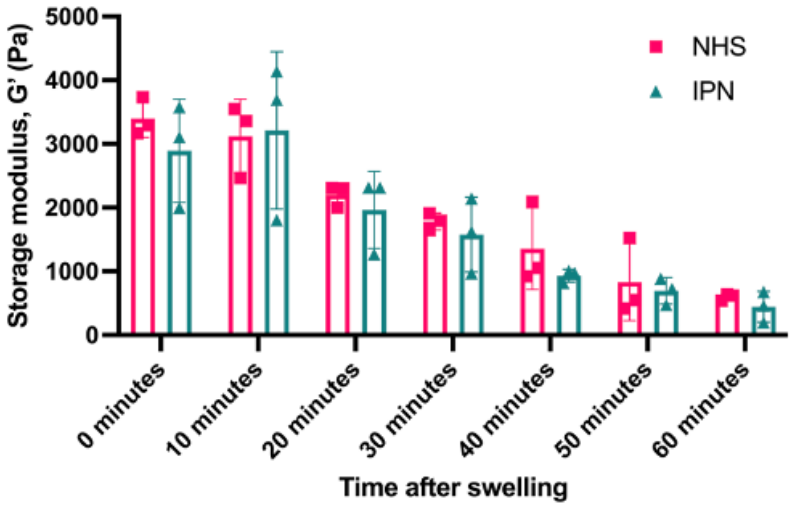

Figure 5.6. Dissolution of IPN and NHS hydrogels when submerged in 0.3M CME, pH 8.5.

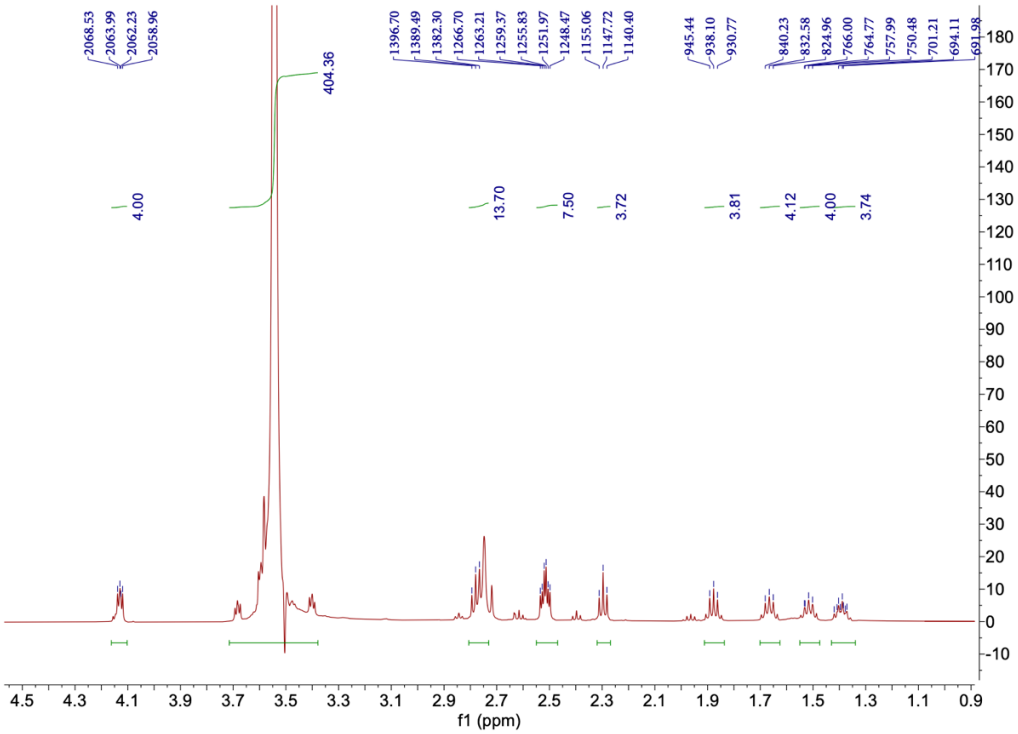

Figure 5.7. ^{1}H NMR spectrum of NHS GA m5 crosslinker.

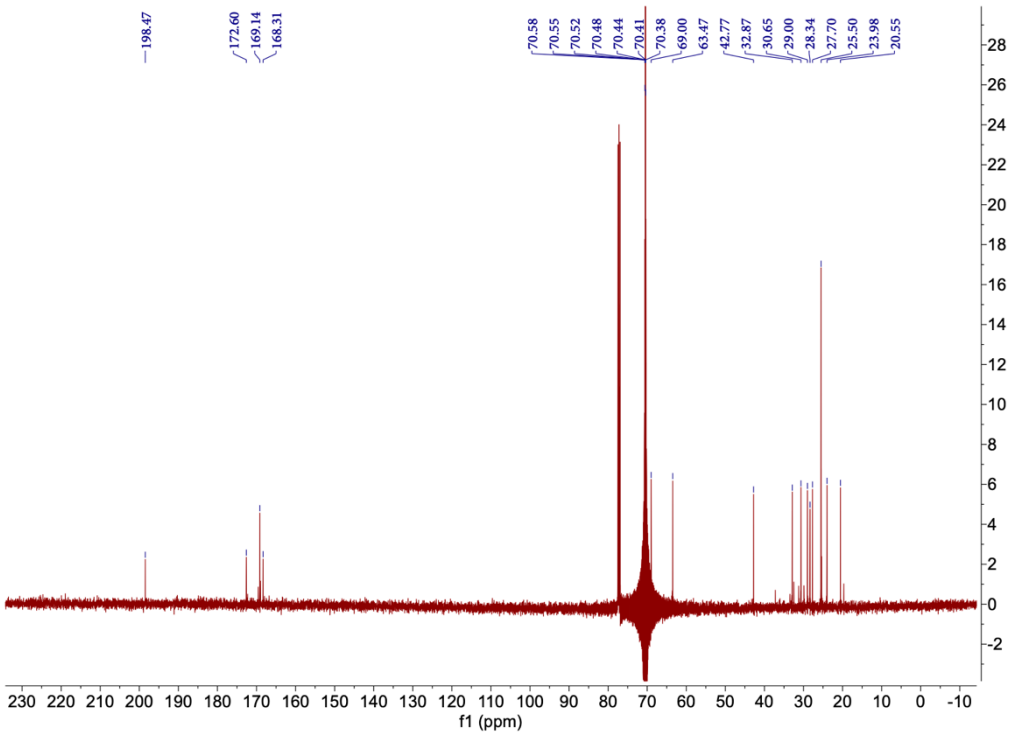

Figure 5.8. ^{13}C NMR spectrum of NHS GA m5 crosslinker.

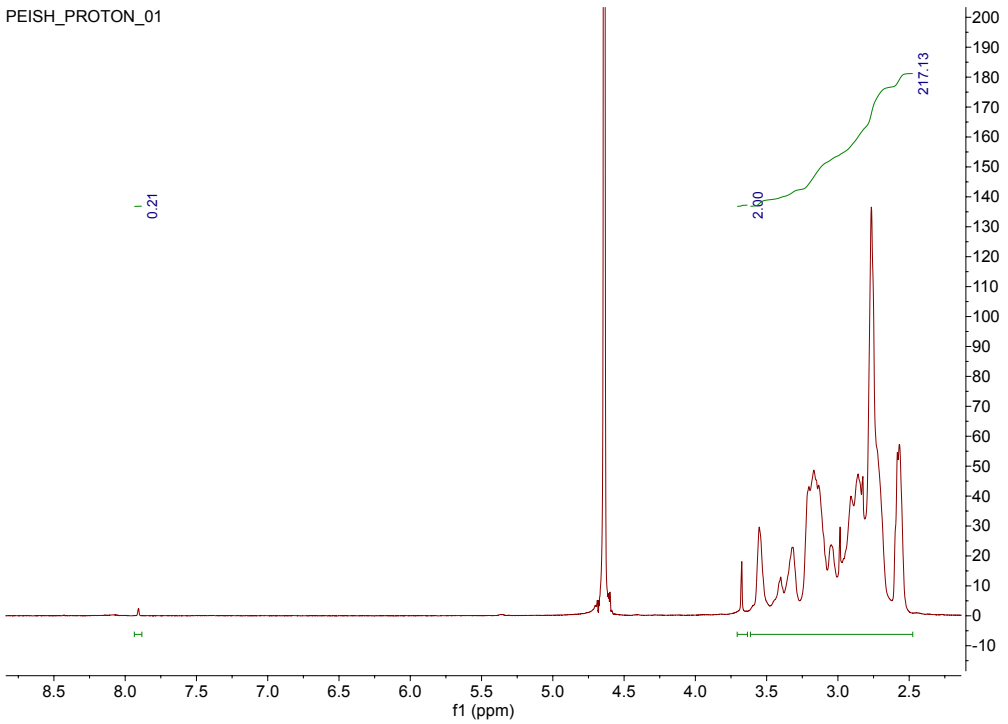

Figure 5.9. ^{1}H NMR spectrum of PEI-SH

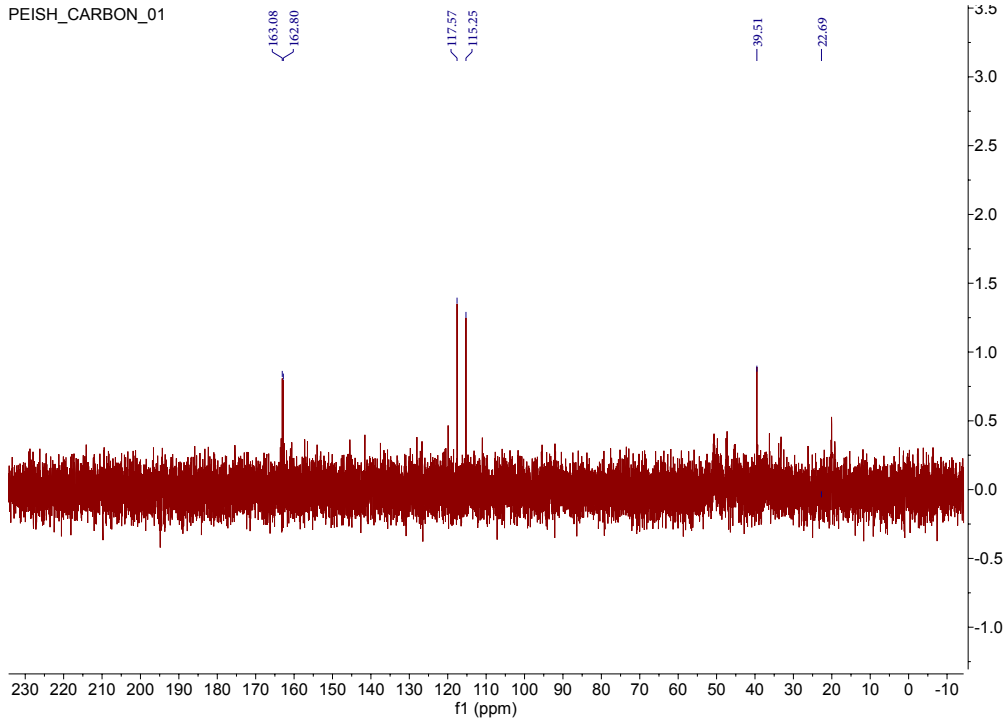

Figure 5.10. ^{13}C NMR spectrum of PEI-SH

Reactivity of functional groups	**NHS crosslinker**	**VS crosslinker**
SH	0.97 min^{-1}	0.63 min^{-1}
NH_2	0.37 min^{-1}	Does not react

Table 5.1. Half-life of NHS and VS crosslinkers reacting with either SH or NH_2 functional groups.

CHAPTER 6. Future work

6.1 Hydrogels as burn wound dressings

The next translational step in the hydrogel burn wound dressing research is to expand the library of hydrogel burn wound dressings and assess bacterial migration and infection through the hydrogels. Expanding the hydrogel library will assist in determining the optimal hydrogel burn dressing formulation. Additionally, bacterial migration and infection studies *in vitro* and *in vivo* will determine the barrier of infection provided by the hydrogels. Bacterial migration studies will evaluate infection capabilities of common bacteria found in burn wounds including Staphylococcus aureus, Pseudomonas and Acinetobacter, common bacteria found in burns. Providing a burn dressing that is easily applied and removed, and protects the wound from bacterial infection *in vivo* will lead to a reduction in pain during a dressing change, infection and death in burn patients.

6.2 Colon polypectomy hydrogel dressing

From an application standpoint, one hydrogel formulation (SA+4-arm PEG-NH_2) meets the design requirements set forth for a colon wound dressing, and possesses a G' similar to native colon, adheres to colon, gels quickly, flows through a dual lumen catheter for subsequent hydrogel formation, and prevents the migration of bacteria. The next translational steps in this project will include *in vivo* efficacy studies for assessment of ease of use and colon tissue healing rate

as well as safety and toxicity studies. *In situ* forming hydrogels are promising wound dressing biomaterials for colon polypectomies and continued research and development in this area will lead to treatments that reduce procedural complications such as bleeding, hemorrhaging, and sepsis.

6.3 Hydrogel-based vascular occlusion device

The hydrogel formulation **4**:PEI$(SH)_4$ possesses characteristics fulfilling the design requirements as a hydrogel vascular occlusion device. The next steps in our hydrogel vascular occlusion research will include an *in vivo* pilot study to assess the ease of use, complete occlusion and dissolution of hydrogel formulation **4**:PEI$(SH)_4$. Additionally, embolism and thrombosis formation will be monitored throughout the experiment to determine the safety of our materials and histopathology analyses will be performed on vascular tissue to evaluate endothelial cell viability post-intervention in both the experimental and standard of care treatment groups. Hydrogels are promising medical device materials for vascular occlusion due to *in situ* application, dissolution, undertaking morphology of the vessel, and minimizing pressure on vascular tissue. Continued research and development will allow for a reduction in trauma during vascular occlusion surgeries, therefore reducing complications such as embolisms, thrombosis, and tissue damage.

6.4 Interpenetrating hydrogel network

From a chemical standpoint, the interpenetrating network described in chapter 5 exhibits similar mechanical properties to the individual hydrogel components alone, while allowing for greater control over the reaction kinetics. Future studies for this work include preparing a library of interpenetrating networks formulated from alternative, simultaneous Sn2 reactions to assess the variability in hydrogel characteristics between the interpenetrating network and the individual hydrogel networks based on reactive end groups. Research and development focusing on controlling reaction kinetics, and outcome characteristics of hydrogels and interpenetrating networks will advance the use of hydrogels as biomaterials reducing risk factors of current standard of care treatments such as toxicity and physical limitations, i.e. cohesive failure and adhesion among others, of the materials.

Structure	m	Macromer	Weight percent	G' (Pa)	Swelling (%)	Hydrolysis (time)	Dissolution (time)	Gelation (seconds)
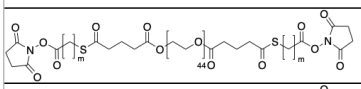	1	PEI	15	3763.89 ± 1924.06	168.39 ± 10.03	48h	<10 min	1.00 ± 0.00
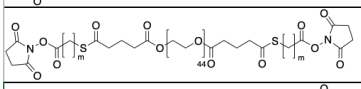	5	PEI	15	7200.64 ± 936.16	147.69 ± 12.90	>30d	30 min	118.33 ± 27.54
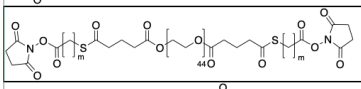	10	PEI	15	18951.50 ± 2963.15	122.75 ± 5.42	>30d	80 min	194.00 ± 14.18
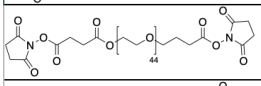	N/A	PEI	15	1564.07 ± 452.41	153.47 ± 36.04	48h	N/A	102.00 ± 16.64
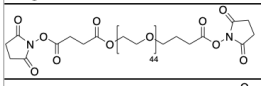	N/A	4-arm PEG-NH2	15	3591.5 ± 621.41	411.46 ± 16.08	7d	N/A	85.00 ± 21.79
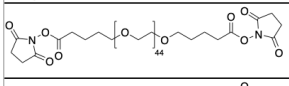	N/A	PEI	15	12436.43 ± 843.03	265.11 ± 33.55	N/A	N/A	90.00 ± 13.75
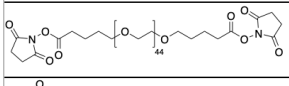	N/A	4-arm PEG-NH2	15	3764.51 ± 1925.58	374.89 ± 4.63	N/A	N/A	40.00 ± 5.00
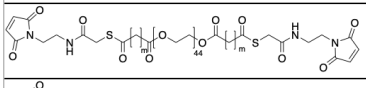	2	PEI-SH	25	1568.83 ± 70.44 *4h time point	192.04 ± 36.23 *4h time point	4h	<10 min	<1s
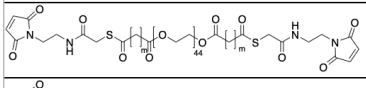	3	PEI-SH	25	711.459 ± 241.83	300.41 ± 92.63	24h	10 min	<1s
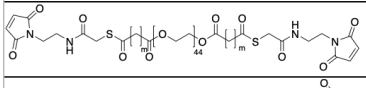	4	PEI-SH	25	3095.70 ± 1555.49	295.27 ± 51.24	7d	10 min	<1s
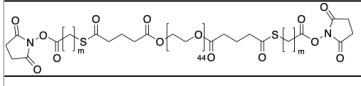	5	PEI	25	5626.52 ± 3157.40	281.82 ± 6.68	>7d	60 minutes	56.33 ± 13.05
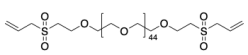	N/A	PEI-SH	30	8045.67 ± 1689.61	291.95 ± 28.95	N/A	N/A	6.33 ± 2.52
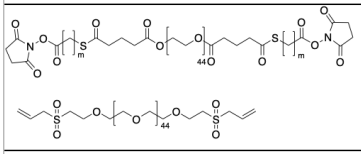	5	PEI and PEI-SH	27.5	9683.90 ± 2633.81	273.87 ± 12.54	>7d	60 minutes	21.67 ± 4.04

Table 6.1. SAR table of hydrogel formulations

REFERENCES

Journal Abbreviations:

AAPS J. ..... AAPS Journal

Acc. Chem. Res. ..... Accounts of Chemical Research

ACS Appl. Mater. Interfaces ..... ACS Applied Materials & Interfaces

Acta Biomater. ..... Acta Biomaterialia

Adv. Mater. ..... Advanced Materials

Adv. Ski. & Wound Care ..... Advances in Skin & Wound Care

Adv. Wound Care ..... Advances in Wound Care

Am. Fam. Physician ..... American Family Physician

Angew. Chemie. – Int. Ed. ..... Angewandte Chemie – International Edition

Ann. Intern. Med ..... Annals of Internal Medicine

Ann. Laparosc. Endosc. Surg. ... Annals of Laparascopic and Endoscopic Surgery

Ann. Plast. Surg. ..... Annals of Plastic Surgery

Ann. Thorac. Surg. ..... Annals of Thoracic Surgery

Ann. Vasc. Surg. ..... Annals of Vascular Surgery

Annu. Rev. Biophys. ..... Annual Review of Biophysics

Asian J. Pharm. Sci. ..... Asian Journal of Pharmaceutical Sciences

Aust. N. Z. J. Surg. ..... Australian and New Zealand Journal of Surgery

Biochem J. ..... Biochemical Journal

Bioeng. Transl. Med. ..... Bioengineering & Translational Medicine

Biol. Pharm. Bull. ..... Biological & Pharmaceutical Bulletin

Biomater. Sci. ..... Biomaterials Science

Biomed Mater. ..... Biomedical Materials

Bull. World Health Organ. ..... Bulletin of the World Health Organization

Burn Trauma ..... Burns and Trauma

Can. J. Chem. ..... Canadian Journal of Chemistry

Cancer Prev. Res ..... Cancer Prevention Research

Carbohydr. Polym. ..... Carbohydrate Polymers

Chem. Eng. J. ..... Chemical Engineering Journal

Chem. Mater. ..... Chemistry of Materials

Chem. Rev. ..... Chemical Reviews

Chem. Soc. Rev. ..... Chemical Society Reviews

Clin. Endosc. ..... Clinical Endoscopy

Clin. Evid. (Online) ..... Clinical Evidence (Online)

Clin. Microbiol. Rev. ..... Clinical Microbiology Reviews

Cochrane Database Syst. Rev. ..... Cochrane Database of Systematic Reviews

Compr. Physiol. ..... Comprehensive Physiology

Cryst. Growth Des. ..... Crystal Growth & Design

Dig. Dis. Sci. ..... Digestive Diseases and Sciences

Eur. J. Heart Fail. ..... European Journal of Heart Failure

Eur. Polym. J. ..... European Polymer Journal

Expert Rev. Med. Devices ..... Expert Review of Medical Devices

Gastrointest. Endosc. ..... Gastrointestinal Endoscopy

Ind. Eng. Chem. Res. ..... Industrial & Engineering Chemistry Research

Indian J. Plast. Surg. ..... Indian Journal of Plastic Surgery

Indian J. Sci. Technol. ..... Indian Journal of Science and Technology

Int. J. Pediatr..... International Journal of Pediatrics

Int. J. Pharm ..... International Journal of Pharmaceutics

Int. J. Pharm. Sci. Rev. Res.....

.....International Journal of Pharmaceutical Sciences Review and Research

Int. Wound J..... International Wound Journal

Interact. Cardiovasc. Thorac. Surg. .....

..... Interactive Cardiovascular and Thoracic Surgery

J. Adv. Res. .....Journal of Advanced Research

J. Am. Chem. Soc. ..... Journal of the American Chemical Society

J. Appl. Polym. Sci. ..... Journal of Applied Polymer Science

J. Burn Care Res .....Journal of Burn Care & Research

J. Burn Care Rehabil. ..... Journal of Burn Care & Rehabilitation

J. Card. Fail. .....Journal of Cardiac Failure

J. Cardiothorac Vasc. Anesth . Journal of Cardiothoracic and Vascular Anesthesia

J. Healthc. Eng. ..... Journal of Healthcare Engineering

J. Macromol. Sci. – Rev. ..... Journal of Macromolecular Science – Reviews

J. Mater. Chem. ..... Journal of Materials Chemistry

J. Mater. Sci. .....Journal of Materials Science

J. Med. Assoc. Thail. ..... Journal of the Medical Association of Thailand

J. Microb. Biochem. Technol. .....
..... Journal of Microbial & Biochemical Technology
J Pak Med Assoc ..... Journal of the Pakistan Medical Association
J Pediatr Surg ..... Journal of Pediatric Surgery
J. Thorac. Dis..... Journal of Thoracic Disease
J. Trauma.....Journal of Trauma
J Trauma Acute Care Surg ..... Journal of Trauma and Acute Care Surgery
J West Afr Coll Surg ..... Journal of the West African College of Surgeons
J. Wound Care.....Journal of Wound Care
Macromol. Biosci. .....Macromolecular Bioscience
Macromol. Mater. Eng. ..... Macromolecular Materials and Engineering
Macromol. Rapid Commun. ..... Macromolecular Rapid Communications
Mar. Drugs ..... Marine Drugs
Mater. Horiz. ..... Materials Horizons
Mater. Technol. .....Materials Technology
Med. Eng. Phys. ..... Medical Engineering & Physics
Mil Med Res.....Military Medical Research
N. Engl. J. Med. ..... The New England Journal of Medicine
Nat. Commun..... Nature Communications
New J. Chem. .....New Journal of Chemistry
Pain Rev. ..... Pain Reviews
Pak. J. Med. Sci. ..... Pakistan Journal of Medical Sciences

Plast Reconstr Surg Glob Open .....
.....Plastic and Reconstructive Surgery. Global Open
Plast Surg Int .....Plastic Surgery International
Polym. Adv. Technol. ..... Polymers for Advanced Technologies
Polym. Bull. .....Polymer Bulleting
Prog. Materi. Sci. ..... Progress in Materials Science
R. Soc. Med. Serv. Int. Cong. Symp. Ser……...
..... Royal Society of Medicine Internal Congress and Symposium Series
Sci. Rep. .....Scientific Reports
Surg. Today ..... Surgery Today
Texas Heart Inst. J.....Texas Heart Institute Journal
Tissue Eng. Part B Rev. ..... Tissue Engineering. Part B, Reviews
World J. Surg. Surg. Res.....World Journal of Surgery and Surgical Research
Wounds Int.....Wounds International

References:

(1) Hall, C.; Hardin, C.; Corkins, C. J.; Jiwani, A. Z.; Fletcher, J.; Carlsson, A.; Chan, R. Pathophysiologic mechanisms and current treatments for cutaneous sequelae of burn wounds. *Compr. Physiol.* **2017,** 8(1), 371–405. https://doi.org/10.1002/cphy.c170016

(2) Lloyd, E. C. O.; Rodgers, B. C.; Michener, M.; Williams, M. S. *Am. Fam. Physician* **2012**, *85* (1), 25–32.

(3) Moss, L. S. *Critical Care Nursing Clinics of North America*. 2004.

(4) Oryan, A.; Alemzadeh, E.; Moshiri, A. Burn wound healing: Present concepts, treatment strategies and future directions. *J. Wound Care* **2017,** 26(1), 5–19. https://doi.org/10.12968/jowc.2017.26.1.5

(5) Son Tran, H.; Hoang Le, T.; Thanh Nguyen, T. *Indian J. Sci. Technol.* **2016**, *9* (45), 1–6.

(6) Singh, V.; Devgan, L.; Bhat, S.; Milner, S. M. *Ann. Plast. Surg.* **2007**, *59* (1), 109–115.

(7) Chaganti, P.; Gordon, I.; Chao, J. H.; Zehtabchi, S. A systematic review of foam dressing for partial thickness burns. *American Journal of Emergency Medicine*. **2019**, 37 (6), 1184–1190. https://doi.org/10.1016/j.ajem.2019.04.014

(8) Khansa, I.; Schoenbrunner, A. R.; Kraft, C. T.; Janis, J. E. *Plast Reconstr Surg Glob Open* **2019**, *7* (8), e2390.

(9) Quinn, K. J.; Courtney, J. M.; Evans, J. H.; Gaylor, J. D. S.; Reid, W. H. Principles of burn dressings. *Biomaterials*. **1985**, 6 (6), 369–377. https://doi.org/10.1016/0142-9612(85)90095-x

(10) Wasiak, J.; Cleland, H.; Campbell, F.; Spinks, A. *Cochrane Database Syst. Rev.* **2013**, *2013* (3).

(11) Sahin, C.; Kaplan, P.; Ozturk, S.; Alpar, S.; Karagoz, H. Treatment of partial-thickness burns with a tulle-gras dressing and a hydrophilic polyurethane membrane: A comparative study. *J. Wound Care* **2019,** 28(1), 24–28. https://doi.org/10.12968/jowc.2019.28.1.24

(12) Tang, H.; Lv, G.; Fu, J.; Niu, X.; Li, Y.; Zhang, M.; Zhang, G.; Hu, D.; Chen, X.; Lei, J.; Qi, H.; Xia, Z. *J Trauma Acute Care Surg* **2015**, *78* (5), 1000–1007.

(13) Yang, B.; Wang, X.; Li, Z.; Qu, Q.; Qiu, Y. *Pak J Med Sci* **2015**, *31* (6), 1334–1339.

(14) Silverstein, P.; Heimbach, D.; Meites, H.; Latenser, B.; Mozingo, D.; Mullins, F.; Garner, W.; Turkowski, J.; Shupp, J.; Glat, P.; Purdue, G. *J Burn Care Res* **2011**, *32* (6), 617–626.

(15) Silverstein, P.; Heimbach, D.; Meites, H.; Latenser, B.; Mozingo, D.; Mullins, F.; Garner, W.; Turkowski, J.; Shupp, J.; Glat, P.; Purdue, G. *J Burn Care Res* **2011**, *32* (6), 617–626.

(16) Yang, B.; Wang, X.; Li, Z.; Qu, Q.; Qiu, Y. *Pak J Med Sci* **2015**, *31* (6), 1334–1339.

(17) Baghel, P. S.; Shukla, S.; Mathur, R. K.; Randa, R. *Indian J Plast Surg* **2009**, *42* (2), 176–181.

(18) Aziz, Z.; Abdul Rasool Hassan, B. *Burns* **2017**, *43* (1), 50–57.

(19) Genuino, G. A.; Baluyut-Angeles, K. V; Espiritu, A. P.; Lapitan, M. C.; Buckley, B. S. *Burns* **2014**, *40* (7), 1267–1273.

(20) Khorasani, G.; Hosseinimehr, S. J.; Azadbakht, M.; Zamani, A.; Mahdavi, M. R. *Surg Today* **2009**, *39* (7), 587–591.

(21) Malik, K. I.; Malik, M. A.; Aslam, A. *Int Wound J* **2010**, *7* (5), 413–417.

(22) Shahzad, M. N.; Ahmed, N. *J Pak Med Assoc* **2013**, *63* (2), 225–230.

(23) Godhi, A. S.; Ram, P.; Powar, R. *J West Afr Coll Surg* **2017**, *7* (1), 57–70.

(24) Khansa, I.; Schoenbrunner, A. R.; Kraft, C. T.; Janis, J. E. *Plast Reconstr Surg Glob Open* **2019**, *7* (8), e2390.

(25) Gravante, G.; Caruso, R.; Sorge, R.; Nicoli, F.; Gentile, P.; Cervelli, V. *Ann Plast Surg* **2009**, *63* (2), 201–205.

(26) Muangman, P.; Chuntrasakul, C.; Silthram, S.; Suvanchote, S.; Benjathanung, R.; Kittidacha, S.; Rueksomtawin, S. *J. Med. Assoc. Thail.* **2006**, *89* (7), 953–958.

(27) Varas, R. P.; O'Keeffe, T.; Namias, N.; Pizano, L. R.; Quintana, O. D.; Tellachea, M. H.; Rashid, Q.; Ward, C. G. *J. Burn Care Rehabil.* **2005**, *26* (4), 344–347.

(28) Al-Waili, N. S.; Salom, K.; Al-Ghamdi, A. A. Honey for wound healing, ulcers, and burns; Data supporting its use in clinical practice. *The Scientific World Journal*. **2011,** 11, 766–787. https://doi.org/10.1100/tsw.2011.78

(29) Aziz, Z.; Abdul Rasool Hassan, B. *Burns* **2017**, *43* (1), 50–57.

(30) Wijesinghe, M.; Weatherall, M.; Perrin, K.; Beasley, R. Honey in the treatment of burns: A systematic review and meta-analysis of its efficacy *New Zealand Medical Journal*. **2009**, 122 (1295), 47–60.

(31) Fletcher, J.; Moore, Z.; Anderson, I.; Matsuzaki, K. *Wounds Int.* **2011**, *2* (4), 1–6.

(32) Phipps A, L. J. B. *Beyond Occlusion Wound Care Proceedings, R. Soc. Med. Serv. Int. Congr. Symp. Ser. No. 136.* **1988**.

(33) Thomas, S. S.; Lawrence, J. C.; Thomas, A. *J Wound Care* **1995**, *4* (5), 218–220.

(34) Wright, A.; MacKechnie, D. W.; Paskins, J. R. *Burns* **1993**, *19* (2), 128–130.

(35) Wright, A.; MacKechnie, D. W.; Paskins, J. R. *Burns* **1993**, *19* (2), 128–130.

(36) Fiachra T Martin Padraic J Regan, Jack McCann, Jack L Kelly, J. B. O. *J Pediatr Surg* **2010**, *45* (3), 600–605.

(37) Cassidy, C.; St Peter, S. D.; Lacey, S.; Beery, M.; Ward-Smith, P.; Sharp, R. J.; Ostlie, D. J. *Burns* **2005**, *31* (7), 890–893.

(38) Poulsen, T. D.; Freund, K. G.; Arendrup, K.; Nyhuus, P.; Pedersen, O. D. *Burns* **1991**, *17* (1), 59–61.

(39) Feng, J. J., See, J. L., Choke, A., Ooi, A., & Chong, S. J. *Mil Med Res* **2018**, *5* (1).

(40) White, R. *Wounds UK* **2005**.

(41) S. L. Hansen P. Wiebelhaus, and C. N. Paul, D. W. V. *Adv. Ski. & Wound Care, 14* (1), 37–45.

(42) Demling, R. H.; DeSanti, L. *Burns* **1999**, *25* (3), 256–261.

(43) Demling, R. H.; DeSanti, L. *Burns* **1999**, *25* (3), 256–261.

(44) Murphy, P. S.; Evans, G. R. *Plast Surg Int* **2012**, *2012*, 190436.

(45) Jones, N.; Ivins, N.; Ebdon, V.; Hagelstein, S.; Harding, K. *Wounds UK* **2017**.

(46) Sood, A.; Granick, M. S.; Tomaselli, N. L. *Adv Wound Care (New Rochelle)* **2014**, *3* (8), 511–529.

(47) Jozsa, G.; Vajda, P.; Garami, A.; Csenkey, A.; Juhasz, Z. Treatment of partial thickness hand burn injuries in children with combination of silver foam dressing and zinc-hyaluronic gel: Case reports. *Medicine* **2018,** 97 (13), e9991. https://doi.org/10.1097/md.0000000000009991

(48) Muangman, P.; Pundee, C.; Opasanon, S.; Muangman, S. *Int Wound J* **2010**, *7* (4), 271–276.

(49) Ghobril, C.; Grinstaff, M. W. *Chem. Soc. Rev.* **2015**, *44* (7), 1820–1835.

(50) Ahmed, E. M. *J. Adv. Res.* **2015**, *6* (2), 105–121.

(51) Fu, J.; In Het Panhuis, M. *J. Mater. Chem. B* **2019**, *7* (10), 1523–1525.

(52) Zhang, Y. S.; Khademhosseini, A. *Science.* **2017**, *356* (6337), 1–27.

(53) Li, X.; Shen, Q.; Su, Y.; Tian, F.; Zhao, Y.; Wang, D. *Cryst. Growth Des.* **2009**, *9* (8), 3470–3476.

(54) Okay, O. *Supramolecular Polymer Networks and Gels*; Springer, Cham, 2015.

(55) Zheng, S. Y.; Ding, H.; Qian, J.; Yin, J.; Wu, Z. L.; Song, Y.; Zheng, Q. *Macromolecules* **2016**, *49* (24), 9637–9646.

(56) You, Y.; Yang, J.; Zheng, Q.; Wu, N.; Lv, Z.; Jiang, Z. *Sci. Rep.* **2020**, *10* (1), 1–8.

(57) Gradinaru, V.; Treweek, J.; Overton, K.; Deisseroth, K. *Annu. Rev. Biophys.* **2018**, *47*, 355–376.

(58) Kamoun, E. A.; Kenawy, E. R. S.; Chen, X. *J. Adv. Res.* **2017**, *8* (3), 217–233.

(59) Mathur, A. M.; Moorjani, S. K.; Scranton, A. B. *J. Macromol. Sci. - Rev. Macromol. Chem. Phys.* **1996**, *36* (2), 405–430.

(60) Stubbe, B.; Mignon, A.; Declercq, H.; Van Vlierberghe, S.; Dubruel, P. *Macromol. Biosci.* **2019**, *19* (8), 1–12.

(61) Ghobril, C.; Charoen, K.; Rodriguez, E. K.; Nazarian, A.; Grinstaff, M. W. *Angew. Chemie - Int. Ed.* **2013**, *52* (52), 14070–14074.

(62) Ye, H.; De, S. Thermal injury of skin and subcutaneous tissues: A review of experimental approaches and numerical models. *Burns*. **2017,** 43 (5), 909–932. https://doi.org/10.1016/j.burns.2016.11.014

(63) Zheng, Y.; Yuan, W.; Liu, H.; Huang, S.; Bian, L.; Guo, R. *Biomater. Sci.* **2020**, *8* (17), 4810–4820.

(64) Lei, H.; Zhu, C.; Fan, D. *Carbohydr. Polym.* **2020**, *239* (January), 116249.

(65) Zhu, C.; Lei, H.; Fan, D.; Duan, Z.; Li, X.; Li, Y.; Cao, J.; Wang, S.; Yu, Y. *J. Mater. Sci.* **2018**, *53* (8), 5909–5928.

(66) Madaghiele, M.; Sannino, A.; Ambrosio, L.; Demitri, C. *Burn. Trauma* **2014**, *2* (4), 153.

(67) Dang, L. H.; Nguyen, T. H.; Tran, H. L. B.; Doan, V. N.; Tran, N. Q. *J. Healthc. Eng.* **2018**, *2018*, 1–14.

(68) Yan, T.; Kong, S.; Ouyang, Q.; Li, C.; Hou, T.; Chen, Y.; Li, S. *Mar. Drugs* **2020**, *18* (5).

(69) Rinehart, S.; Campbell, T. *J. Microb. Biochem. Technol.* **2016**, *08* (02), 65–70.

(70) Jackson, J.; Burt, H.; Lange, D.; Whang, I.; Evans, R.; Plackett, D. *Nanomaterials* **2021**, *11* (1), 1–19.

(71) Boonkaew, B.; Suwanpreuksa, P.; Cuttle, L.; Barber, P. M.; Supaphol, P. *J. Appl. Polym. Sci.* **2014**, *131* (9), 1–10.

(72) Kim, M. H.; Park, H.; Nam, H. C.; Park, S. R.; Jung, J. Y.; Park, W. H. *Carbohydr. Polym.* **2018**, *181* (November 2017), 579–586.

(73) Johnson, K. anne; Muzzin, N.; Toufanian, S.; Slick, R. A.; Lawlor, M. W.; Seifried, B.; Moquin, P.; Latulippe, D.; Hoare, T. *Acta Biomater.* **2020**, *112*, 101–111.

(74) Wang, P.; Huang, S.; Hu, Z.; Yang, W.; Lan, Y.; Zhu, J.; Hancharou, A.; Guo, R.; Tang, B. *Acta Biomater.* **2019**, *100*, 191–201.

(75) Samadi, A.; Azandeh, S.; Orazizadeh, M.; Bayati, V.; Rafienia, M.; Karami, M. A. *Mater. Technol.* **2020**, *00* (00), 1–11.

(76) Konieczynska, M. D.; Grinstaff, M. W. *Acc. Chem. Res.* **2017**, *50* (2), 151–160.

(77) Lu, W.; Xu, X.; Imbernon, L.; Zhu, J.; Hoogenboom, R.; Du Prez, F. E.; Pan, X. *Biomacromolecules* **2020**, *21* (8), 3308–3317.

(78) Mock, C.; Peck, M.; Peden, M.; Krug, E.; Ahuja, R.; Albertyn, H.; Bodha, W.; Cassan, P.; Godakumbura, W.; Lo, G.; Partridge, J.; Potokar, T. Burns https://www.who.int/news-room/fact-sheets/detail/burns.

(79) Church, D.; Elsayed, S.; Reid, O.; Winston, B.; Lindsay, R. *Clin. Microbiol. Rev.* **2006**, *19* (2), 403–434.

(80) Atchison, N. E.; Osgood, F.; Carr, D. B.; Szyfelbein, K. *Pain* **1991**, *47*, 41–45.

(81) Beushausen, T.; Mücke, K. *Int Pediatr Surg* **1997**, 327–333.

(82) Judkins, K. Pain management in the burned patient. *Pain Rev.* **1998**, 5(3), 133–146. https://doi.org/10.1191/096813098666525736

(83) Peck, M.; Molnar, J.; Swart, D. *Bull. World Health Organ.* **2009**, *87*, 802–803.

(84) Iv, G. Management of Burns https://www.who.int/surgery/publications/Burns_management.pdf.

(85) Wasiak, J.; Cleland, H. *Clin. Evid. (Online).* **2015**, No. January 2014, 1–44.

(86) Daristotle, J. L.; Lau, L. W.; Erdi, M.; Hunter, J.; Djoum, A.; Priya, J.; Xiaofang, S.; Mousumi, W.; Ayyub, O. B.; Sandler, A. D.; Kofinas, P. *Bioeng. Transl. Med.* **2020**, No. July 2019, 1–12.

(87) Latarjetl, J Choinere, M. *Burns* **1995**, *21* (5), 344–348.

(88) Dane, E. L.; Grinstaff, M. W. Poly-amido-saccharides: Synthesis via anionic polymerization of a β-lactam sugar monomer. *J. Am. Chem. Soc.*

2012, 134 (39), 16255–16264. https://doi.org/10.1021/ja305900r

(89) Duchowny, K. *J. Burn Care Res.* **2020**, *40*, 2008–2010.

(90) Fullenkamp, D. E.; Rivera, J. G.; Gong, Y. kuan; Lau, K. H. A.; He, L.; Varshney, R.; Messersmith, P. B. *Biomaterials* **2012**, *33* (15), 3783–3791.

(91) Queen, D.; Evans, J. H.; Gaylor, J. D. S.; Courtney, J. M.; Reid, W. H. *Burns* **1987**, *13*, 218–228.

(92) Gandhi, M.; Thomson, C.; Lord, D.; Enoch, S. *Int J Pediatr.* **2010**, *2010*.

(93) Loo, Y.; Wong, Y.; Cai, E. Z.; Ang, C.; Raju, A.; Lakshmanan, A.; Koh, A. G.; Zhou, H. J.; Lim, T.; Moochhala, S. M.; Hauser, C. A. E. *Biomaterials* **2014**, *35* (17), 4805–4814.

(94) Campbell, J. M.; Kavanagh, S.; Kurmis, R.; MClinSci, Z. M. *J. Burn Care Res.* **2017**, *38* (2), 552–567.

(95) Konieczynska, M. D.; Villa-Camacho, J. C.; Ghobril, C.; Perez-Viloria, M.; Tevis, K. M.; Blessing, W. A.; Nazarian, A.; Rodriguez, E. K.; Grinstaff, M. W. *Angew Chemie Int. Ed.* **2016**, *55* (34), 9984–9987.

(96) Wright, J. K.; Kalns, J.; Wolf, E. a; Traweek, F.; Schwarz, S.; Loeffler, C. K.; Snyder, W.; Yantis, L. D.; Eggers, J. *J. Trauma* **2004**, *57* (2), 224–230.

(97) Oelker, A. M.; Berlin, J. A.; Wathier, M.; Grinstaff, M. W. *Biomacromolecules* **2011**, *12* (5), 1658–1665.

(98) Hawker, C. J.; Wooley, K. L. *Science.* **2005**, *309* (August), 1200–1206.

(99) Watabe, H.; Yamaji, Y.; Okamoto, M.; Kondo, S.; Ohta, M.; Ikenoue, T.; Kato, J.; Togo, G.; Matsumura, M.; Yoshida, H.; Kawabe, T.; Omata, M.

Gastrointest. Endosc. **2006**, *64* (1), 73–78.

(100) Zohuriaan-Mehr, M. J.; Omidian, H.; Doroudiani, S.; Kabiri, K. *J. Mater. Sci.* **2010**, *45* (21), 5711–5735.

(101) Tang, S.; Richardson, B. M.; Anseth, K. S. *Prog. Mater. Sci.* **2020**, No. September, 100738.

(102) Huang, W.; Wang, Y.; Huang, Z.; Wang, X.; Chen, L.; Zhang, Y.; Zhang, L. *ACS Appl. Mater. Interfaces* **2018**, *10*, 41076–41088.

(103) Lee, K. Y.; Mooney, D. J. Hydrogels for tissue engineering. *Chem. Rev.* **2001**, *101* (7), 1869–1880.

(104) Singh, A.; Sharma, P. K.; Garg, V. K.; Garg, G. *Int. J. Pharm. Sci. Rev. Res.* **2010**, *4* (2), 97–105.

(105) Zhu, J.; Marchant, R. E. *Expert Rev. Med. Devices* **2011**, *8* (5), 607–626.

(106) Op't Veld, R. C.; Walboomers, X. F.; Jansen, J. A.; Wagener, F. A. D. T. G. Design considerations for hydrogel wound dressings: Strategic and molecular advances. *Tissue Eng. Part B Rev.* **2020**, *26* (3), 230–248. https://doi.org/10.1089/ten.teb.2019.0281

(107) Cascone, S.; Lamberti, G. *Int. J. Pharm.* **2020**, *573* (November 2019), 118803.

(108) Zhao, Y.; Li, Z.; Li, Q.; Yang, L.; Liu, H.; Yan, R.; Xiao, L.; Liu, H.; Wang, J.; Yang, B.; Lin, Q. *Macromol. Rapid Commun.* **2020**, *2000441*, 1–11.

(109) Pailler-mattei, C.; Bec, S.; Zahouani, H. *Med. Eng. Phys.* **2008**, *30*, 599–606.

(110) Ghobril, C.; Grinstaff, M. W. *Chem. Soc. Rev.* **2015**, *44* (7), 1820–1835.

(111) Burke, S. A.; Ritter-Jones, M.; Lee, B. P.; Messersmith, P. B. *Biomed. Mater.* **2007**, *2* (4), 203–210.

(112) Lee, S. H.; Joo, Y.; Kim, H. G. *Endoscopy* **2013**, *45*, 202–207.

(113) Lam, W.; Times, M. *Ann. Laparosc. Endosc. Surg.* **2019**, *4* (97), 1–9.

(114) Levin, T. R.; Zhao, W.; Conell, C.; Seeff, L. C.; Manninen, D. L.; Shapiro, J. A.; Schulman, J. *Ann. Intern. Med.* **2006**, *145*, 880–886.

(115) Grossberg, L. B.; Papamichael, K.; Leffler, D. A.; Sawhney, M. S.; Feuerstein, J. D. *Dig. Dis. Sci.* **2019**, *65*, 1964–1970.

(116) Cardoso, R.; Niedermaier, T.; Chen, C.; Hoffmeister, M.; Brenner, H. *Cancer Prev. Res.* **2019**, *12* (9), 617–629.

(117) Calonge, N.; Petitti, D. B.; DeWitt, T. G.; Dietrich, A. J.; Gregory, K. D.; Harris, R.; Isham, G.; LeFevre, M. L.; Leipzig, R. M.; Loveland-Cherry, C.; Marion, L. N.; Melnyk, B.; Moyer, V. A.; Ockene, J. K.; Saway, G. F.; Yawn, B. P. *Ann. Intern. Med.* **2008**, *149* (9), 627–638.

(118) Hong, S. P. *Clin. Endosc.* **2012**, *45* (3), 282–284.

(119) Heldwein, W.; Dollhopf, M.; Meining, A.; Schmidtsdorff, G.; Hasford, J.; Hermanek, P.; Burlefinger, R.; Birkner, B.; Schmitt, W. *Endocsopy* **2005**, *37* (11), 1116–1122.

(120) Hui, A. J.; Wong, R. M. Y.; Ching, J. Y. L.; Hung, L. C. T.; Chung, S. C. S.; Sung, J. J. Y. *Gastrointest. Endosc.* **2004**, *59* (1), 44–48.

(121) Colorectal (colon) cancer.

(122) Myung, D.; Waters, D.; Wiseman, M.; Duhamel, P.-E.; Noolandi, J.; Ta, C. N.; Frank, C. W. *Polym. Adv. Technol.* **2008**, *19* (April 2008), 647–657.

(123) Chai, Q.; Jiao, Y.; Yu, X. Hydrogels for biomedical applications: Their characteristics and the mechanisms behind them. *Gels*, **2017**, 3 (1), 6. https://dx.doi.org/10.3390%2Fgels3010006

(124) Ghobril, C.; Rodriguez, E. K.; Nazarian, A.; Grinstaff, M. W. *Biomacromolecules* **2016**, *17* (4), 1235–1252.

(125) Ghobril, C.; Rodriguez, E. K.; Nazarian, A.; Grinstaff, M. W. *Biomacromolecules* **2016**, *17* (4), 1235–1252.

(126) Konieczynska, M. D.; Villa-Camacho, J. C.; Ghobril, C.; Perez-Viloria, M.; Blessing, W. A.; Nazarian, A.; Rodriguez, E. K.; Grinstaff, M. W. *Mater. Horiz.* **2017**, *4* (2), 222–227.

(127) Comisar, C. M.; Hunter, S. E.; Walton, A.; Savage, P. E. *Ind. Eng. Chem. Res.* **2008**, *47* (3), 577–584.

(128) Bergmann, F.; Segal, R.; Shimoni, A.; Wurzel, M. *Biochem. J.* **1956**, *63* (4), 684–690.

(129) Nojima, Y.; Iguchi, K.; Suzuki, Y.; Sato, A. *Biol. Pharm. Bull.* **2009**, *32* (3), 523–526.

(130) Cline, G. W.; Hanna, S. B. *J. Am. Chem. Soc.* **1987**, *109* (10), 3087–3091.

(131) Liu, M.; Zhang, J.; Shan, W.; Huang, Y. *Asian J. Pharm. Sci.* **2014**, *10* (4), 275–282.

(132) Crater, J. S.; Carrier, R. L. *Macromol. Biosci.* **2010**, *10* (12), 1473–1483.

(133) Chen, S.; Li, L.; Zhao, C.; Zheng, J. *Polymer.* **2010**, *51* (23), 5283–5293.

(134) Cheng, G.; Xue, H.; Zhang, Z.; Chen, S.; Jiang, S. *Angew. Chemie* **2008**, *120* (46), 8963–8966.

(135) Mechanic, O. J.; Grossman, S. A. *StatPearls* **2019**.

(136) Metra, M.; Teerlink, J. R.; Felker, G. M.; Greenberg, B. H.; Filippatos, G.; Ponikowski, P.; Teichman, S. L.; Unemori, E.; Voors, A. A.; Weatherley, B. D.; Cotter, G. *Eur. J. Heart Fail.* **2010**, *12*, 1130–1139.

(137) Torre-amione, G.; Milo-cotter, O.; Kaluski, E. D. O.; Perchenet, L.; Kobrin, I.; Frey, A.; Rund, M. M.; Weatherley, B. D. *J. Card. Fail.* **2009**, *15* (8), 639–644.

(138) Alexander, J. H.; Smith, P. K. *N. Engl. J. Med.* **2016**, *374* (20), 1954–1964.

(139) Erkut, B.; Ates, A. *World J. Surg. Surg. Res.* **2019**, *2*, 2–5.

(140) Babin-Ebell, J.; Gimpel-Henning, K.; Sievers, H.-H.; Scharfschwerdt, M. *Interact. Cardiovasc. Thorac. Surg.* **2010**, *10* (2), 168–171.

(141) Christenson, J. T.; Vala, D. L.; Licker, M.; Sierra, J.; Kalangos, A. *Texas Hear. Inst. J.* **2005**, *32* (4), 515–521.

(142) Takeda, S.; Nakanishi, K.; Ikezaki, H.; Kim, C.; Sakamoto, A.; Tanaka, K.; Ogawa, R. *J. Cardiothorac. Vasc. Anesth.* **2002**, *16* (4), 421–425.

(143) Margovsky, A. I.; Lord, R. S.; Chambers, A. J. *Aust. N. Z. J. Surg.* **1997**, *67* (7), 448–451.

(144) Calafiore, A. M.; Di Mauro, M.; Teodori, G.; Di Giammarco, G.; Cirmeni, S.; Contini, M.; Iacò, A. L.; Pano, M. *Ann. Thorac. Surg.* **2002**, *73* (5),

1387–1393.

(145) Melly, L.; Torregrossa, G.; Lee, T.; Jansens, J. L.; Puskas, J. D. *J. Thorac. Dis.* **2018**, *10* (3), 1960–1967.

(146) Onan, B.; Erkanli, K.; Onan, I. S.; Ersoy, B.; Canillioglu, Y. E.; Senturk, G. E.; Hurdag, C.; Yeniterzi, M. *Ann. Vasc. Surg.* **2014**, *28* (5), 1113–1122.

(147) Zaikina, O. E.; Dolgov, V. V.; Ivanov, V. N.; Bondarenko, M. F.; Repin, V. S. *Atherosclerosis* **1982**, *41* (2–3), 141–154.

(148) Sturtz, K. L.; Danitz, D. J.; Carnegie, J.; Baughman, T. L. Surgical Clamp Inserts with Microtractive Surfaces, 2014. US Patent US20040143276A1 https://patents.google.com/patent/US20040143276

(149) Gitsov, I.; Zhu, C. *J. Am. Chem. Soc.* **2003**, *125* (37), 11228–11234.

(150) Wei, Z.; Gerecht, S. *Biomaterials* **2018**, *185*, 86–96.

(151) Freedman, B. R.; Mooney, D. J. *Adv. Mater.* **2019**, *31* (19), 1–53. https://doi.org/10.1002/adma.201806695

(152) Koehler, J.; Brandl, F. P.; Goepferich, A. M. *Eur. Polym. J.* **2018**, *100* (August 2017), 1–11.

(153) Brown, T. E.; Anseth, K. S. *Chem. Soc. Rev.* **2017**, *46* (21), 6532–6552.

(154) Konieczynska, M. D.; Grinstaff, M. W. *Acc. Chem. Res.* **2017**, No. 1, acs.accounts.6b00547.

(155) Barnard, P. W. C.; Robertson, R. E. *Can. J. Chem.* **1961**, *39* (6212), 881–888.

(156) Sharifi, M.; Ghafourian, T. Estimation of biliary excretion of foreign compounds using properties of molecular medicine. *AAPS J.* **2014**, *16* (1), 65–78. https://doi.org/10.1208/s12248-013-9541-z

(157) Hirom, P. C.; Millburn, P.; Smith, R. L.; Williams, R. T. *Biochem. J.* **1972**, *129* (5), 1071–1077.

(158) Abou-el-Makarem, M. M.; Millburn, P.; Smith, R. L.; Williams, R. T. *Biochem. J.* **1967**, *105* (3), 1269–1274.

(159) Stockman, K.; Carnahan, M. A.; D'Alessio, K.; Grinstaff, M. W. CROSSLINKED GELS COMPRISING POLYALKYLENEIMINES, AND THEIR USES AS MEDICAL DEVICES. US 2007/0196454 A1, 2007.

(160) Konieczynska, M. D.; Villa-Camacho, J. C.; Ghobril, C.; Perez-Viloria, M.; Blessing, W. A.; Nazarian, A.; Rodriguez, E. K.; Grinstaff, M. W. *Mater. Horiz.* **2017**, *64*, 24.

(161) Wathier, M.; Johnson, M. S.; Carnahan, M. A.; Baer, C.; McCuen, B. W.; Kim, T.; Grinstaff, M. W. *ChemMedChem* **2006**, *1* (8), 821–825.

(162) Waters, D. J.; Engberg, K.; Parke-Houben, R.; Ta, C. N.; Jackson, A. J.; Toney, M. F.; Frank, C. W. *Macromolecules* **2011**, *44* (14), 5776–5787.

(163) Farooq, U.; Teuwen, J.; Dransfeld, C. *Polymers (Basel).* **2020**, *12* (9), 1–29.

(164) Raina, N.; Rani, R.; Khan, A.; Nagpal, K.; Gupta, M. *Polym. Bull.* **2020**, *77* (9), 5027–5050.

(165) Silverstein, M. S. *Polymer (Guildf).* **2020**, *207*, 122929.

(166) Dragan, E. S. *Chem. Eng. J.* **2014**, *243*, 572–590.

(167) Shivashankar, M.; Mandal, B. K. *Int. J. Pharm. Pharm. Sci.* **2012**, *4* (SUPPL. 5), 1–7.

(168) Feig, V. R.; Tran, H.; Lee, M.; Bao, Z. *Nat. Commun.* **2018**, *9* (1), 1–9.

(169) Chen, F.; Le, P.; Lai, K.; Fernandes-Cunha, G. M.; Myung, D. *Chem. Mater.* **2020**, *32* (12), 5208–5216.

(170) Zhyhailo, M.; Horechyy, A.; Meier-Haack, J.; Formanek, P.; Malanin, M.; Arnhold, K.; Schneider, K.; Yevchuk, I.; Fery, A. *Macromol. Mater. Eng.* **2021**, *2000776*, 1–11.

(171) Liu, E.; Lin, X.; Zhang, D.; Xu, W.; Shi, J.; Hong, Y. *New J. Chem.* **2021**, *45* (2), 725–734.

(172) Zhang, X.; Liu, K.; Liu, J.; Ding, Y.; Li, W.; Zhang, A. *Eur. Polym. J.* **2020**, *141*, 1–7.

CURRICULUM VITAE